# The coding of safety-danger boundaries by the amygdala and hippocampus: an ecological risky foraging investigation in rats

Mi-Seon Kong

A dissertation

submitted in partial fulfillment of the

requirements for the degree of

Doctor of Philosophy

University of Washington

2019

Reading Committee:

Jeansok Kim, Chair

Sheri Mizumori

David Gire

Program Authorized to Offer Degree:

Department of Psychology

University of Washington

## Abstract

The coding of safety-danger boundaries by the amygdala and hippocampus: an ecological risky foraging investigation in rats

Mi-Seon Kong

Chair of the Supervisory Committee:
Professor Jeansok J. Kim
Department of Psychology

Contemporary fear research focuses heavily on learned/acquired fear, as opposed to innate/instinctive fear, through the use of the Pavlovian fear conditioning paradigm. However, fear conditioning studies have limited translational applicability because, by focusing on specific responses (such as freezing) in a small experimental chamber, they confine the natural behaviors of animals. In contrast, ethological approaches can provide a more comprehensive understanding of the brain's fear system because they mimic the risky situations that animals face in the real world. This dissertation investigated how the basal nucleus of the amygdala (BA; implicated in fear processing) and the dorsal hippocampus (dHPC; implicated in spatial processing) interact during 'approach food-avoid predator' conflict situations in rats. The first study employed a

simultaneous recording technique to reveal the characteristics of BA and dHPC cells during risky foraging behaviors. The results showed that the BA neurons encode the valence of events whereas the dHPC place cells build the spatial representation with a distance gradient of fear. The two regions together showed selective modulation of neural activity based upon spike synchrony during the interaction with a predatory threat; that is, dHPC cells that displayed synchronized firing with the BA cells displayed remapping of their place fields. The second study demonstrated that optogenetic stimulation of BA neurons was sufficient to produce defensive behaviors in the absence of explicit threats. The third study showed that optical stimulations of BA cells altered the stability of place cells in the dHPC. Based on these findings, I propose a neural model of fear signals from the BA influencing spatial coding in the dHPC, which serves to provide the safety-danger boundary information.

# TABLE OF CONTENTS

# LIST OF FIGURES

# LIST OF TABLES

# ACKNOWLEDGEMENTS

I would like to thank everyone who supported my graduate school journey. First, great thanks to my advisor Professor Jeansok Kim, who brought me from Korea and gave me the opportunity to study and pursue my goals in the United States. I enjoyed every discussion we had, and I respect his insights for research and his depth of knowledge. Thanks also to each of the Kim lab members; Eun Joo, Bryan, and Peter who have been very supportive and inspiring to me. I appreciate my committee members for their valuable comments and insight into my dissertation. To my parents, I am very grateful for being their daughter and thankful for their emotional and financial support. Sung, who is the best husband and father to our children, thank you for being right next to me always. Without your support and love, this day would have never come. Finally, thanks to God, who is the reason why I live.

# Chapter 1. BACKGROUND AND INTRODUCTION

Fear is an unpleasant emotion caused by the belief that someone or something is dangerous, likely to cause pain or even death. The main function of fear is to protect animals and humans from dangers and threats. Thus, fear is normally an adaptive behavior. However, when the fear system becomes dysfunctional, it could lead to various mental illnesses such as anxiety disorder, panic disorder, phobia, and posttraumatic stress disorder (PTSD). Understanding the brain's fear system therefore has clinical significance.

Contemporary fear studies have traditionally employed the standard Pavlovian fear conditioning paradigm to understand the neural basis of fear. In this paradigm, a neutral stimulus (conditioned stimulus, CS) becomes capable of eliciting fear responses (conditioned response, CR) through associations with an aversive stimulus (unconditioned stimulus, US), which naturally evokes fear responses (unconditioned response, UR). The typical way fear conditioning research done in rodents is that the animal is placed in a small chamber and presented with CS such as a tone followed by US such as a footshock. Afterward, when the tone is presented alone, the animal freezes to the tone. This freezing behavior is commonly observed in prey animals and is characterized by changes in blood pressure, increased time in crouching position, shortness of breath, sweating, increased heart rate, and choking sensations. In the laboratory setting, freezing is measured by the duration of crouching time, which indicates the level of fear in rodents.

Fear conditioning, which is centered on fear that is acquired through learning, represents only one facet of fear as an adaptive behavior. This oversimplification of fear in fear research diminishes transnationality. When fear conditioning is compared to what happens in real life fear situations, critical differences are observed. First, there is no discrete cue (i.e., the CS in fear

conditioning) that signals danger in real life. Second, localizable external agents that cause harm in real life-threatening situations—such as predators, offenders, or enemy combatants—do not exist in fear conditioning experiments. Lastly, fear conditioning focuses on a limited set of specific responses (namely, duration of freezing) in small experimental chambers, despite the abundance of various risky situations in the natural world that require a diversity of fear-related behaviors, such as fleeing, risk assessment, avoidance, etc.

Moving forward, it is advisable that fear research implement an ethological approach to effectively expand the scope of fear to include innate fear (i.e., unlearned fear), which provides greater translational relevance. Utilizing stimuli that naturally evoke defensive behaviors without previous learning experience supports a realistic model of fear more than the fear framed by associative learning. It is therefore paramount that we elucidate the neural circuits of innate fear as well. Among all brain regions that are part of fear circuits, the studies presented in this dissertation focus on the interaction between the amygdala and hippocampus in innate fear. These two structures are critical in fear processing and their roles will be examined in the following sections (LeDoux, 2000).

In this chapter, the following contents will be covered: i) the roles of the amygdala in learned fear and innate fear, ii) spatial, nonspatial, and fear information processing by the hippocampus, iii) direct interaction between the amygdala and hippocampus in learned fear, and iv) importance of ethological approaches in fear studies. Finally, a brief discussion of the series of studies in this dissertation will be provided.

*Amygdala, a core of fear circuitry.*

The amygdala is located in the medial part of the temporal lobe in the brain and has been identified to be necessary for the various functions such as emotional information processing, learning and memory, and reward processing (Lalumiere, 2014). It consists of heterogeneous nuclei that include the basolateral complex (BLA), central nucleus (CeA), cortical nucleus, medial nucleus, and intercalated cell masses (ICMs). The BLA involves the lateral (LA) and basal (BA) nuclei and the CeA is divided into lateral (CeL) and medial (CeM) parts. The multifaceted function of the amygdala comes from not only the heterogeneous nuclei but also from heterogeneous cells in each nucleus. For example, within the BLA, there are genetically and functionally distinct neuronal types that process positive or negative valence coding, respectively (Gore et al., 2015; J. Kim, Pignatelli, Xu, Itohara, & Tonegawa, 2016; Paton, Belova, Morrison, & Salzman, 2006).

The most important function of the amygdala is regulating emotion and emotional expressions. Observations from cases of Kluver-Bucy syndrome, which results from damage to the temporal lobe (including the amygdala) and is characterized by behavioral and emotional abnormalities in rhesus monkeys, support this function (Klüver & Bucy, 1937). Monkeys and patients with Kluver-Busy syndrome show both diminished fear responses and aggressive behaviors. Other than reduced fear and anger responses, this syndrome is also characterized by inappropriate sexual behaviors, mouthing objects, a diminished ability to visually organize objects, amnesia, seizures, and dementia.

Learning and memory functions of the amygdala, especially from aversive learning, have been identified. One study found that BLA stimulation in the gamma frequency (40 Hz) enhances emotional memory consolidation (Huff, Miller, Deisseroth, Moorman, & LaLumiere,

2013). More about the role of the BLA in learning and memory, especially fear learning, will be covered in the next section. The amygdala is also crucial for reward processing and addiction-related behaviors (Di Ciano & Everitt, 2004; Everitt et al., 1999; See, Fuchs, Ledford, & McLaughlin, 2003). Anatomically, glutamatergic neurons in the BLA project to the nucleus accumbens (NAc), which is a well-known structure for motivated behaviors. Stimulation of these projections promotes reward-seeking behavior (Stuber et al., 2011).

*An amygdala microcircuit for fear learning.* Decades of studies have established an essential role of the amygdala in fear learning (LeDoux, 2000; Maren & Quirk, 2004; Pape & Pare, 2010). Pavlovian fear conditioning is widely used partially because it is easy to implement, and only a small number of pairings are required to form a lifelong memory (Gale et al., 2004; McAllister, McAllister, Scoles, & Hampton, 1986). Among the subnuclei of the amygdala, the roles of the BLA and CeA in fear conditioning have been the focus of most researchers. In this section, we will discuss how the BLA and CeA participate in fear learning and examine their intrinsic connectivity (Figure 1.1).

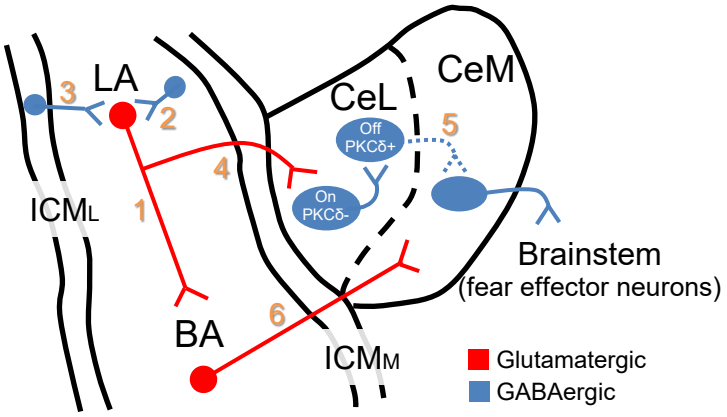


Figure 1.1. Intrinsic connectivity of the amygdala.

*Lateral Amygdala.* The prominent information flow within the BLA is unidirectional, and most projections have a preferential directionality, which runs dorsoventrally, from LA to BA (Figure 1.1, line 1). Due to this directionality, the cortical sensory and thalamic inputs containing CS and US information first arrive in the LA (Romanski, Clugnet, Bordi, & LeDoux, 1993). Based on these anatomical connections, it was proposed that the LA is the place where the CS and US convergence occurs [but not the sole place of plasticity for fear conditioning; the auditory thalamus and cortex are thought to also be loci of plasticity (Letzkus et al., 2011; Weinberger, 2011)], and CS-US association memory is stored in the BLA (LeDoux, 2000). Indeed, reversible inactivation of the LA during fear conditioning prevents the acquisition of fear learning (Maren, Yap, & Goosens, 2001; J. Muller, Corodimas, Fridel, & LeDoux, 1997; Wilensky, Schafe, & LeDoux, 1999). Furthermore, LA neurons develop increased CS-evoked responses after fear conditioning, which implicates potentiation of synapses as a result of learning (Collins & Pare, 2000; Quirk, Repa, & LeDoux, 1995; Repa et al., 2001). This potentiation eventually leads to fear responses by recruiting cells in charge of fear expression such as CeM.

GABAergic transmission in the LA has also been indicated to regulate fear conditioning and the underlying synaptic plasticity (Pare, Royer, Smith, & Lang, 2003). LA principal neurons are under strong inhibition by local interneurons and intercalated cells (Figure 1.1, line 2 and 3, repectively). As mentioned above, reversible inactivation of the LA impairs fear conditioning. This is mediated by activation of GABA-A receptors, which adds more inhibition onto the principal neurons, thereby suppressing acquisition of fear memory. Conversely, when GABAergic inhibition is reduced, greater activity-dependent synaptic plasticity is induced in the

LA (Bissiere, Humeau, & Luthi, 2003; Shaban et al., 2006). These results together suggest that disinhibition of the LA principal neurons is an essential factor of fear conditioning.

*Basal Amygdala, relaying information from LA to CeM.* To express fear, CS-US association information has to be delivered from the LA to CeM, which is the output station of the amygdala. However, there has been no direct connection identified between the LA and CeM (Pitkanen, Savander, & LeDoux, 1997; Y. Smith & Pare, 1994)). Instead, the LA and CeM are connected through the CeL (Figure 1.1, line 4 → 5) or BA (Figure 1.1, line 1 → 6) supposedly exerting opposite effects onto CeM; inhibitory control via the CeL and excitatory control via the BA due to differential cell types in each region (GABAergic vs. glutamatergic).

Fear conditioning induces sustained activity in CeM neurons during the CS presentations (Ciocchi et al., 2010; Duvarci, Popa, & Pare, 2011). Moreover, optogenetic activation of CeM neurons elicits freezing responses, whereas inhibition impairs expression of fear responses (Ciocchi et al., 2010). Optogenetics is a biological technique used to control cells that have been genetically modified to respond to light (Deisseroth et al., 2006). To control neural activities, a light-sensitive protein called opsin must be expressed in neurons. More detailed information about optogenetics will be covered in chapter 3. Taken together, the positive correlation between the CeM neuronal activity and the expression of fear suggests that the CeM receives excitatory inputs during fear learning. This indicates that CS information is relayed through the BA. Indeed, BA receives abundant input from the LA (Figure 1.1, line 1) and sends robust excitatory projections to the CeM (Figure 1.1, line 4) (Krettek & Price, 1978; Pare, Smith, & Pare, 1995; Pitkanen et al., 1997; Y. Smith & Pare, 1994).

However, this pathway (LA → BA → CeM) is not the only pathway from the LA that provides CS information onto CeM neurons. This was demonstrated by the fact that pre-training

lesion of the BA does not affect fear learning (Amorapanth, LeDoux, & Nader, 2000; Goosens & Maren, 2001; Nader, Majidishad, Amorapanth, & LeDoux, 2001), but post-training BA lesion abolishes conditioned fear responses (Anglada-Figueroa & Quirk, 2005). These results suggest that in the absence of the BA from the beginning, CS information relayed to CeM bypasses the BA, but with an intact BA, CS information is mainly relayed and partially stored in the BA. Consistent with the lesion studies, fear conditioning induces either CS-evoked phasic responses (Herry et al., 2008) or sustained responses in the BA (Amano, Duvarci, Popa, & Pare, 2011). The existence of sustained activities in the BA resembles the persistent activities of the CeM, which correlates conditioned fear responses.

*Microinhibitory circuit within CeA.* Traditionally, the role of the CeA has been limited to the expression of conditioned responses suggesting its passive role in fear conditioning. However, a newer model of fear conditioning provides ample evidence that CeA is necessary for both acquisition and expression of conditioned fear and that the CeA, in fact, may also be a site of plasticity in fear conditioning (Goosens & Maren, 2003; Samson & Pare, 2005; Wilensky, Schafe, Kristensen, & LeDoux, 2006). Further studies found a functional dissociation between the CeL and CeM suggesting that neural activity of CeL is required for acquisition, whereas CeM drives for expression of conditioned fear responses (Ciocchi et al., 2010).

The connection between the CeL and CeM gives a more complicated picture of the microcircuits within the CeA. As discussed above, CeM neurons show increased activity during the CS after fear conditioning. However, how the CeM becomes excited even with the CeL inhibitory connection needs to be explained. Interestingly, there are two types of neuronal responses to the CS after fear learning: CeL_ON, which shows increased activity during the CS and CeL_OFF, which shows decreased activity during the CS (Ciocchi et al., 2010; Duvarci et

al., 2011). Before fear learning, CeM receives tonic inhibition by CeL_OFF neurons. After fear conditioning, CeL_ON neurons get increase their activity, which then leads to inhibition of the CeL_OFF neurons (Figure 1.1, line 5). Decreased activity of CeL_OFF neurons allows the CS to excite the CeM more readily. Thus, disinhibition is the key factor that allows CeM to respond to the CS (Ciocchi et al., 2010; Haubensak et al., 2010). This functional distinction between CeL_OFF and CeL_ON neurons corresponds to the genetic distinction between neurons expressing protein kinase C-δ (PKC-δ+) and neurons not expressing PKC-δ (PKC-δ–) (Haubensak et al., 2010).

*Innate fear and amygdala.* The term innate fear refers to perceived danger to stimuli which was not associated with threat through previous learning, and it is expressed as a collection of defensive behaviors. Defensive behavior can be expressed to either discrete and present stimuli such as predators, conspecifics, dangerous objects (fear/defense) or ambiguous and intangible stimuli such as predatory odor or perceived dangerous situations (anxiety/defense) (R. J. Blanchard & Blanchard, 1989). Neural circuits processing innate fear cover whole sets of threatening stimuli. The circuit for each stimulus has been identified differently (Silva, Gross, & Graff, 2016). In this section, among the circuits, the roles of the amygdala will be examined, especially where they can be studied in a laboratory setting.

The neural representations of unconditioned stimuli (US), which naturally evokes defensive responses (UR) without learning, have confirmed the role of the amygdala in innate fear. One study conducted a series of experiments showing that an aversive US (footshock) is represented in a different subset of neurons from neurons representing an appetitive US and that these distinct neurons are intermingled within the BLA (Gore et al., 2015). Furthermore, optogenetic stimulation of shock representation neurons elicits fear responses such as decreases

in both heart rate and respiration rate, and increased time being immobile. Consistent with this, optogenetic stimulation of the LA is utilized as a US in fear conditioning because it itself elicits freezing responses (Johansen et al., 2010). These findings suggest that the amygdala not only gains learned fear information by fear conditioning, but also it naturally has neural representations of stimuli that induce innate fear responses.

By implementing ethological aspects into research designs, rats' innate fear of predatory threat can be studied in a laboratory setting. Choi and Kim developed a semi-naturalistic foraging task in which hunger motivated rats forage for food in the presence of a predator-like robot (Choi & Kim, 2010). To date, the main findings regarding neural mechanisms underlying defensive behavior in a risky foraging situation are i) the amygdala bidirectionally regulates risky foraging behavior; reduced and heightened activity of the amygdala increases and decreases a chance of pellet procurement with the robot predator, respectively (Choi & Kim, 2010), ii) the magnitude of hippocampal place cell remapping depends on the distance from the threat source; place fields near the threat are disrupted more than the fields near the safe nest (E. J. Kim et al., 2015), iii) dorsal periaqueductal gray (dPAG) conveys unconditioned stimulus information to the BLA, which causes both innate and learned fear responses (E. J. Kim et al., 2013). Additionally, the PAG, which is thought to generate defensive behaviors, has been commonly considered as a downstream of the amygdala (Depaulis, Keay, & Bandler, 1992; Gray & Magnuson, 1992; Lavond, Kim, & Thompson, 1993). However, Kim et al., 2013 found that fear information is actually delivered from the dPAG to BLA because defensive behavior by the dPAG stimulation was completely abolished with BLA lesion/inactivation.

*Hippocampus, from spatial processing to an extended fear circuit.*

*Hippocampal place cells.* Hippocampal place cells were first found in the rodent hippocampus showing location-specific firing patterns; selective burst firings when an animal visits a particular location in space (R. U. Muller & Kubie, 1987; O'Keefe & Dostrovsky, 1971). A given place cell shows one or a few place fields in a small environment but tends to have more fields in a larger environment (Fenton et al., 2008). Place cells in the hippocampus do not show apparent topography (no correlation between the anatomical location and the location of place fields in the environment), which is a common characteristic found in sensory cortices (O'Keefe, Burgess, Donnett, Jeffery, & Maguire, 1998).

The location-specific property, which takes up a considerable fraction of the cells in the hippocampus (O'Keefe, 1976), is the evidence of a cognitive map (O'Keefe & Nadel, 1987). However, place cells were also shown to process nonspatial information (Hampson, Heyser, & Deadwyler, 1993; E. J. Kim et al., 2015; Lu & Bilkey, 2010; D. M. Smith & Mizumori, 2006; B. J. Young, Fox, & Eichenbaum, 1994). Experience-dependent spatial encoding is the most compelling evidence that place cells are important for not only spatial encoding but also memory (Mizumori, 2008). Next, the roles of spatial encoding and nonspatial encoding of the place cells will be discussed.

*Spatial information in place cells.* Place cells have proven to have the ability to suddenly alter their firing patterns in response to changes in external environments, a phenomenon known as ‘remapping’ (Colgin, Moser, & Moser, 2008). Because of the remapping property, place cells are thought to be involved in space discrimination, which is a fundamental aspect of spatial information processing. The earliest attempt to quantify the ability of place cells to encode environmental changes by remapping was done by Muller and Kubie (R. U. Muller & Kubie, 1987). They tested how place cell firing properties would be affected by changes in the animal’s

environment. A standard environment consisted of a cylinder shape apparatus, a cue card on the inside wall, and no obstacles on the floor. Each of these major features of the environment was changed while the others were kept constant. The results were i) rotating the cue card produced equal rotation on the place field of single cells, but changing the width of the card or removing the card was not effective to draw dramatic changes in place fields, ii) changing the size and the shape of the apparatus resulted in remapping of place fields, iii) bisecting the floor with a barrier abolished place fields, but the effectiveness of barriers was restricted to their vicinity.

There is evidence that the spatial representation by hippocampal place cells includes geometric information (e.g. the distances and directions of features in the environment) as well as nongeometric information. Anderson and Jeffery found that hippocampal place fields were modulated by nongeometric information such as colors and odors (Anderson & Jeffery, 2003). From the results, they proposed a model of remapping, in which the representation of the entire spatial environment would require heterogeneous modulation by geometric and nongeometric information.

*Nonspatial information in place cells.* Hippocampal place cells encode nonspatial information as well. The contemporary view of hippocampal place cells is that place fields are affected by previous experience, which can be referred to as memory (Hill & Best, 1981; Markus, Barnes, McNaughton, Gladden, & Skaggs, 1994; R. U. Muller, Kubie, & Saypoff, 1991; Quirk, Muller, & Kubie, 1990). In addition, there is a subset of place fields that are unchanged following changes in the context. This pattern of responses, called ‘partial reorganization’, is some evidence that hippocampal place fields are not only shaped by environmental changes through visual information but also by nonspatial aspects of information (Lu & Bilkey, 2010; D. M. Smith & Mizumori, 2006).

Examples of nonspatial factors that affect place fields have been examined. One study found that factors modulated by self-motion such as motor efference and proprioception are the primary factors that change place cell firing rates (Lu & Bilkey, 2010). Task demands also affect place fields. When the task was to discriminate two contexts based on reward locations, place cells showed markedly different place fields in the two contexts. (D. M. Smith & Mizumori, 2006). In this study, other than the reward location, spatial information between the two contexts were identical. These results suggest that hippocampal place cells are modulated by nonspatial factors as well.

*Fear conditioning and hippocampus.* The role of the hippocampus in fear conditioning has been widely studied. Even though there has been controversy as to the exact role of the hippocampus during fear conditioning (Gewirtz, McNish, & Davis, 2000), the hippocampus, in general, is thought to be required for processing the contextual information in which fear learning occurs (J. J. Kim & Fanselow, 1992; J. J. Kim, Rison, & Fanselow, 1993; Maren & Fanselow, 1997; Phillips & LeDoux, 1994; Selden, Everitt, Jarrard, & Robbins, 1991; S. L. Young, Bohenek, & Fanselow, 1994). During Pavlovian fear conditioning, contextual representations are incidentally encoded (e.g. by exploring the context before presentation of an aversive stimulus), and these representations are associated with the fear-evoked events. Thus, the subject will show fear responses to that context as well as to a stimulus predicting the occurrence of the aversive stimulus. If the hippocampus is not fully functioning, the context-induced fear responses will be abolished. In one study, when rats underwent bilateral hippocampal electrolytic lesions after fear conditioning where a tone was paired with a footshock, they showed reduced freezing behavior during exposure to the shock-paired context (J. J. Kim & Fanselow, 1992). This result suggests that failures in forming and storing the

contextual representation (i.e., context encoding), which should have been processed by the intact hippocampus, lead to deficits in adaptive fear responses to that context.

Relatively recently, as a result of optogenetic manipulation, hippocampal subfield cornu ammonis field 1 (CA1) was found to be especially important for contextual fear memory (Goshen et al., 2011). During contextual fear conditioning, dorsal CA1 pyramidal neurons were suppressed by optogenetic inhibition, and mice were tested the next day in the absence of light. Mice with dorsal CA1 inhibition during training showed lower contextual freezing than the non-inhibition control group. Apparently, the context information could not be encoded due to the inhibition of CA1 pyramidal neurons and this led to inadequate fear responses.

*Innate fear and hippocampus.* Hippocampal lesions disrupt not only conditioned responses but also unconditioned freezing responses (D. C. Blanchard, Blanchard, Lee, & Fukunaga, 1977; R. J. Blanchard & Blanchard, 1972). Animals without the hippocampus tended to show reduction in fear as well as in aggressive behaviors. Functional inactivation of the hippocampus by tetrodotoxin also disrupted avoidance behaviors (Telensky et al., 2011). In this study, rats had to avoid a moving object or else they received footshocks. However, when the hippocampus was inactivated, rats received significantly more footshocks than the control rats.

Hippocampal place cells are also affected by innate fear (e.g. predatory threat). Utilizing a naturalistic setting using predatory-like robots, rats were placed in an 'approach food-avoidance predator' situation (E. J. Kim et al., 2015). Under this condition, place cells that had exhibited place fields located near the threat (high fear) remapped after encountering the robot. By contrast, place fields inside and nearby the nest (no/low fear) remained stable. Likewise, the theta rhythm (6–10 Hz) in the hippocampus was selectively increased near the threat. On the other hand, the amygdala lesioned rats did not show avoidance behavior to the robot predator nor

remapping of place fields. These findings suggest a possible scaling relationship between the magnitude of fear, which varies in a relation to the nest-foraging distance and the stability of hippocampal place fields.

*Cooperative functions of the amygdala and hippocampus in learned fear.*

Anatomical studies have shown that reciprocal connections between the amygdala and hippocampus provide strong evidence to their functional relevance (Pitkanen, Pikkarainen, Nurminen, & Ylinen, 2000; Tannenholz, Jimenez, & Kheirbek, 2014). Anatomically, the temporal end of CA1 has substantial reciprocal connections with the amygdala, with the BA in particular having most extensive interconnections with the hippocampus (Pitkanen et al., 2000). The connection from the hippocampus to the amygdala including direct and indirect projections seems to be necessary for fear renewal after extinction, which is considered as a form of context-specific learning (Orsini, Kim, Knapska, & Maren, 2011). Second, the hippocampus has also been found to be integral for extinction learning (Corcoran & Maren, 2001). Orsini and his colleagues disconnected the hippocampus and the amygdala (direct connection) or the hippocampus and the mPFC (indirect connection to the amygdala) with asymmetric unilateral lesions in each structure. The lesions were conducted after extinction learning, and the fear renewal was assessed. When rats were placed in the different context as the extinction context, they showed higher levels of fear responses (i.e., fear renewal). However, rats with disconnection of the hippocampus-amygdala or the hippocampus-mPFC pathways exhibited significantly lower freezing levels compared to those of the control groups (no lesion or ipsilateral lesions). These results suggest that a direct connection (hippocampus-amygdala) and indirect connection

(hippocampus-mPFC-amygdala) are both important for contextual regulation of fear after extinction.

Interaction between the hippocampus and the amygdala in regard to fear seems to be through theta synchronization. One study was designed to characterize patterns of neural activity between those two areas related to fear memory retrieval. This was achieved by simultaneous recording of neuronal activity in the LA and the CA1 in freely behaving fear-conditioned mice. In the results, increased synchronized activity at theta frequencies (4 to 8 Hz) were found when mice showed freezing behaviors when exposed to the conditioned context not to a neutral context (Seidenbecher, Laxmi, Stork, & Pape, 2003). Furthermore, theta inputs from the hippocampus to the amygdala gate heterosynaptic plasticity, eventually modulating fear responses via feedforward inhibition (FFI) (Bazelot et al., 2015). This FFI arises from interneurons in the amygdala, which is reduced by repeated theta frequency firing of ventral CA1 hippocampal neurons. This depression of FFI enables the induction of LTP at the LA-BA synapses which causes stronger output from the BA. Ultimately this projection will lead to fear responses. These results suggest that the amygdala and hippocampus actively communicate during fear learning to promote appropriate behavioral responses.

*Importance of the ethological approach in studying fear.*

We have discussed in the previous sections that contemporary fear research largely focuses on acquired fear responses using Pavlovian fear conditioning. Thus, the current neurobiological models of fear provide only a partial explanation of the brain's fear system. These models oversimplify molecular, genetic, and behavioral factors underlying an organism's fear system because animals in this model are tested in small experimental chambers and simply

receive tone-footshock pairings. To better understand the brain mechanisms of fear, real-world threat situations should be simulated in a laboratory setting. Thus, in this section, how fear researchers have employed stimuli that evoke innate fear in a laboratory setting will be introduced, and the importance of adopting an ethological approach to study fear will be examined.

Factors or stimuli that readily evoke fear have been identified. For example, 'looming stimuli', which mimic an advancing predator, elicits defensive behaviors in various species (Sun & Frost, 1998; Yilmaz & Meister, 2013). Recently, Yilmaz and Meister showed that overhead visual display of a rapidly expanding dark disc simulating a shadow of an approaching aerial predator triggers immediate flight and/or freezing behavior in mice (Yilmaz & Meister, 2013). Rapid behavioral responses to the looming stimuli can be supported by the fact that there are 'OFF' retinal ganglion cells that are selectively responsive to stimuli approaching or increasing in size but not to stimuli shrinking in size or laterally moving (Munch et al., 2009). Another study also found that several types of motion-sensitive retinal ganglion cells directly project to the superior colliculus (Huberman et al., 2009), and that neurons in the medial intermediate layers of the superior colliculus, which project to the BLA via the lateral posterior thalamus, have been implicated to be necessary for the defensive responses to looming stimuli (Wei et al., 2015). These anatomical evidence suggest that rapid fear responses to imminent threats can be generated without the need for cortical processing.

Predator odor has also been reported to evoke innate fear responses in mice and rats. When animals detect predator odors such as cat fur/saliva (Papes, Logan, & Stowers, 2010) or fox urine/feces (Ferrero et al., 2011; Rosen, Asok, & Chakraborty, 2015), they exhibit defensive behaviors including avoidance, freezing, and risk assessment, as well as fear-related autonomic

and endocrine changes. Several brain mechanisms implicated in the processing of predator odor have been identified. For instance, the main (MOS) and accessory olfactory systems (AOS) both detect predator odors, with specific receptors in the MOS or AOS sensing different types of predator odors, respectively. Other brain areas, such as the dPAG, paraventricular nucleus (PVN) of the hypothalamus, ventral hippocampus, bed nucleus of the stria terminalis and the amygdala also appear to be broadly involved in predator odor processing (Takahashi, 2014). Understanding circuits that process different types of predator odors will provide significant insight as to how distinct predator odors initiate innate fear responses.

Another approach to studying innate fear is to engender predator-prey interactions in the laboratory setting. During predator-prey interactions, rats naturally display diverse, intricate behaviors (R. J. Blanchard, Blanchard, Rodgers, & Weiss, 1990; McNaughton & Corr, 2004). Typically, predator-prey interactions are studied in tasks incorporating an approach-avoid conflict (Choi & Kim, 2010; Telensky et al., 2009; Wilson et al., 2015) . Due to its complexity, however, this approach has been neglected in fear research, even though it is requisite for the brain to deal with this conflicted situation in a predatory threat. Fortunately, there have been recent efforts to resurrect this ethological approach to study fear in the laboratory setting.

One study by Telensky et al., developed an enemy avoidance task where rats avoided a moving object, which delivered  cutaneous shocks whenever rats came near the object (Telensky et al., 2011; Telensky et al., 2009). Their results indicate that the hippocampus is necessary for actively updating spatial representation (Choi & Kim, 2010)ns to avoid threats, a result that could not be found by using simple fe(Amir, Lee, Headley, Herzallah, & Pare, 2015)ar conditioning. Another study created a predator-prey interaction using a robotically controlled laser beam that chased the animals (Wilson et al., 2015). The software used to track animals'

locations can provide systematic understandings of animals' avoidance behavior. Finally, the paradigm that was developed by Choi and Kim introduced an 'approach food-avoid predator' conflict in a foraging situation (Choi & Kim, 2010) and been utilized in several of studies (Amir, Headley, Lee, Haufler, & Pare, 2018; Amir et al., 2015; Choi & Kim, 2010; E. J. Kim et al., 2013; E. J. Kim et al., 2018; E. J. Kim et al., 2015). This scenario is realistic and ubiquitous in nature, and that the brain's fear system has likely evolved to handle such scenarios. The studies presented in this dissertation utilized this paradigm to understand the roles of the amygdala and hippocampus in innate fear (as apposite to their roles in learned fear, which was covered in the previous section). We suspect that their cooperative functions cannot be fully explained by fear conditioning and may show different pictures in a naturalistic setting. Therefore, results from studies using an ethological approach will provide a more comprehensive understanding of an organism's fear system (Pellman & Kim, 2016).

*In this dissertation.*

The studies presented in this dissertation examine how the amygdala and hippocampus interact in innate fear situations using the aforementioned risky foraging task (Choi & Kim, 2010). In chapter 2, simultaneous recording was used to reveal how the BA of the amygdala and dHPC of the hippocampus process a risky foraging situation where animals confront a robot predator. From each region, single neuron and local field potentials (LFPs) responses to the risky situation were assessed. Subsequently, spike synchrony during the predator confrontation was examined to see how the BA and dHPC work together to guide an optimal behavior. In chapter 3, we tested whether stimulation of the neurons in the BA was sufficient to generate defensive behaviors in the foraging task. Selective activation of neurons was established by optogenetic

manipulation. Technical validity was confirmed by optrode recordings, which showed that the light successfully evoked neuronal firing in the BA. Next, in chapter 4, we tested the necessity and sufficiency of the amygdala on the stability of place cells. For the experiments establishing necessity of amygdala input to dHPC, electrolytic lesions were used to exclude the function of the amygdala for defensive behaviors and stability of place cells. Sufficiency was examined by the optogenetic stimulation of the BA, which showed defensive behaviors even without the explicit threat. The effect of optogenetic stimulation of BA on the stability of place cells was also investigated.

# Chapter 2. ROLES OF THE AMYGDALA AND HIPPOCAMPUS IN RISKY FORAGING BEHAVIORS

## 2.1 INTRODUCTION

Each role of the amygdala and the hippocampus in fear research has been widely studied as described in chapter 1. However, relatively a small number of studies have suggested the importance of their cooperativity during fear situations. Additionally, studies that investigated the interaction between the amygdala and hippocampus mostly focused on the ventral hippocampus (vHPC), not dHPC since vHPC has substantial interconnections with the amygdala (Allsop, Vander Weele, Wichmann, & Tye, 2014; Beyeler et al., 2018; Maren & Fanselow, 1995; Pitkanen et al., 2000; Richardson, Strange, & Dolan, 2004). These extensive connections are thought to be important for the expression of anxiety-related behaviors (Bannerman et al., 2003; Fanselow & Dong, 2010; Kheirbek et al., 2013; Kjelstrup et al., 2002). One study suggested that the selective manipulation of the projection from the amygdala to vHPC modulates anxiety-related behaviors such that rats spend more time in the closed arm in the elevated plus maze and stay longer in the periphery of the open field when the projections are excited (Felix-Ortiz et al., 2013). However, the vHPC does not seem to be crucial for spatial learning even though it also has place cells (Bannerman et al., 2003; Jung, Wiener, & McNaughton, 1994; Kheirbek et al., 2013; Poucet, Thinus-Blanc, & Muller, 1994; Royer, Sirota, Patel, & Buzsaki, 2010). These functional dissociations provide a rationale for why we focused on the function of the dHPC and not vHPC, along with the function of the amygdala. The aim of the current study is not simply to focus on how defensive behaviors are expressed, but more on how animals build a cognitive map to guide their defensive behaviors when confronted with danger. Additionally, one study suggests that

dHPC is necessary to avoid a moving object (Telensky et al., 2011), which also supports the role of the hippocampus on dynamic cognitive processes in a fearful situation.

As mentioned in chapter 1, the amygdala is a collection of distinct nuclei. Based on the directionality of the primary information flow (see chapter 1), the LA does not have a direct connection with the CeM, which is important for eliciting freezing responses (Ciocchi et al., 2010; Duvarci et al., 2011). Rather, the CS information is relayed through the CeL to CeM or through the BA to CeM. Evidence that the BA is not a passive relay center for CS information but actively extends the CS information to other downstream brain regions include: i) BA neurons showed increased CS responses after fear conditioning (Amano et al., 2011; Herry et al., 2008), ii) BA inactivation reduced expressions of conditioned fear (Amano et al., 2011), iii) most BA neurons showed sustained activities during the entire CS (Amano et al., 2011), iv) glutamatergic inputs from the BA are crucial in learned fear (Duvarci & Pare, 2014).

Combining the roles of the BA in learned fear and innate fear toward predatory threat, and assuming the underlying framework between the two roles may be similar due to the anatomical connections within the amygdala, we decided to target the BA and not the LA

To support the importance of the BA in innate fear, there have been studies of the function of the BA in risky foraging situations (Amir et al., 2018; Amir et al., 2015). The findings from these studies showed that the majority of neurons in the BA encoded the speed of behavioral outputs (Amir et al., 2015). However, high gamma rhythm (75-95 Hz) from the local field potentials strongly entrained BA neuronal firing and was pronounced with predatory threats (high-vigilance state) (Amir et al., 2018). Interestingly, high gamma and theta coupling in the BLA is enhanced to the fear conditioned tone (Stujenske, Likhtik, Topiwala, & Gordon, 2014). Combining

the role of the BA in learned fear and innate fear, we agreed to target the BA not the LA in the amygdala.

Using the same semi-naturalistic foraging task, we implicated the amygdala (Choi & Kim, 2010), the LA and prelimbic area of the medial prefrontal cortex (PL) (E. J. Kim et al., 2018), the amygdala and PAG (E. J. Kim et al., 2013), and the dHPC in predatory interaction (E. J. Kim et al., 2015). From these findings, we hypothesize that the amygdala plays a central role of eliciting innate fear (amygdala-PAG) and making optimal subsequent decisions (amygdala-PL). The function of the hippocampus itself during predatory interactions has been shown to provide spatial representations as a function of threat distance (E. J. Kim et al., 2015). However, most importantly, we have not studied the underlying mechanisms regarding the functional connection between the dorsal hippocampus and the amygdala, despite the existence of a direct anatomical connection between them (Rei et al., 2015). Thus, we posit that the BA-dHPC pathway provides the safety-danger boundary information in a risky foraging situation.

In this chapter, the roles of the amygdala and the hippocampus in risky foraging situations were investigated using simultaneous recording. Neural data were analyzed to reveal how these regions encoded risky foraging environments at the single unit and a population level via LFPs. How predatory threat altered spike synchrony between the two regions was also examined. These findings suggest that the amygdala and the hippocampus encode threatening and non-threatening contexts differently and work together to produce a boundary of safety-danger, which leads to an appropriate behavioral output during a risky foraging situation.

## 2.2 Materials and Methods

*Subjects.*

Male Long-Evans rats (initial weight range of 325-350 g) were individually housed in a climate-controlled vivarium (accredited by the Association for Assessment and Accreditation of Laboratory Animal Care) and maintained on a reversed 12-h light/dark cycle (lights on at 7 PM). Rats were on a standard food-deprivation schedule with free access to water to gradually reach their 85% of normal weights. All experiments were performed during the dark phase of the cycle in strict compliance with the University of Washington Institutional Animal Care and Use Committee guidelines.

*Surgery.*

Under anesthesia (94 mg/kg ketamine and 6 mg/kg xylazine, intraperitoneally), four rats were mounted in a stereotaxic instrument (Kopf) and implanted with a microdrive of tetrode bundles (formvar-insulated nichrome wires, 14 μm diameter; Kanthal) into the right dHPC (coordinates: 4.0 mm posterior, 2.0 mm lateral from bregma; 1.5 mm ventral from dura) and the right BA (coordinates: 2.8 mm posterior, 5.0 mm lateral from bregma; 6.5 mm ventral from dura, Figure 2.1A and B). Three tetrodes per region were implanted for the two rats, and six tetrodes per region were implanted for the other two rats. The microdrive was fixed by dental cement with anchoring

*Behavioral paradigms.*

Rats maintained their body weights at ~ 85% of normal weight throughout the sessions. The experiment was conducted in a specialized foraging apparatus (E. J. Kim et al., 2018; E. J. Kim et al., 2015). The composition of sessions for the experiment is represented in Figure 2.1C.

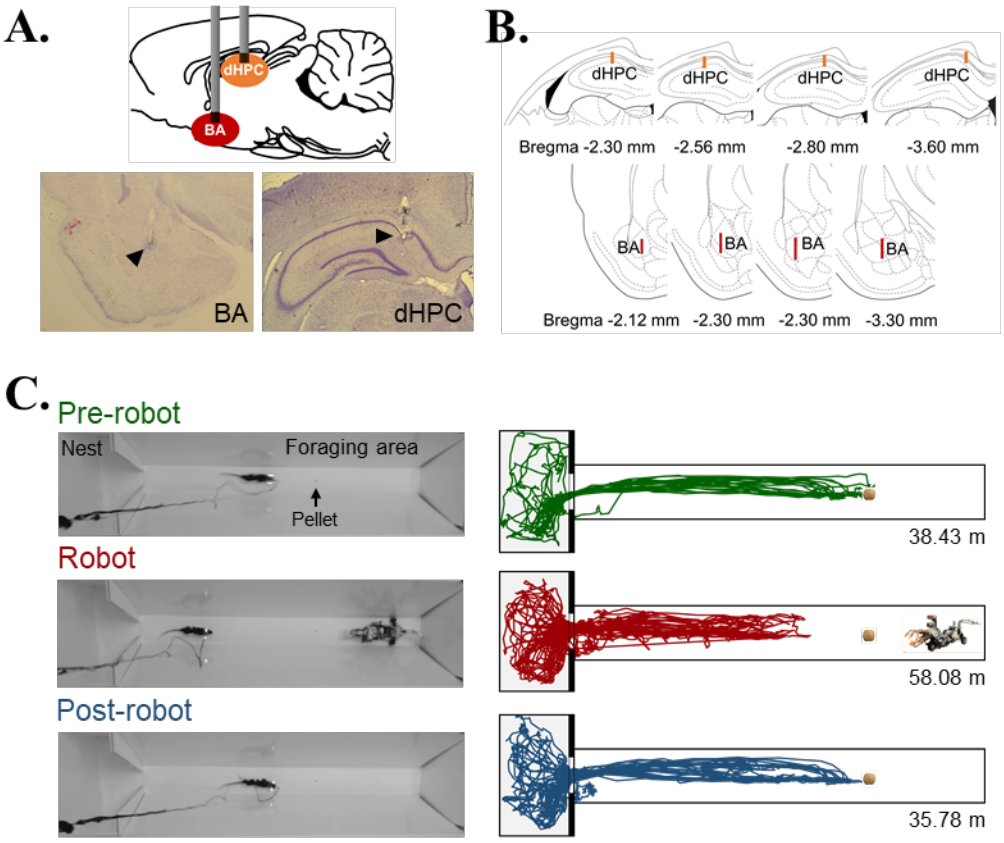


Figure 2.1. Simultaneous recording from the BA and the dHPC in risky foraging situations. **(A)** Schematic image of simultaneous recording (top) and photomicrographs of tetrode tips in the BA and (arrowhead, bottom left) the dHPC (arrowhead, bottom right). **(B)** Histological reconstructions of the recording sites in the dHPC (top) and BA (bottom). Bars indicate the trajectory of the recording sites. **(C)** Photographs of the foraging apparatus during the three sessions (left column) and representative trajectories of a rat during each session (right column). The number below each apparatus indicates the total distance traveled from the representative trajectory data.

*Habituation*. Rats were placed in the nest for 30 min/day for 2 consecutive days with twenty food pellets (0.5 g, F0171, Bio-Serv) to acclimate to the nest area and the experimental room.

*Baseline foraging*. After two minutes in the nest, the gateway to the foraging area opened, and the rat was allowed to explore and procure a food pellet placed at variable distances (25 cm, 50 cm, 75 cm, 100 cm, and 125 cm from the nest). After the rat took the pellet back into the nest, the gateway closed. When the rat learned to procure a pellet from the longest distance, the pellet distance was fixed, and unit screening started. Rats underwent baseline foraging until unit responses were detected.

*Robot testing.* Units from the BA and the dHPC were recorded throughout the three sessions; pre-robot, robot, and post-robot. During the pre-robot session, 8-10 trials of foraging with a pellet placed at 125 cm from the nest were conducted to collect baseline unit activities. After the pre-robot session, rats underwent the robot session with a robot predator (Mindstorms robotic kit, LEGO Systems) placed at the end of the foraging area (Choi & Kim, 2010). After the gateway opened, each time the rat approached the vicinity of the pellet, the robot surged 23 cm toward the pellet, snapped its jaws once, and returned to its original position. Rats were permitted at least 10 attempts to procure the pellet. If the rats made an attempt again within 10 s following the previous robot activation, the second attempt was excluded from the analyses to limit units' responsiveness to the robot. Once the rats finished the robot session, another 8-10 trials of foraging without the robot were conducted to collect post manipulation unit activities (post-robot session).

*Behavioral data acquisition and analyses.*

The ANY-maze video tracking system (Stoelting Co.), with an HD webcam (C920, Logitech) affixed over the apparatus was used to capture video images and automatically track the rats' movements (30 frames/s) from both nest and foraging areas. ANY-maze was connected to

the recording system (Neuralynx) and provided the rats' tracking information. It also provided locomotor data including distance traveled, speed, and the number of entries to specified zones.

*Electrophysiological data acquisition and analyses.*

The impedance of electrode tips was matched to 100-300 kΩ measured at 1 kHz through gold plating. After the postoperative recovery period, electrodes were gradually advanced (≤ 160 μm per day) until they reached to the target regions. Unit isolation and cluster cutting procedures have been described before (J. J. Kim et al., 2007). Briefly, unit signals were amplified (× 10,000), filtered (600 Hz to 6 kHz), and digitized (32 kHz) by using the Cheetah data acquisition system (Neuralynx). Unit isolation was performed by using an automatic spike-sorting program (SpikeSort 3D; Neuralynx) and additional manual cutting as previous studies (E. J. Kim et al., 2018; E. J. Kim et al., 2015). Raster plots and peristimulus time histograms were generated by NeuroExplorer (Nex Technologies).

*Classification of BA units.* BA units were classified as putative pyramidal cells and interneurons based on the average spike with and the firing rate of each cell (Figure 2.2A) [Hierarchical unsupervised cluster (E. J. Kim et al., 2018)]. The majority of the cells recorded from the BA were pyramidal cells (n = 247, 96.1%). The response patterns of pyramidal neurons and interneurons were similar, so both cell types were included for the analyses.

All units' activities were binned at 0.5 s and aligned by the events of pellet acquirements (pre- and post-robot sessions) or the robot activations (robot session) by using NeuroExplorer (version 5.118, Nex Technologies) (Figure 2.2B). Approach Time Zone (ATZ) is defined as the three 0.5 s bins before the pellet procurements or the robot activations (E. J. Kim et al., 2018). All unit activities were normalized to 3.5 s before the ATZ period (-5 s to -1.5 s of the pellet

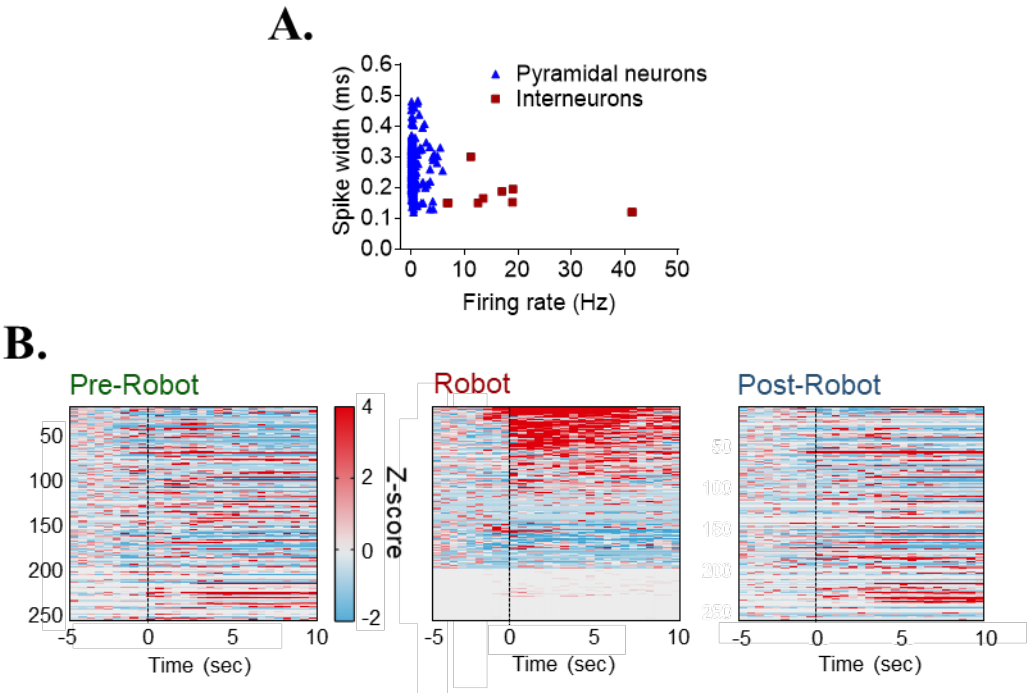


Figure 2.2. Single unit activities in the BA during the encounter of the robot predator. **(A)** Units recorded from the BA were classified as putative pyramidal neurons (blue triangles) and putative interneurons (red square). **(B)** Z-scored BA unit activities during each session. Each cell is represented in the same row of each session. Unit activities were aligned by the activities during the robot session.

.

acquirements or robot activations). Units were classified as Pellet cells or Robot cells when at least one of the z-scores was greater than 3 during the ATZ or 3 s after the events (total of 4.5 s period). If a cell showed significant changes ($Z > 3$) during the ATZ, it is classified as an approach cell. If a cell showed significant changes ($Z > 3$) after the event, it is classified as a triggered cell. Nest-in cells showed $Z > 3$ presumably when the rats went back to the nest. Percentages of each cell type are shown in Table 2.1.

*Place cell analyses*. Criteria that was used for the place cell analyses has been described in the previous study (E. J. Kim et al., 2015). Hippocampal place cells that showed i) stable, well-discriminated complex spike waveforms, ii) a refractory period of at least 1 ms, iii) peak firing > 2Hz in any session, iv) spatial information > 1.0 bit per/s in any session were included. Firing rate maps consisted of square pixel bins measuring 3 cm/side. The threshold of the visit was 0.05 s and undersampled pixel bins were excluded from the analyses. The firing rate in each bin was calculated as the number of spikes divided by the time spent in that bin. Rate maps were smoothed by a single iteration of convolution with Gaussian kernel spanning a 3 × 3 pixel region. The peak firing rate was identified as the rate of the highest pixel bin in the smoothed rate map. The field size was the summed extent (in $cm^2$) of all continuous regions of pixel bins whose firing rate exceeded the mean rate by at least one standard deviation. Contour plots were generated using NeuroExplorer.

Based on the location of place fields during the pre-robot session, cells were classified into three different types; nest cells (cells fired maximally in the nest), proximal cells (near the nest), and distal cells (distant from the nest, close to the threat). A pixel-by-pixel spatial correlation analyses by a customized R program (R Foundation for Statistical Computing) calculated the similarity of the place maps between three different sessions; pre- vs. robot, robot vs. post-, and

pre- vs. post- sessions for each place cell. R values from a Fisher Z' transformation were compared across sessions by cell types. The customized R program also gives us the information of the average firing rates, maximal firing rates, peak distance, place field size, and spatial information for each cell (E. J. Kim et al., 2015).

*Cross-correlation analyses.* Cross-correlograms (CCs) of simultaneously recorded BA and dHPC units were generated by NeuroExplorer with BA cells as references. The procedure of the analyses was identical as the previous study except that the current study includes 5 s of each time window (E. J. Kim et al., 2018). The shift predictors generated by applying 100 random trial shuffles were subtracted from the raw CCs. CCs were calculated at four 5-s-windows; pre-retrieval, post-retrieval, pre-surge, and post-surge. During each window, cell pairs showing significant spike synchrony were examined. To be significant, following criteria should be met: i) the average firing rate is more than 0.1 Hz in both BA and dHPC units, ii) CCs shows significant peaks, which exceed z-score of 3, iii) the peak z-score is fallen into a -100 ms and +100 ms time window around the BA spikes.

*Local field potential analyses.* LFP analyses were conducted as the study by Amir et. al., 2018 (Amir et al., 2018) except for those that we did not normalize the time. LFP signals were processed with the following steps: i) signals were down-sampled to 32.5Hz, ii) one LFP channel from one tetrode was extracted based on the signal quality, iii) using the Chronux spectral analysis MATLAB toolkit, spectrograms were calculated for all foraging trials (from three sessions) on each day and for each LFP channel, iv) the average and standard deviation of the spectrogram for each day and each LFP channel was calculated, v) each trial was normalized by the average and standard deviation from above, vi) the average of all normalized spectrogram across LFP channels was generated, and lastly, vii) a grand average of all trials was computed. Events such as pellet

procurements, robot activations, or outing from the nest were used to see event-evoked changes in the LFPs.

In addition, power spectral densities (PSD) were calculated by NeuroExplorer. For the calculations, the number of frequency value was 655,536 with no pre-processing for each window. Single taper with Hann windowing function was used and a percentage of total PSD was displayed for each analysis.

*Histology.*

After the completion of the experiment, electrolytic currents (10 μA, 10 s) were applied to tips of each tetrode to confirm the placement of the electrodes. Rats were overdosed with Beuthanasia and perfused intracardially with 0.9% saline and 10% formalin. Extracted brains were stored in 10% formalin at 4°C overnight followed by a 30% sucrose solution until they sank. Transverse sections (50 μm) were washed with phosphate-buffered saline (PBS) and mounted onto slides with a gelatin solution. Staining with Cresyl violet and Prussian blue confirmed the location of tips.

*Statistical analyses.*

Statistical significance was determined with repeated measures ANOVA, two-way ANOVA, linear regression, Pearson's *r*, unpaired *t* test, or Friedman test using Bonferroni *post hoc* or Dunn's multiple comparisons tests (SPSS or Prism). The detailed information is described in the following section, Results. Kolmogorov-Smirnov normality test was also used to determine the application of parametric or nonparametric tests. Statistical significance was set at $P < 0.05$. Graphs were made using GraphPad Prism (version 8).

## 2.3 RESULTS

*Changes in foraging behavior during the encounter of the robot predator.*

A fearful situation with presence of a predator increased foraging time compared to a safe situation without a predator. To address this, we measured the outbound foraging time. The definition of outbound foraging is travel time from the nest to a pellet (pre- and post-robot sessions) or travel time from the nest to until a robot is triggered (robot session). The outbound foraging time during the robot session (5.532 ± 0.5740 s) increased significantly compared to the pre-robot (2.727 ± 0.2869 s) and post-robot (5.532 ± 0.5740 s) sessions (repeated measures ANOVA, $F_{2,62}$ = 27.21, $P < 0.001$ using Bonferroni *post hoc* test; Figure 2.3A). Representative trajectories during each session showed that the rats traveled more distance during the robot session but still could not procure the pellet because of the robot predator (Figure 2.1C, right). In addition, rats traveled significantly more distance when the robot was present (repeated measures ANOVA, $F_{2,34}$ = 15.11, $P < 0.001$ using Bonferroni *post hoc* test; Figure 2.3B) with a higher speed (repeated measures ANOVA, $F_{2,34}$ = 13.43, $P < 0.001$ using Bonferroni *post hoc* test; Figure 2.3C) compared to pre- and post-robot sessions. Rats took longer to finish the robot session compared to the pre- and post-robot sessions (repeated measures ANOVA, $F_{2,34}$ = 13.32, $P < 0.001$ using Bonferroni *post hoc* test; Figure 2.3D). Without the robot predator, rats spent most of the time in the nest to consume the food (pre-robot, 85.4 ± 1.2%; post-robot, 85.9 ± 1.2% of the total session time) and spent very little time in the foraging area since they succeeded in food obtainment. During the robot session, however, rats tried to procure the food while staying in the foraging area but still proximal to the nest (foraging area zone 1, 69.2 ± 2.2%). The chance of getting closer to the pellet was significantly lower due to the robot; rats barely reached the pellet (pre-robot, 3.6 ± 0.4% of the total session time; robot, 1.0 ± 0.2%; post-robot, 3.2 ± 0.3%; two-way ANOVA, main effect of session: $F_{2,51}$ =

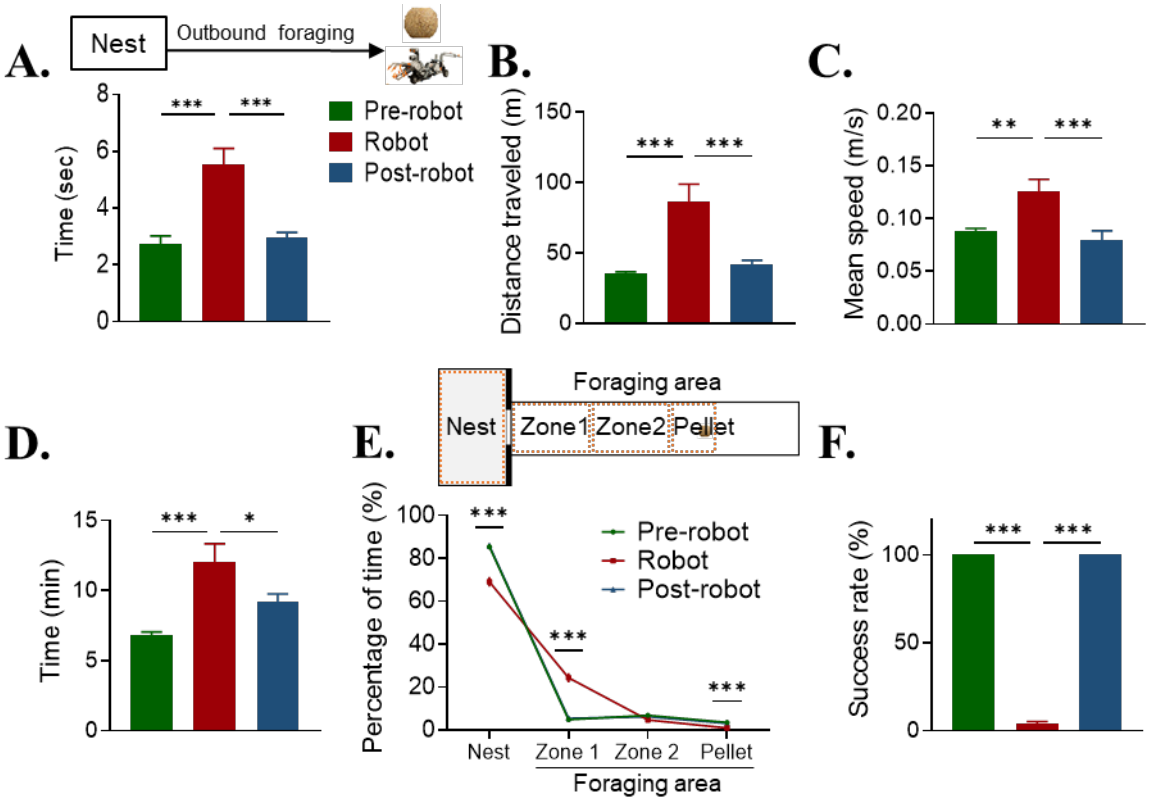


Figure 2.3. The difference in foraging behaviors with and without the robot predator.
**(A)** Time spent in outbound foraging during pre-robot, robot, and post-robot sessions. **(B)** Distance traveled during each session. **(C)** The mean speed during each session. **(D)** Time spent to finish each session. **(E)** Percentage of time spent in the nest and foraging area (zone 1, zone 2, and pellet zone) during each session. **(F)** The success rate of pellet acquirement during each session. Data are presented as mean ± s.e.m. * $P < 0.05$; ** $P < 0.01$; *** $P < 0.001$.

52.11, $P < 0.0001$; nest: pre and post > robot, $P < 0.0001$; zone1: pre and post < robot, $P < 0.0001$; pellet: pre and post > robot, $P < 0.0001$; Figure 2.3E). The success rate of procurement was significantly lower in the robot session than pre- and post-robot sessions (Figure 2.3F).

*BA unit activities during the encounter of the robot predator.*

Single unit activities from the BA were recorded during the three sessions that rats performed in the foraging task. Since we tracked each neuron throughout the sessions, neuronal responses during each session can be compared directly.

A total of 258 neurons were recorded and they were classified based on their responses to the pellet or the robot (Table 2.1). Among all neurons, there was a subset of neurons that were excited to the robot (Robot cells including robot-excited and pellet-inhibited, n = 54, 20.9%; Figure 2.4E). These cells can be also divided into two types; whether they showed activities before the robot activation (robot-approach, n = 17, 6.6%; Figure 2.4A) or after the robot activation (robot-triggered, n = 37, 14.3%). Other than Robot-excited cells, 31 neurons showed Pellet-excited responses (Pellet cells, 12%; Figure 2.4C) and 20 neurons showed excitation to both (7.8%). There was one more excitation category, which showed excitation when the rats went into the nest after procuring the pellet and/or after fleeing from the robot (Nest-in cells, n = 21, 8.2%; Figure 2.4D). Cells not only showed excitation, but also showed inhibition to the robot (n =2, 0.8%), to the pellet (n = 6, 2.3%), or to both (n = 2, 0.8%). Lastly, there were 122 neurons that had no response (47.3%).

Robot-excited neurons showed sustained activities after the robot activation during the robot session (two-way ANOVA using Bonferroni *post hoc* tests, session: $F_{2,1590} = 26.95$, $P <$

Table 2.1. Percentage of BA cell types during pre-robot and robot session

| Cell type | Response type | % | Appr. | Trigg. |
|---|---|---|---|---|
| **Robot cell** | | | | |
| | Excitation | 18.6 | 5.8 (6.6) | 12.8 (14.3) |
| | Inhibition | 0.8 | 0.4 | 0.4 |
| **Pellet cell** | | | | |
| | Excitation | 12.0 | 4.3 | 7.8 |
| | Inhibition | 2.3 | 1.6 | 0.4 |
| **Both** | (pellet + robot) | | | |
| | Excitation + Excitation | 7.8 | | |
| | Inhibition + Inhibition | 0.8 | | |
| | Inhibition + Excitation | 2.3 | | |
| **Nest-in** | (after procuring the pellet + after fleeing from the robot) | | | |
| | Excitation + Excitation | 0.8 | | |
| | Excitation after procuring the pellet | 6.6 | | |
| | Excitation after fleeing from the robot | 0.8 | | |
| **No response** | | | | |
| | | 47.3 | | |
| **Total** | | 100 | | |

| | |
|---|---|
| Same responses between the pre-robot and robot sessions | 9.3 |
| Different responses between the pre-robot and robot sessions | 43.4 |
| Non-responsive during the pre-robot and robot sessions | 47.3 |
| Total | 100 |

A total of 258 units were recorded. The bottom table indicates the percentage of cells showing the same, different or no response between the pre-robot and the robot sessions. Appr. = approach cells, Trigg. = triggered cells.

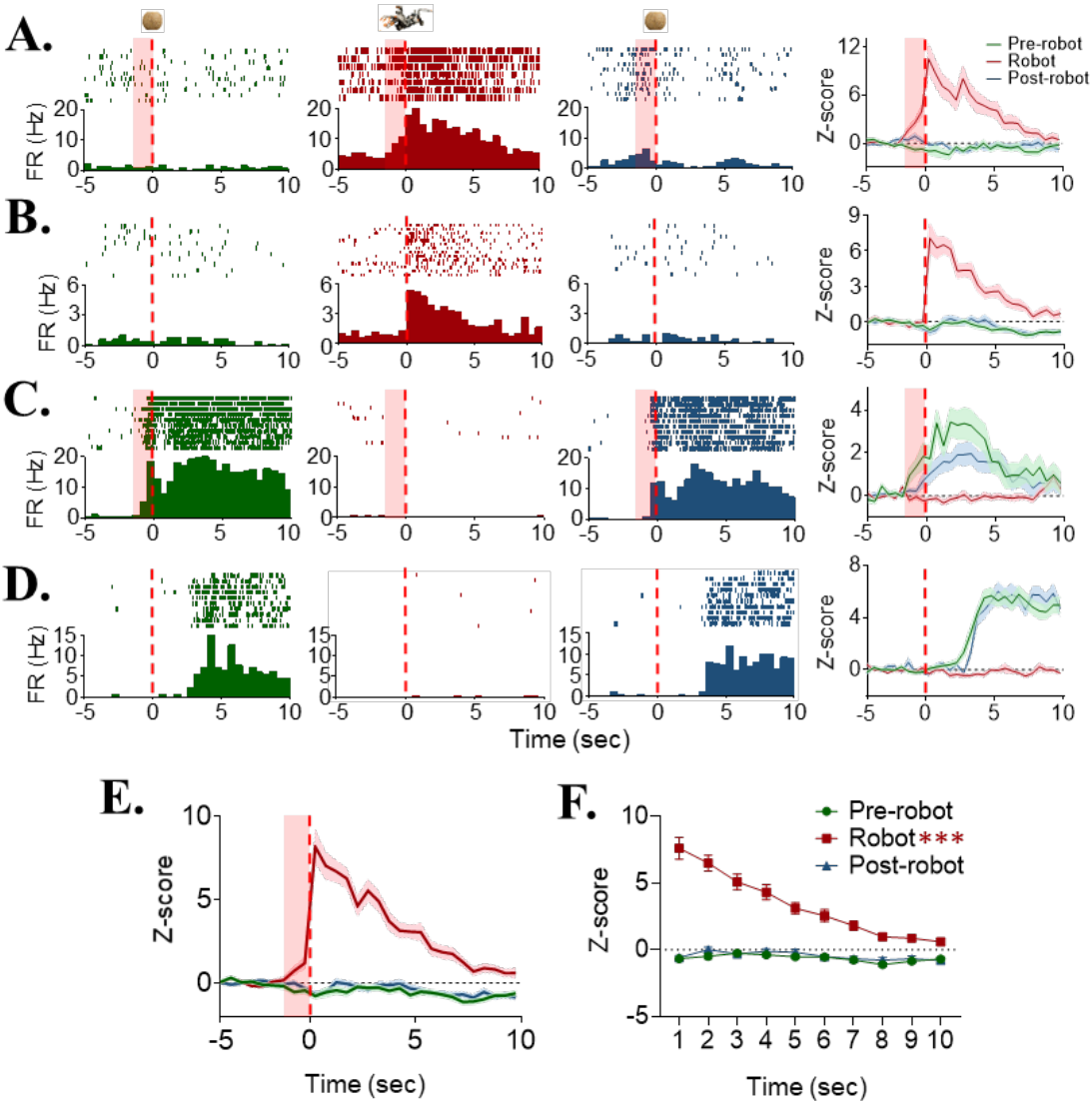


Figure 2.4. Examples and population activities of each cell type in the BA.
**(A)** An example unit that showed significant excitation before the robot was activated and population activity of the same cell type. Raster plots and peri event histograms of a representative robot cell during each session are shown (the first three columns). The last column illustrates the population activity of all robot cells. **(B)** An example unit that showed significant excitation after the robot was activated and a population activity of the same cell type. **(C)** An example unit that responded to the pellet and population activity of the same cell type (excitation, n = 31, 12%). **(D)** An example unit that showed increased responses after the rat went into the nest during the pre-robot session and population activity of the same cell type (n = 17, 6.6%). **(E)** The average z-scored firing rates for all robot-excited cells. Robot-excited and pellet-inhibited cells were also included. **(F)** Comparison of z-scored activities after the pellet acquirement and robot activation. t = 0, pellet acquirements for the pre- and post-robot sessions, robot activations for the robot session. Red shaded area indicates the ATZ. The dark lines represent the mean with the shaded band representing s.e.m. Data are presented as mean ± s.e.m. *** $P < 0.001$.

0.0001; Figure 2.4F). These activities were significant up to 10 s compared to pre- and post-robot sessions (pre vs. robot at 10 s, $P = 0.0101$; post vs. robot at 10 s, $P = 0.0045$).

*BA LFP activities during the encounter of the robot predator.*

We next examined local field potentials (LFPs) from the BA during the foraging behaviors. Changes in event-evoked LFPs were evaluated from spectrograms of z-scored power in different frequency bands (theta, 6-10 Hz; low-gamma, 35-55 Hz; mid-gamma, 55-75 Hz; high-gamma, 75-95 Hz) (Amir et al., 2018). Figure 2.5A shows averaged LFP changes from four rats and all trials (pre-robot, 829 trials; robot, 899 trials; post-robot, 820 trials) when the time zero point was set to pellet acquirements for the pre- and post-robot sessions and robot activations for the robot session. From the spectrograms, increased z-scored power of all four frequency bands was found near the time point of attacking (jaw snapping of the robot predator) in the robot session. To quantify the increased power, the z-scored power for each frequency bands was averaged, but only 3 seconds after pellet acquirements or robot activations were included (Figure 2.5B). Robot session had significantly higher z-scored power of theta, low-gamma, mid-gamma, and high-gamma than pre- and post-robot sessions (two-way ANOVA using Bonferroni *post hoc* tests, session: $F_{2,972} = 551.1$, $P < 0.001$; session × frequency: $F_{6,972} = 23.20$, $P < 0.001$; Figure 2.5B). The elevated power in theta and gamma during this period was not simply due to running speed because the mean running speed was higher in the pre- and post-robot sessions whereas the mean z-score of theta and gamma were higher in the robot session (theta: two-way ANOVA; session × theta z-score: $F_{2,702} = 26.28$, $P < 0.0001$; gamma: two-way ANOVA, session × gamma z-score: $F_{2,702} = 28.18$, $P < 0.0001$; Figure 2.5C). Altogether, these

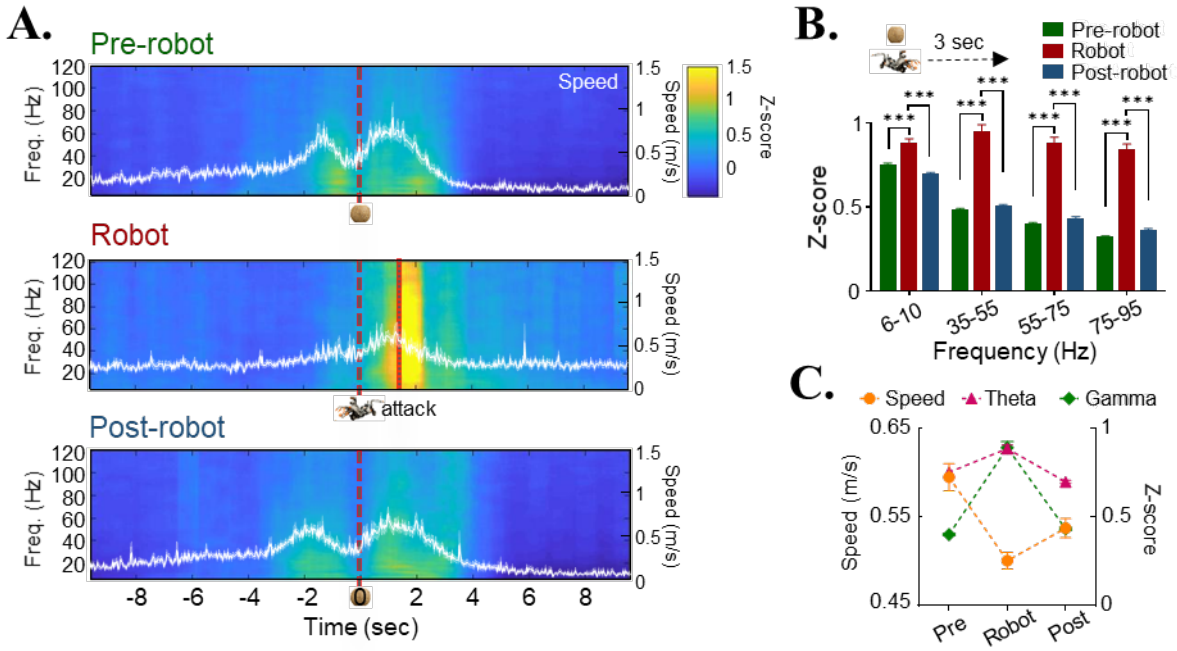


Figure 2.5. BA LFPs and the robot predator.
**(A)** Spectrograms of z-scored power in different frequency bands during each session are shown (t = 0, pellet acquirements for the pre- and post-robot sessions, robot activations for the robot session). White line with shades graphs inside of each spectrogram indicate the mean speed ± s.e.m. during each session. **(B)** In 3 seconds after the pellet acquirements or robot activations, the averaged z-scores in theta (6-10 Hz), low gamma (35-55 Hz), mid gamma (55-75 Hz), and high gamma (75-95 Hz) bands were calculated throughout the three sessions. **(C)** Increased z-scored theta and gamma power for 3 seconds after the robot activation during the robot session was not by the running speed. The dark lines represent the mean with the shaded band representing s.e.m. Data are presented as mean ± s.e.m. *** $P < 0.001$.

results demonstrate that the BA responds differently to the food and predator at both a single unit level and LFPs level.

*dHPC place cell activities during the encounter of the robot predator.*

Hippocampal place cells from the dorsal CA1 were recorded throughout the three sessions. Place fields from each cell during the three sessions were compared and examined to the degree of remapping. A total of 318 place cells from four rats were recorded, and they were classified into three cell types by the location of maximal firing during the pre-robot session; inside of the nest (nest cell, n = 212), near the nest (proximal cell, n = 26, zone 1 in Figure 2.3E), and near the threat (distal cell, n = 80). Place maps from each session were compared by the analysis of a pixel-by-pixel spatial correlation ($Z'_{\text{pre vs. robot}}$, $Z'_{\text{robot vs. post,}}$ and $Z'_{\text{pre vs. post}}$). The differences in the spatial correlations between the pre- and robot sessions ($Z'_{\text{pre-robot vs. robot}}$) were significantly lower in distal cells than in nest and proximal cells (one-way ANOVA using Bonferroni *post hoc* tests, $F_{2,315} = 9.728$, $P < 0.001$; nest, 0.499 ± 0.027; proximal, 0.671 ± 0.081; distal, 0.341 ± 0.028; Figure 2.6B, see examples in Figure 2.6A). The next parameter was peak distance, which is calculated by the difference of distance where the cell fired most during each session. The differences of peak distance between pre- and robot session were significantly longer in distal cells than in nest and proximal cells (one-way ANOVA, $F_{2,315} = 8.797$, $P =$ 0.0002 using Bonferroni *post hoc* test; nest, 11.114 ± 0.849 cm; proximal, 7.821 ± 1.262 cm; distal, 17.006 ± 1.438 cm; Figure 2.6C). Figure 2.6D shows scatter plots displaying differences of Z' between sessions as a function of X positions of peak firing during the pre-robot session (0, nest; 2, the end of the foraging arena). Differences in spatial correlations between the pre- and robot sessions ($Z'_{\text{pre vs. robot}}$) are negatively correlated with the distances from the nest ($r$ = -

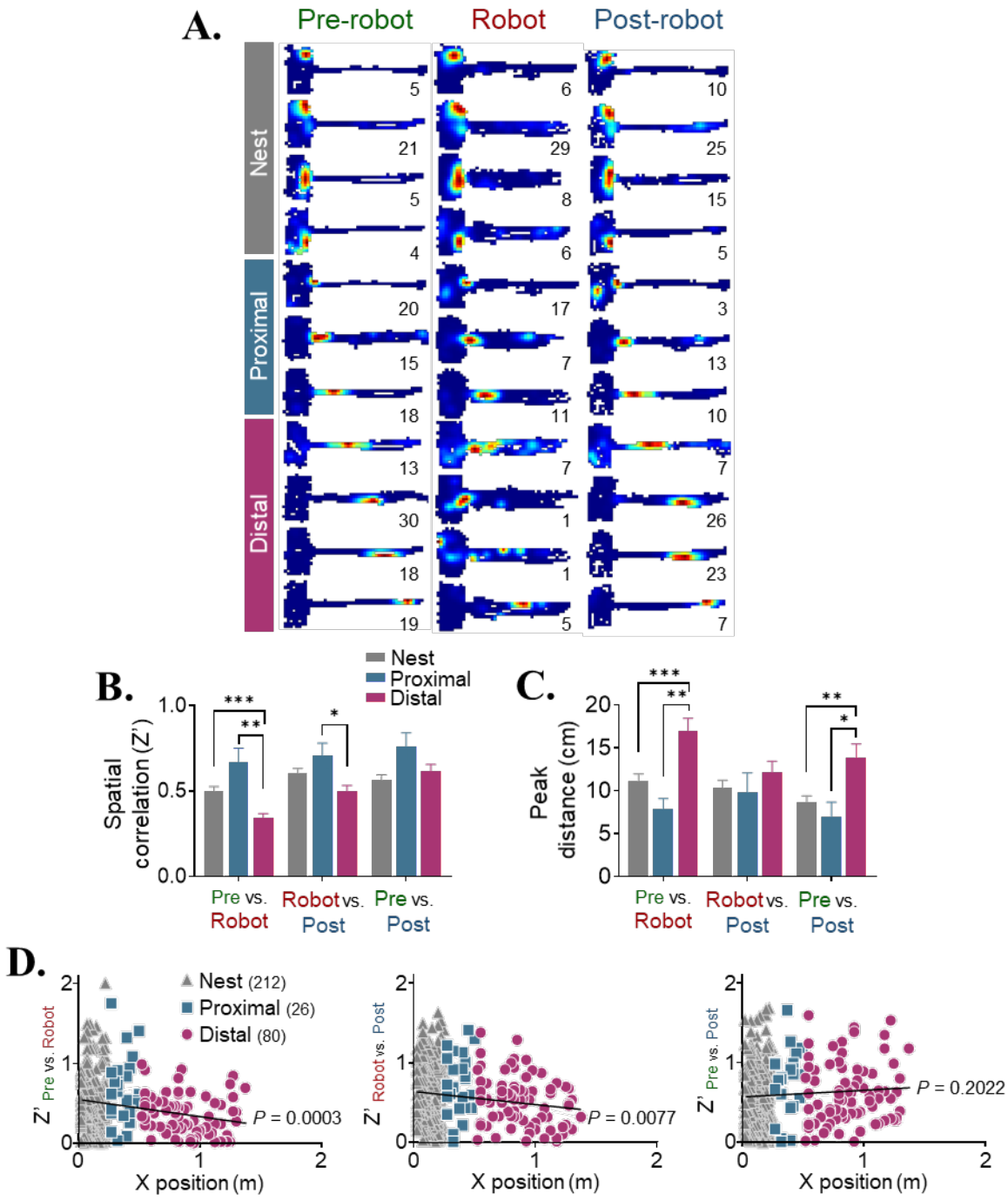


Figure 2.6. Hippocampal place cells and the robot predator.
**(A)** Examples of place fields of thenest, proximal, and distal cells during each session.
**(B)** Differences in the pixel-by-pixel spatial correlations (Z') value between sessions.
**(C)** Differences in peak distance between sessions. **(D)** Scatter plot displaying X positions of peak firing during the pre-robot session vs. differences of Z' between sessions. Data are presented as mean ± s.e.m. * $P < 0.05$; ** $P < 0.01$; *** $P < 0.001$.

0.2009, $P = 0.0003$). This negative correlation was also found in the X position and spatial correlation between the robot and post-robot sessions ($r = -0.1492$, $P = 0.0077$) but not between the pre- and post-robot sessions ($r = 0.0717$, $P = 0.2022$). These results confirm the previous findings that while place fields inside and near the nest are stable, place fields near the source of threat become unstable by the robot predator (E. J. Kim et al., 2015). Table 2.2 displays the characteristics of place cells that were recorded from this experiment.

*dHPC LFP activities during the encounter of the robot predator.*

Subsequently, we examined changes of event-evoked LFPs in the dHPC using z-scored power spectrograms from four rats and all trials (pre-robot, 935 trials; robot, 1034 trials; post-robot, 931 trials). Figure 2.7A shows z-scored power spectrograms with combined plots of running speed for the three sessions. All graphs were aligned to the time points when the rats came out of the nest. During the pre- and post-robot sessions, z-scored theta power was increased when the running speed also increased. The correlation between the z-scored theta power and the running speed of pre-robot session was significant ($r = 0.9324$, $P < 0.0001$; Figure 2.7B, top). Also, the z-scored theta power strongly correlated with the running speed of the post-robot session ($r = 0.7588$, $P < 0.001$; Figure 2.7B, bottom). However, there was no theta peak when the running speed was fastest during the robot session. There was a strong theta peak near 8 s after leaving the nest, but there was no correlation found between the theta power and the running speed ($r = -0.01115$, $P = 0.8511$; Figure 2.7B, middle). There is a possibility that positive correlations between the theta power and the pre- and post-robot sessions could be drawn from the different range of running speed as the robot session. When we matched the running speed from the pre- and post-robot sessions to the range of running speed during robot

Table 2.2. Firing properties of place cells during the pre-robot, robot, and post-robot sessions.

| Properties | | Pre-robot | Robot | Post-robot |
|---|---|---|---|---|
| Average firing rate (Hz) | Nest | 0.38 (0.17, 0.88) | 0.55 (0.30, 1.03) | 0.51 (0.28, 1.01) |
| | Proximal | 0.46 (0.21, 0.70) | 0.51 (0.33, 1.14) | 0.39 (0.30, 1.14) |
| | Distal | 0.39 (0.17, 0.67) | 0.52 (0.29, 0.89) | 0.57 (0.34, 0.94) |
| Field size ($cm^2$) | Nest | 381.48 ± 14.32 | 468.59 ± 11.28 | 375.28 ± 13.28 |
| | Proximal | 505.73 ± 39.60 * | 454.15 ± 30.45 | 417.15 ± 27.97 |
| | Distal | 508.50 ± 23.36 *** | 537.86 ± 22.33 *** | 499.73 ± 21.98 *** |
| Peak rate (Hz) | Nest | 4.62 (2.35, 8.65) | 5.75 (2.99, 10.12) | 5.82 (2.60, 11.72) |
| | Proximal | 5.43 (3.24, 13.25) | 5.09 (3.06, 10.68) | 5.89 (3.66, 12.45) |
| | Distal | 5.31 (2.73, 10.07) | 5.27 (3.12, 11.21) | 7.19 (3.69, 12.74) |
| Spatial info (bits/s) | Nest | 10.18 (5.61, 21.63) | 7.67 (4.66, 11.72) | 10.32 (4.72, 20.53) |
| | Proximal | 5.94 (3.58, 9.86) ** | 5.70 (2.91, 10.32) | 4.78 (2.75, 13.56) * |
| | Distal | 3.91 (2.21, 7.75) *** | 3.84 (2.63, 7.41) *** | 4.07 (1.92, 7.90) *** |
| Running speed (cm/s) | Nest | 13.31 (12.72, 14.54) | 18.13 (16.61, 19.96) | 11.49 (10.30, 12.49) |
| | Proximal | 13.66 (13.10, 14.40) | 16.52 (14.85, 18.13) ** | 11.26 (10.05, 12.27) |
| | Distal | 14.28 (13.12, 15.02) * # | 18.42 (16.61, 19.48) # | 11.59 (10.78, 12.49) |

* $P < 0.05$; ** $P < 0.01$; *** $P < 0.001$ compared to the nest cells. # $P < 0.05$ compared to the proximal cells.

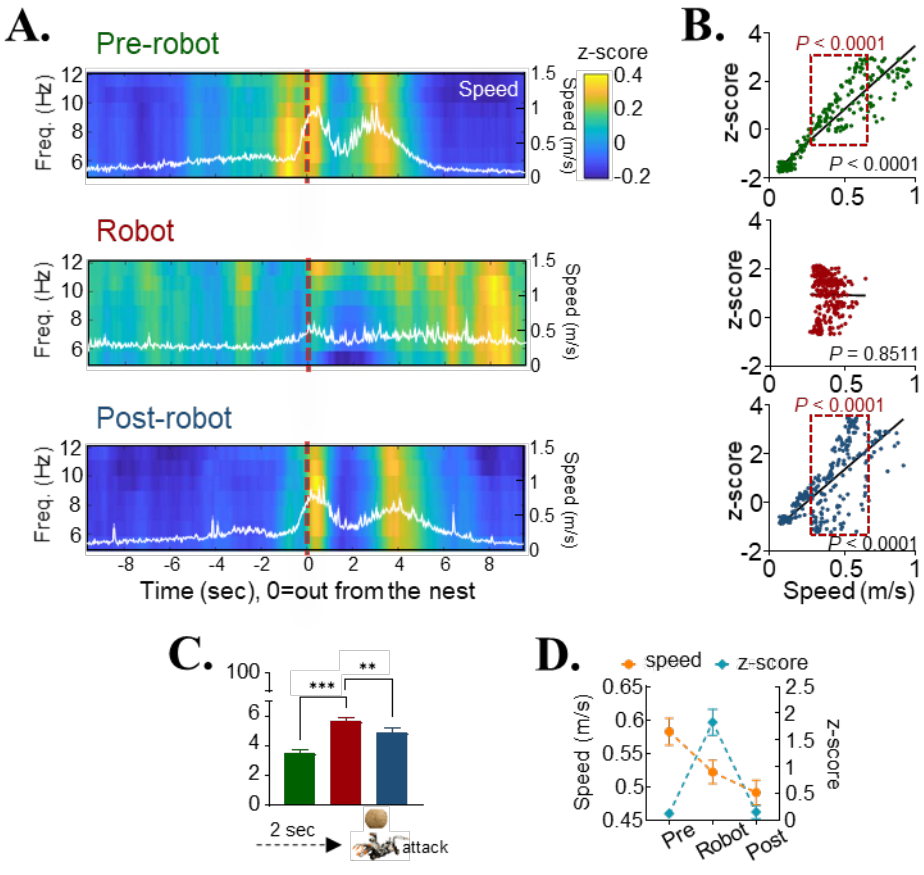


Figure 2.7. Hippocampal LFPs and the robot predator.
**(A)** Spectrograms of z-scored power in different frequency bands and combined plots of speed and position for each session are shown (t = 0, out from the nest). **(B)** Correlations between the running speed and z-scored theta power during each session (10 seconds after the outings from the nest) confirmed that increased theta power during the robot session is not correlated to the increase of running speed. Red dotted boxes indicate that matching running speed of pre- and post-robot sessions to robot session did not affect the results. **(C)** Power spectral densities (PSD) of theta were compared during each session (for 2 seconds before the pellet acquirement for pre- and post-robot sessions, for 2 seconds before the robot attack for the robot session). **(D)** Increased z-scored theta power before the robot attack during the robot session was not by the running speed. Data are presented as mean ± s.e.m. ** $P < 0.01$; *** $P < 0.001$.

session, they still maintained positive correlations (pre-robot$_{matched}$: $r$ = 0.7356, $P$ < 0.001; post-robot$_{matched}$: $r$ = 0.6359, $P$ <0.001; Figure 2.7B, red dotted box from top and bottom). From these data, it appears that increased theta during the pre- and post-robot sessions are due to the increased running speed, whereas increased theta during the robot session is not solely related to the running speed. PSD analysis was also used to further investigate the elevated theta power during the robot session. When the rats approached the pellet (2 seconds before the pellet acquirement or robot activations), there was a significant increase of theta percentage during the robot session (pre-robot, 3.497 ± 0.271%; robot, 5.568 ± 0.356%; post-robot, 4.862 ± 0.366%, repeated measures ANOVA, $F_{2,194}$ = 9.729, $P$ < 0.001 using Bonferroni *post hoc* test; Figure 2.7C). Again, the increased theta was not attributed to the increase of running speed because running speed was fastest during the pre-robot session, but the z-scored power of theta was highest during the robot session (two-way ANOVA, session × theta z-score: $F_{2,240}$ = 8.318, $P$ = 0.0003; Figure 3.7D). Previously, we measured the theta power from place cell activities and found that theta from the distal cells was only increased during the robot session (E. J. Kim et al., 2015). Combining these findings together, a robot predator induced more theta power in the dHPC, and this may be the outcome of selective increased power from distal cells.

*Spike synchrony between the BA and dHPC units during an encounter of the robot predator.*

Next, how the BA and dHPC units fire together in response to the robot was addressed by examining spike synchrony from simultaneously recorded units. To directly assess spike synchrony while rats attempted to procure a pellet in a fearful situation, CCs with the BA cells as references were generated. Among simultaneously recorded 2687 pairs, 145 pairs showed significant spike synchrony during the pre-surge (repeated measures ANOVA, $F_{2,40}$ = 124.7, $P$ <

0.001 using Bonferroni *post hoc* test; Figure 2.8A, bottom left). The same pairs did not show any significant synchrony during post-surge and pre-retrieval. During the post-surge, 209 pairs showed significant spike synchrony but not during pre-surge and post-retrieval (repeated measures ANOVA, $F_{2,40} = 59.00$, $P < 0.001$ using Bonferroni *post hoc* test; Figure 2.8A, bottom right). Representative CCs are shown in Figure 2.8B. Left and right columns display two different cell pairs that show significant synchrony during the pre-surge and post-surge, respectively.

*Directionalities of communication between the dHPC and the BA.*

From CCs, we also explored the directionality of spike synchrony. If the dHPC spike peak was between –100 ms and 0 ms from the BA spikes, this pair was identified as a dHPC leading pair (dHPC → BA). On the other hand, if the dHPC spike peak was between 0 ms and +100 ms from the BA spikes, this pair was defined as a BA leading pair (BA → dHPC). Figure 2.9A shows the percentage of each pair type during the pre-surge and post-surge. During the pre-surge, there were 84 BA leading pairs and 61 dHPC leading pairs. During the post-surge, there were 99 BA leading pairs and 110 dHPC leading pairs. Z-scored dHPC spikes from BA spikes as references for each time window are shown in Figure 2.9B.

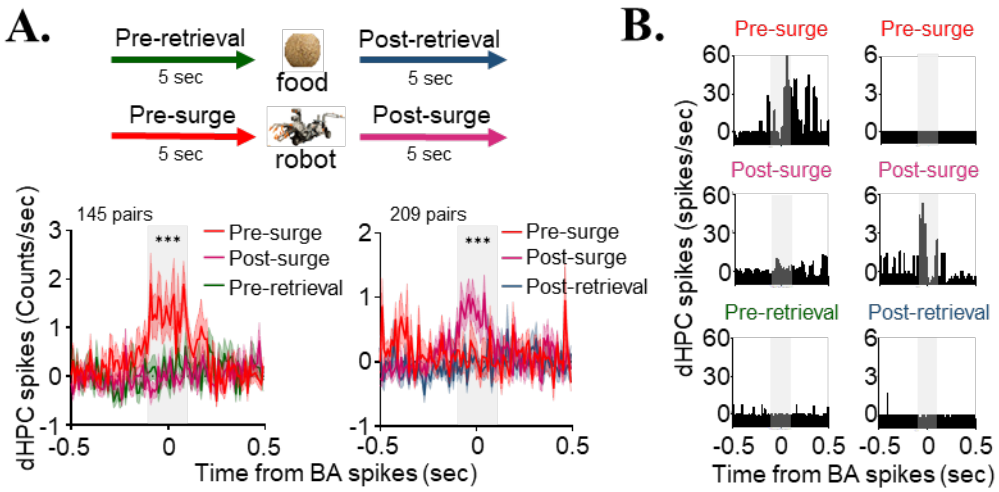


Figure 2.8. Spike synchrony between the BA units and dHPC units encountering the robot. Synchronized spikes between the two regions were evaluated by cross-correlation analysis with BA cells as references. **(A)** The averaged BA-dHPC cross-correlograms (CCs) of pairs that showed significant synchrony peak is shown. Among simultaneously recorded 2687 pairs, 145 pairs showed significant spike synchrony during the pre-surge (left) and 209 pairs showed significant spike synchrony during the post-surge (right). The dark lines represent the mean with the shaded band representing s.e.m. **(B)** Representative CCs of pairs showed significant synchrony during pre-surge (left column) and post-surge (right column), respectively. *** $P < 0.001$.

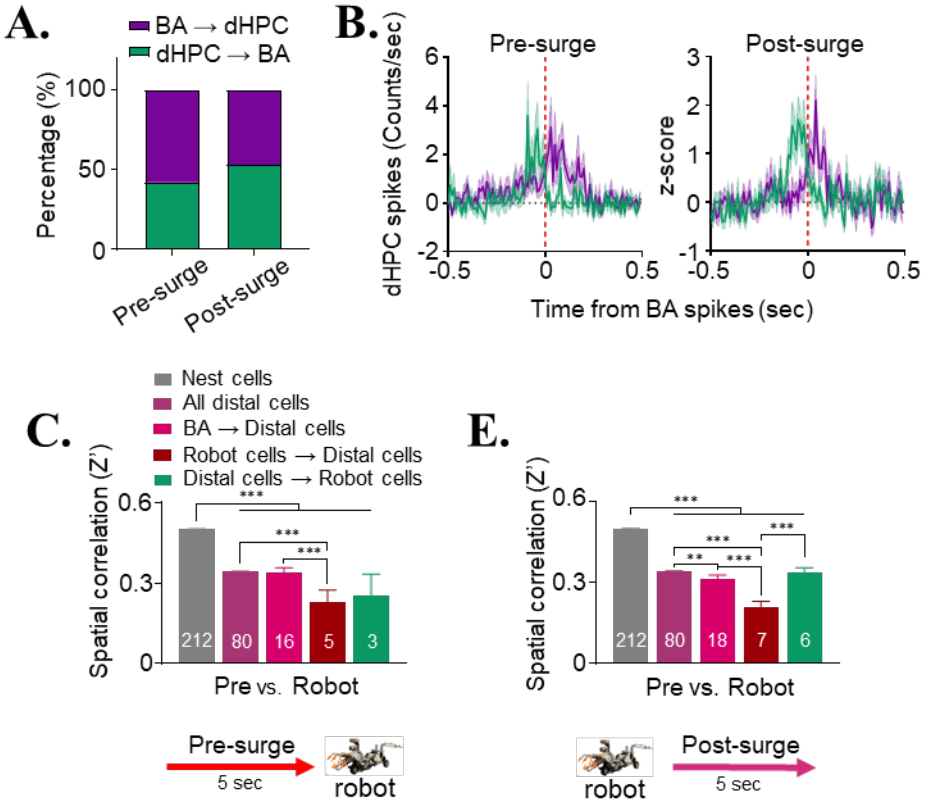


Figure 2.9. Directionalities of communication between the dHPC and the BA.
**(A)** The number of BA leading pairs (BA → dHPC) and dHPC leading pairs (dHPC → BA) during pre-surge and post-surge. **(B)** The averaged BA → dHPC or dHPC → BA CCs of pairs that showed significant synchrony peaks during the pre-surge (left) or post-surge (right). **(C, E)** Spatial correlations (Z') value between the pre-robot and robot sessions of the nest cells, all distal cells, BA leading distal cells (BA → distal cells), Robot cell leading distal cells (Robot cells → distal cells), and distal cells preceding robot cells (distal cells → robot cells) during the pre-surge **(C)** or the post-surge **(E)**. Data are presented as mean ± s.e.m. ** $P < 0.01$; *** $P < 0.001$.

*BA units affect stability of dHPC distal cells.*

Considering the neuronal responses of Robot cells and instability of distal cells during the robot session, how BA units affect place cells' stability when the robot is surging to rats was examined. The hypothesis is that BA units with a significant spike synchrony during the pre-surge or post-surge would induce more remapping in distal cells. To study this, significant BA → dHPC pairs during the pre-surge or post-surge were included because Robot cells fired before the robot activation (robot-approach) or after the robot activation (robot-triggered). In Figure 2.9C and D, spatial correlations between the pre- and robot sessions from different types of distal cells were compared: i) all distal cells, ii) BA leading distal cells (BA → distal cells), iii) Robot cell leading distal cells (Robot cells → distal cells). We also added iv) distal cells preceding Robot cells (distal cells → Robot cells) to see whether the direction of synchrony matters. As mentioned in Figure 2.6B, all distal cells showed significantly lower Z' when compared to the nest cells. During the pre-surge, BA → distal cells showed significant decrease of Z' when compared to the nest cells (one-way ANOVA, $F_{4,323} = 451.1$, $P < 0.001$ using Bonferroni *post hoc* test; BA leading, $P < 0.001$ compared to the nest cells; Figure 2.9C). Since BA units include not only Robot cells but also all other cell types, subsequently only Robot cells were included. Interestingly, distal cells receive Robot cells' leading showed much lower Z' than BA → distal cells ($P < 0.001$ compared to the BA leading distal cells). This indicates that among BA cells, Robot cells even more reduced the stabilities of distal cells. Distal cells preceding Robot cells also showed lower Z' and it was not different from Robot cells leading distal cells ($P = 0.988$).

Similar results were also found in the post-surge pairs with a stronger effect. Unlike pre-surge, BA → distal cell showed lower Z' than all distal cells ($P = 0.010$, pre-surge: a comparison of all distal cells and BA → distal cell was $P > 0.999$). This indicates that preceding BA

activities affected the remapping of distal cells more after the predatory attack than before the attack. Same as the pre-surge, Robot cells → distal cells' stability was even more decreased than BA leading distal cells ($P < 0.001$). We suspect that sustained activities from the Robot cells (Figure 2.4F) had much more impact on the stability of distal cells. Z' of distal cells → Robot cells was significantly higher than Robot cells → distal cells ($P < 0.001$). These results reflect that directionality, distal cells firing before or after Robot cells, is a good indicator of the magnitude of remapping after the predatory attack.

## 2.4 DISCUSSION

The present study investigated how the amygdala and the hippocampus encode the safety-danger boundary as animals navigate their environment using simultaneous recording. The amygdala, especially the BA, showed robust responses to either the pellet or the robot predator at the single-unit level and showed increased theta and gamma rhythms in a LFP level during the robot interactions. In the hippocampus, only the place fields near the source of threat had been remapped but not the place fields in the nest. Theta oscillation was increased during the robot interaction, which was not due to change of running speed. We also found that the amygdala and hippocampus work together, showing spike synchrony at the time of robot interaction. Notably, distal cells tended to be remapped more than nest cells when they showed spike synchrony with Robot cells in the amygdala. These results indicate that the amygdala sends fear signals though sustained activity to the hippocampus to develop an internal representation of a safety-danger boundary, which finally results in selections of optimal behaviors during the risky foraging situation.

From the current study, we found that BA neurons responded differently to positive and negative valence. Contrary to these findings, one study using a similar foraging paradigm found that BA activity does not seem to be modulated by the threat nor reward (Amir et al., 2015). In this study, when the firing rates of BA neurons were compared during four periods (in the nest with the door closed, waiting with the door opened, foraging, and escaping), the majority of units (69% of the pyramidal neurons and 58% of interneurons) showed a significant decrease in firing rate from the nest to foraging area. These patterns were found regardless of the trial types; the absence or presence of the robot predator. These results led the authors to conclude that BA activity encodes behavioral output such as movement velocity. In the current study, however, we found that BA activity is not correlated with rat's behavior output, but session type. Only 9.3% of the BA neurons showed the same response during the pre-robot and robot sessions (blue shaded in Table 1). Among them, only 0.8% showed inhibition to both pellet and robot, which was the prevalent type in the abovementioned study (Amir et al., 2015). Instead, most of the neurons in the current study showed different responses to the pellet and the robot (red shaded in Table 1, 43.4%). Cells responded to either pellet-exclusively (14.3%) or robot-exclusively (19.4%). If Robot BA cells actually encoded animal speed and not valence, then we would expect to see Robot BA cells firing during periods of locomotor activity in the pre and post-robot sessions (when the robotic threat is not present). However, this was not observed. Ultimately, the presence of Pellet and Robot cells provide evidence that the BA encodes valence of events by having different activity to threat or reward.

Characteristics of Robot-excited cells in the BA are different from neurons of the LA neurons. Previously, we found that there are also robot-approach cells and robot-triggered cells in the LA (E. J. Kim et al., 2018). However, the definition of robot-triggered cells was different

from the current study; LA neurons showing maximal firing when the rats were approaching the stationary robot. When we applied this definition to the current study, there were no robot-triggered cells, since BA neurons showed maximum firing rates after robot activations even though they showed a significant increase before robot activations ($Z > 3$). Significant but not maximal firing rates in the BA still indicate that BA neurons encode the internal state such as expectation of predatory attack. BA neurons also showed much longer sustained activity compared to LA neurons. Specifically, BA neurons persisted their activities for 10 seconds after the robot activation (Figure 2.4F), whereas LA neurons showed higher firing rates only during the first 2 seconds after robot activations. BA's sustained activities are very similar to the PL neurons from the same study (PL-RT cells) but with a shorter latency. These results suggest that BA serves to bridge the LA and PL in predatory information processing. This hypothesis regarding the direction of the communication is supported by the plethora of studies investigating learned fear.

Phasic responses in the LA and sustained responses in the PL have been reported from studies using fear conditioning paradigms (Burgos-Robles, Vidal-Gonzalez, & Quirk, 2009; Collins & Pare, 2000; N. Kim, Kong, Jo, Kim, & Choi, 2015; Quirk et al., 1995; Repa et al., 2001), whereas BA neurons have been shown to have sustained activity during the entire CS (Amano et al., 2011). To examine whether LA-BA-PL circuit converts phasic LA signals to sustained PL signals, one study built a biophysical model of the BA-PL network putting parameters such as synaptic weights, percentage connectivity, and distribution of neuromodulator receptors (Pendyam et al., 2013). The model revealed that activity in the BA was the most crucial factor for sustained activity in the PL, because BA activity leads to neuromodulator release. Interestingly, projections from the PL to BA were most important for

sustained BA activity. Even though we cannot fully apply the results obtained from studies of learned fear, they can still provide an outline of communication between nuclei related to fear behaviors.

The relationship between the theta oscillation in the hippocampus and the running speed deserves careful examination. During the pre- and post-robot sessions, we found that increased theta power strongly correlated with the running speed. These results replicated previous findings that theta power increases with faster running speed (Geisler, Robbe, Zugaro, Sirota, & Buzsaki, 2007; Maurer, Burke, Lipa, Skaggs, & Barnes, 2012; Sheremet, Burke, & Maurer, 2016; Sheremet et al., 2019). However, during the robot session, especially during the 10 seconds after the door opened, we found that the strong positive correlation between the theta power and the running speed disappeared, although overall, elevated theta was observed. These findings reflect the fact that the theta oscillation in the hippocampus is not a sole outcome of the running velocity. The function of the hippocampal theta other than the simple relationship with the running speed has been reported. It includes arousal and its control by attentional mechanism (Kemp & Kaada, 1975; Klimesch, 1999), context-dependent memory encoding and retrieval (Hasselmo, 2005), and spatial experiences (Gupta, van der Meer, Touretzky, & Redish, 2012). One interesting paper suggests that the theta may depend not only on the locomotion speed but also on the rats' motivational-emotional state that is associated with ongoing locomotion (Slawinska & Kasicki, 1998). From their findings, electrically induced locomotion led to much a higher power of theta than the expected power by spontaneous locomotion, which reflects the relationship between the locomotion speed and theta. Another finding from the same study supports the relationship between the emotional state and theta showing that the theta power was increased when the posterior hypothalamus was stimulated, which is closely related to aversive

behavior such as attack or escape. In light of such findings, the elevated theta power observed during the robot session may be explained by the aroused state due to defensive behaviors.

The communication between the amygdala and hippocampus at the LFP level could be addressed through coherence or coupling analyses of specific oscillatory rhythms. One study showed that the amygdala and hippocampus showed synchronized theta rhythm during fear memory retrieval using the fear conditioning paradigm (Seidenbecher et al., 2003). Another study found increased coherence of theta and gamma between the two regions when there was high expectation of reward (Terada, Takahashi, & Sakurai, 2013). These data support the new that there is communication between the amygdala and the hippocampus at the LFP level. However, the current study failed to analyze the direct comparison of oscillations due to large variance in LFP channel pairs that were recorded simultaneously. Even with the same LFP channel in the amygdala, pairing with different channels in the dHPC showed great variance. We tried to use normalized data to analyze coherence and coupling of signals, but it was not enough to solve the variance problems. We can also select 'responsive' channels in the same way as separating responsive vs. non-responsive units in the single-unit analysis, but we did not come to agreement in terms of how to choose channels. Additionally, if a certain area of each region communicates more, the location of the electrodes might matter since the BA and the dHPC are not small structures. For a future experiment, recording from the area where the direct connections are between the two regions may be helpful in obtaining cleaner results.

# Chapter 3. OPTOGENETIC MANIPULATION OF THE AMYGDALA AND DEFENSIVE BEHAVIORS

## 3.1 INTRODUCTION

Previous studies have reported that electrical stimulation of the amygdala produces behavioral, motor, and emotional responses both in animals and humans (Allikmets, 1966; Goddard, McIntyre, & Leech, 1969; Johansen et al., 2010; Lanteaume et al., 2007). These changes are closely related to the function of the amygdala mentioned in chapter 1 because heightened activities by the stimulation exaggerate the function of the amygdala (Di Ciano & Everitt, 2004; Huff et al., 2013). Amygdala stimulation also induces defensive behaviors such as freezing or fleeing (E. J. Kim et al., 2013), which are the main focus of the current study. Interestingly, the same electrical stimulation can lead to different types of defensive behaviors. For example, when the amygdala was stimulated when rats were in small chambers, rats tended to elicit freezing responses and 22-kHz ultrasonic vocalizations (E. J. Kim et al., 2013; Weingarten, 1978). On the other hand, when the amygdala was stimulated when rats were in a large arena with a safe nest, rats showed fleeing behavior rather than freezing (E. J. Kim et al., 2013). These results indicate that stimulation-induced freezing or fleeing behavior are dependent on the context where the stimulation occurs.

Electrical stimulation techniques, however, have fatal drawbacks; they stimulate the whole area including cell bodies in the same region, axon terminals coming from other regions, and fibers passing the stimulated region. Due to this disadvantage, it cannot be explained whether the amygdala is in directly responsible for generating defensive behaviors or other brain regions sending projections to the amygdala are in charge. To confirm that amygdala neurons are directly

involved in the expression of defensive behaviors, neurons in the amygdala must to be selectively stimulated. For this reason, a recent technique known as optogenetics can be utilized to target only amygdalar neurons.

As described in chapter 1, optogenetics is used to control cells that expressing light-sensitive opsins. Upon shining the light, cells show excitation (channelrhodopsin) or inhibition (halorhodopsin and archaerhodopsin) dependent on the opsin types. These opsins are responsive to the light within milliseconds so that neural control can be achieved with a great temporal resolution.

The strongest advantage of optogenetics over other conventional techniques is that it permits cell-type specific control (Do-Monte, Manzano-Nieves, Quinones-Laracuente, Ramos-Medina, & Quirk, 2015; Johansen et al., 2010; Wolff et al., 2014). For example, the calmodulin-dependent protein kinase II (CamKII) promotor is widely used to specifically target glutamatergic pyramidal neurons (Van den Oever et al., 2013). In the current study, we also used CamKII promoter to target pyramidal neurons in the BA since this cell type comprises nearly 80% of the total cell population (McDonald, 1982). Embracing the technologies from optics, genetics, and bioengineering, optogenetics became a powerful tool for better understanding the neural circuits.

In this chapter, it was tested whether pyramidal cells in the amygdala, especially BA as mentioned in chapter 1, are responsible for generating defensive behaviors using optogenetics. To test this, experiment 1 verified that light evoked neuronal responses from virus infected cells in the BA. Neuronal responses were recorded from rats implanted with an optrode (a bundle of optic fiber and tetrodes). After the technique was verified, virus injected animals were behaviorally tested during the foraging task (Choi & Kim, 2010). Despite the fact that there was no explicit

threat for the rats, stimulating pyramidal cells in the amygdala successfully generated defensive behaviors.

## 3.2 Materials and Methods

*Subjects.*

Male Long-Evans rats (initially weighing 325-350 g) were individually housed in a climate-controlled vivarium (accredited by the Association for Assessment and Accreditation of Laboratory Animal Care) and maintained on a reversed 12-h light/dark cycle (lights on at 19:00 hours). Rats were placed on a standard food-deprivation schedule, with free access to water, to gradually reach and maintain 85% of their normal weight. All experiments were conducted during the dark phase of the cycle in strict compliance with University of Washington Institutional Animal Care and Use Committee guidelines.

*Surgery.*

*Experiment 1.* Under anesthesia (94 mg/kg ketamine and 6.2 mg/kg xylazine, i.p.), four rats were injected with a virus expressing channelrhodopsin (ChR2) into the right BA (coordinates from bregma: 2.8 mm posterior, 5.0 mm lateral, 8.8 mm ventral) via a microinjection pump (UMP3-1, World Precision Instruments) with a 33-gauge syringe (Hamilton). The total volume was 0.5 µl and the injection speed was 0.05 µl/min. The microinjector needle was left in place for 10 minutes to prevent back flow. After injection, an optrode which consisted of six tetrodes and one optic fiber with a ferrule (optic fiber: 0.22 NA, 200 µm core; ferrule: 2.5 mm diameter; Doric Lenses) was implanted in the right BA (coordinates: 2.8 mm posterior, 5.2 mm lateral from bregma; 5.5 mm ventral from dura). The

optrode was secured by Metabond (C&b metabond®) and dental cement with anchoring screws. Behavioral experiments started after 4–5 weeks of recovery and viral expression.

*Experiment 2.* Nine rats were anesthetized and injected with one of the viruses subsequently described (ChR2, n = 5; EYFP, n = 4). The viruses were delivered into the bilateral BA (coordinates from bregma: 2.8 mm posterior, 5.0 mm lateral, 8.8 mm ventral). The total volume was 0.5 µl per site and the injection speed was 0.05 µl/min. To avoid back flow of the virus, the injection needle was left in place for 10 minutes. After the virus injection, optic fibers attached to ferrules were implanted 0.4 mm dorsal to the injection sites. The optic ferrules were secured by Metabond and dental cement with anchoring screws. Behavioral experiments started after 4–5 weeks of recovery and viral expression.

*Viruses.*

Adeno-associated viruses (AAVs; serotype 5) to express Channelrhodopsin-EYFP (AAV5-CaMKIIa-hChR2(H134R)-EYFP) or EYFP only (AAV5-CaMKIIa-EYFP) were injected in the BA. Viral titers were 8.5 x $10^{12}$ virus molecules/mL for AAV5-CaMKII-hChR2(H134R)-EYFP and 4.3 x $10^{12}$ virus molecules/mL for AAV5-CaMKII-EYFP. Viruses were stored in a -80°C freezer until the day of surgery. All viruses were obtained from the University of North Carolina Vector Core.

*Behavioral paradigms.*

Rats maintained their body weights at ~ 85% of normal weight throughout the experiment.

*Habituation.* Rats stayed in the nest for 30 min/day for 2 consecutive days with twenty food pellets to acclimate to the nest and experimental room.

*Experiment 1.* Baseline foraging procedure was the same as the experiment of chapter 2. Once rats learned to procure pellets up to 125 cm distance away from the nest, the baseline session lasted until photostimulation-responsive units were detected. During the stimulation session, a pellet location was fixed at 125 cm from the nest while the BA units were recorded. Photostimulation-responsive units were detected by introducing laser stimulation (2 sec, 20 Hz, 10 ms width, 5-10 mW). Response latency to the photostimulations was counted for each light pulse (10 ms, 20 Hz, 2 sec). The optrode was lowered after each recording session and multiple days of tests occurred. Some test days, photostimulations were delivered while rats were under anesthesia. This prevented seizure-like behaviors due to overstimulation of the BA. There was no robot session for the optrode experiment.

*Experiment 2.* After two minutes in the nest, the gateway to the foraging area opened, and the rat was allowed to explore and procure a food pellet placed at the S distance (25 cm from the nest). After the rat took the pellet back into the nest, the gateway closed (first trial). Consecutive trials commenced in the same way, except the pellet distance from the nest increased to the M distance (50 cm) for the second trial and L distance (75 cm) for the third trial. Rats underwent 4-5 days of baseline foraging for the behavioral experiment.

Once rats learned the baseline foraging behavior, the stimulation session began (Figure 3.1A). During the stimulation session, rats were first tested with three trials of baseline foraging with a L distance pellet. For the photostimulation trial, bilateral BA were activated by laser (473 nm; Opto Engine LLC) connected to Master-8 (A.M.P.I.) to deliver photostimulations (2 sec, 20 Hz, 10 ms width, 5-10 mW) whenever the rat approached the vicinity (~ 25 cm) of the L distance

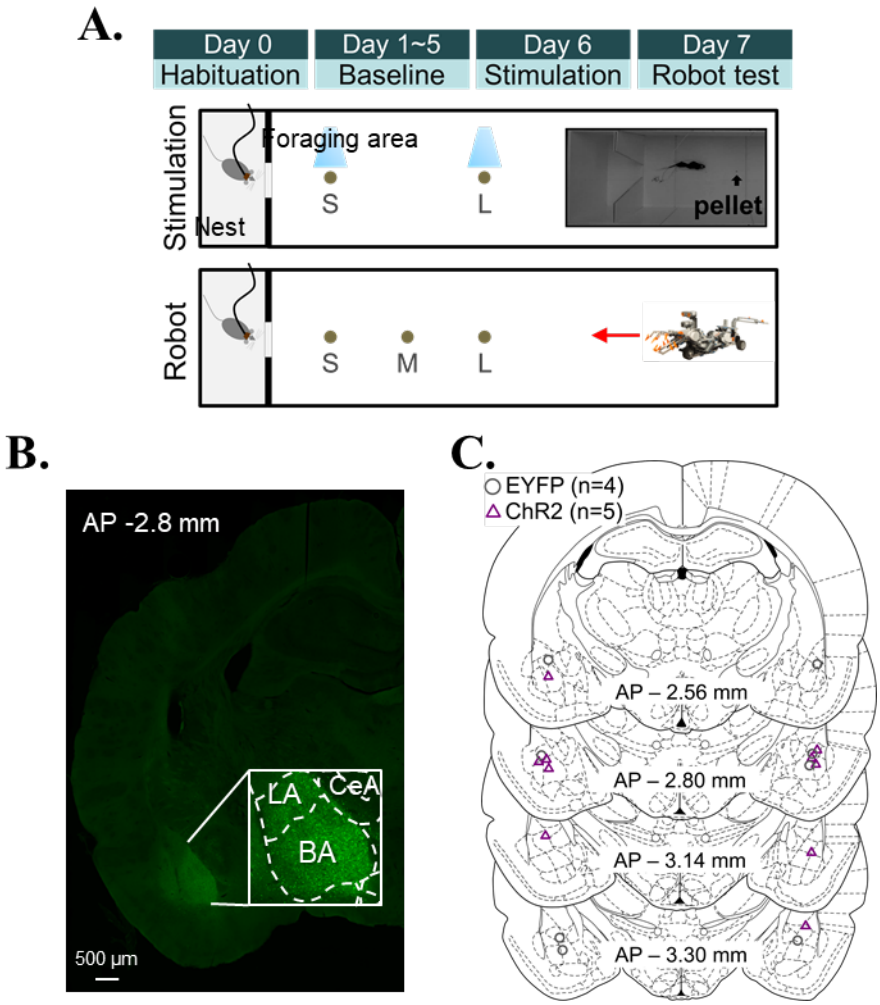


Figure 3.1. Foraging task and ChR2 expression in the BLA.
**(A)** Illustrations of the experimental design. S: short, M: medium, L: long distance pellet from the nest. A pellet set at each distance per trial. Insert: a photograph of the foraging apparatus. **(B)** Viral expression in the amygdala. **(C)** Placements of optic fiber tips in the BLA (EYFP: gray circles, ChR2: purple triangles). BA, basal amygdala; LA, lateral amygdala; CeA, central amygdala

pellet. If the rat failed to procure the L-pellet within 3 minutes, the gateway closed, and the rats were tested with S-pellet distances for another 3 minutes. If the rat succeeded with the L-pellet, testing with the S-pellet did not occur (ChR2 group only). For the EYFP group, rats were tested with both L- and S-pellets. One week after the stimulation session, all rats were tested with the robot predator. Rats were allowed to procure the L-pellet without the robot, and rats underwent the first robot-predator encounter trial with the L-pellet. The robot surged 23 cm toward the pellet, snapped its jaws once, and returned to its original position. If the rat was unsuccessful for 3 minutes, the pellet was moved to M and S distances on the following trials.

*Unit recording and analyses for experiment 1.*

The impedance of the electrode tips was matched to 100-300 kΩ measured at 1 kHz through gold plating. After the postoperative recovery period, electrodes were gradually advanced (≤ 160 μm per day) until they reached the target regions. Unit isolation and cluster cutting procedures have been described in chapter 2.

All units' activities were aligned to the time of photostimulations and were binned at 0.2 s. Photostimulation-evoked responses were defined as times when the activity change occurred during the laser delivery (2 s). To quantify neural changes by the stimulation, activities were normalized to 2 s before the stimulation. Units were classified as excitation when at least one of the z-scores was greater than 3 during the stimulation period. Inhibition was defined when at least one of the z-scores was less than -2 during the stimulation.

*Behavioral data acquisition and analyses for experiment 2.*

Behavioral data analyses for experiment 2 were the same as described in the chapter 2 experiment. The ANY-maze and a webcam were used to analyze behavioral data.

*Histology.*

For experiment 1, the tip of optrode was marked through electrolytic currents to confirm the location of the tetrodes. To verify viral expression, rats were overdosed with Beuthanasia and perfused intracardially with 250-300 ml of PBS followed by 400 ml of 4% paraformaldehyde. Brains were extracted, stored in 4% paraformaldehyde at 4°C overnight then transferred to a 30% sucrose solution until they sank. Transverse sections (50 μm) were washed with PBS, mounted onto slides and coverslipped with Flouromount-G™ with DAPI (eBioscience). Expression of ChR2-EYFP was examined using a Nikon fluorescence microscope (Model E400) equipped with a digital camera (Hitachi HV-C20). Rats with no EYFP expression or misplacement were excluded from the analyses.

*Statistical analyses.*

Statistical significance was determined with Mann-Whitney U test and repeated measures ANOVA (SPSS or Prism). The detailed information is described in Results. Kolmogorov-Smirnov normality test was also used to determine the application of parametric or nonparametric tests. Statistical significance was set at $P < 0.05$. Graphs were made using GraphPad Prism (version 8).

## 3.3 RESULTS

*Experiment 1: Photostimulations reliably evoked neuronal responses in the BA.*

One of the main findings from the experiment in chapter 2 was the presence of Robot cells in the BA, which show sustained activities to robot activations. To mimic the role of Robot cells, we used optogenetic manipulations to activate neurons in the BA specifically (Figure 3.1B and C). Optogenetic stimulation has the advantage of targeting specific cell types and targeting localized neurons, not passing fibers in the BA. These advantages give us a precise manipulation of the BA. Before we tested the effects of optogenetic stimulation of the BA on behavioral change, we tested whether optogenetic stimulation generated the expected neuronal responses in the virus infected cells (Figure 3.2). To confirm this, a different subset of animals was injected with a ChR2-expressing virus and implanted with an optrode in the BA. We found that optogenetic stimulation elicited excitation (n = 45), inhibition (n = 8), or no response (n = 18) from the neurons in the BA (Figure 3.2A). In the case of the excitation, optogenetic stimulation reliably evoked neuronal firing in the BA (jitter: median 1.3 ms; Figure 3.2B; latency: median 7.7 ms; Figure 3.2C). The representative excited responses by the photostimulation are shown in Figure 3.2D and Z-scored activities of three responsive types are shown in Figure 3.2E. These results confirmed that optogenetic stimulation reliably induced changes in neuronal firings in the BA.

*Experiment 2. Optogenetic stimulation of the BA elicited defensive behaviors.*

Next, we tested whether the optogenetic stimulation of the BA generates defensive behaviors. AAV-ChR2 (ChR2) or AAV-EYFP (EYFP) expressed rats were tested with 2 s of

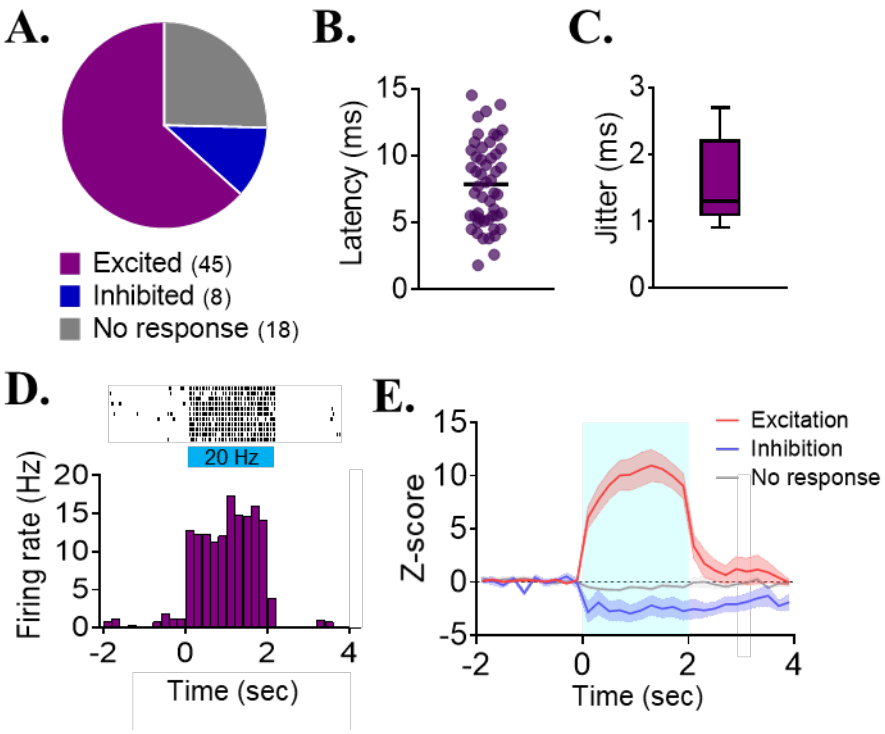


Figure 3.2. Photostimulation evoked neuronal responses in the BLA.
**(A)** Firing rate changes in response to photostimulation of BLA in rats expressing ChR2. **(B)** The latency of BLA neuronal responses to photostimulation measured in bins of 0.1 ms. **(C)** The jitter of photostimulation-evoked responses. **(D)** Raster plot and peristimulus time histogram (PSTH) showing the firing rate of a representative BLA neuron before, during, and after the photostimulations in a rat expressing ChR2 in the BLA. **(E)** Averaged z-scored activities from the excitation, inhibition, or no response units.

photostimulation delivered whenever the rats came near the pellet (same distance as the robot trigger). Before the stimulation, ChR2 and EYPF rats were able to procure a pellet successfully ($P = 0.9995$). However, with the stimulations, ChR2 showed longer latency of pellet procurements than EYFP when the photostimulations were delivered near the pellet (L-pellet, $P < 0.0001$; S-pellet, $P = 0.0317$; Figure 3.3A). This effect was not due to tissue damage by the photostimulations because when the rats were tested with the robot predator, both groups ran away and took similar time to acquire the pellet (two-way ANOVA, group: $F_{1,7} = 0.025$, $P = 0.8788$; Figure 3.3B).

With the L-pellet, ChR2 rats traveled more distance but with slower average speed than EYFP rats during the attempts (distance travelled: Mann-Whitney test, $P = 0.016$; Figure 3.4A; speed: Mann-Whitney test, $P = 0.016$; Figure 3.4B). The number of photostimulations received during the foraging task was significantly more in ChR2 than in EYFP (Mann-Whitney U test, $P = 0.016$). Representative tracking data of ChR2 and EYPF are shown in Figure 3.4D. The number of entries to Nest and L zones (nest: Mann-Whitney U test, $P = 0.048$; L: Mann-Whitney U test, $P = 0.048$; Figure 3.4E) and distance traveled by zones during the stimulation session with L-pellet were different from the two groups (two-way ANOVA, group: $F_{1,7} = 14.39$, $P = 0.0068$; Figure 3.4F). In response to the photostimulations, ChR2 rats showed various defensive behaviors (retract their bodies, pause, or flee; Figure 3.4G). Similar results were found with the S-pellet (Figure 3.5). Only four rats from ChR2 group were tested with S-pellet since one rat successfully procured the L-pellet. These results demonstrate that the increased activities of the BA, especially pyramidal neurons, caused defensive behaviors even though there was no explicit threat.

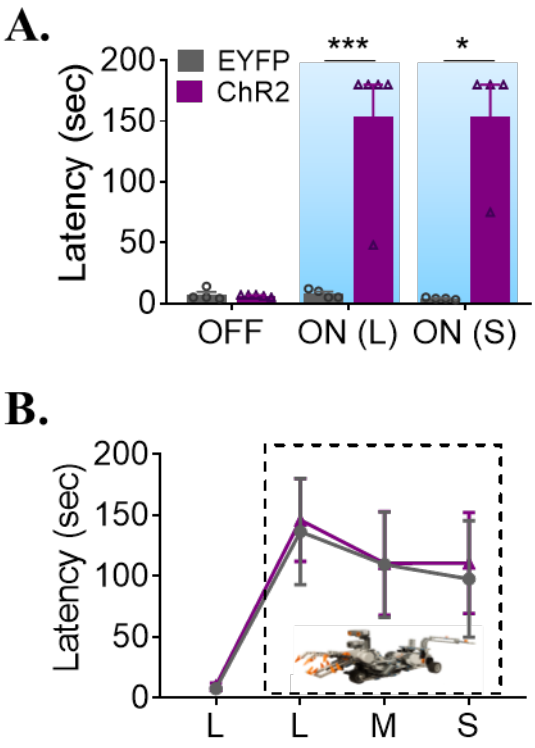


Figure 3.3. ChR2 activation of BLA neurons altered foraging behaviors.
**(A)** The latency of procuring pellets without photostimulations (OFF) and with photostimulations (ON) at L and S distance pellets. **(B)** Latency of procuring pellets during Robot test. Data are presented as mean ± s.e.m. and individual data are represented as symbols. * $P < 0.05$; ** $P < 0.01$ compared to EYFP.

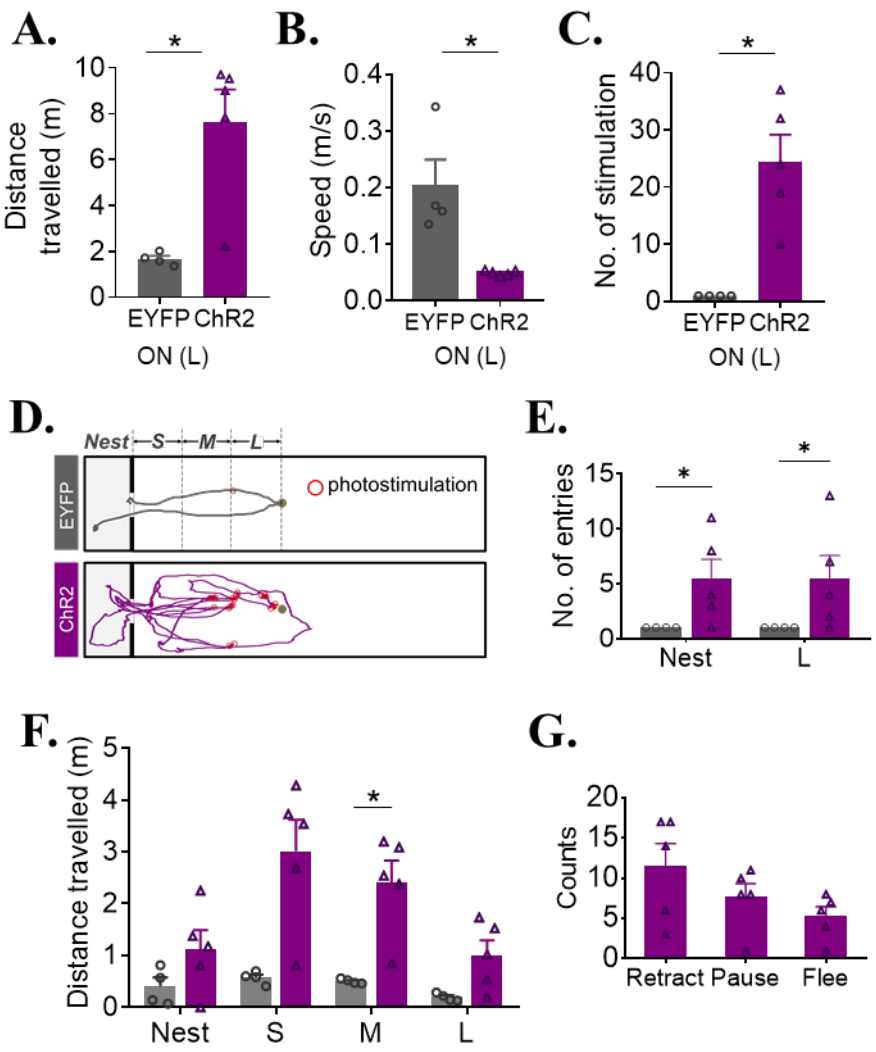


Figure 3.4. Locomotor data during the photostimulation with L distance pellet.
**(A)** The number of photostimulations during the stimulation session with L pellet. **(B)** Distance traveled during the stimulation session with L pellet. **(C)** The speed difference between groups during the stimulation session with L pellet. **(D)** Representative tracking data of EYFP- and ChR2-expressing rats. Red circles indicate the time of photostimulation delivery. **(E)** The number of entries to Nest and L zones. **(F)** Distance traveled by zones during the stimulation session with L pellet. **(G)** Types of defensive behavior elicited by photostimulation. Data are presented as mean ± s.e.m. and individual data are represented as symbols. * $P < 0.05$; ** $P < 0.01$ compared to EYFP

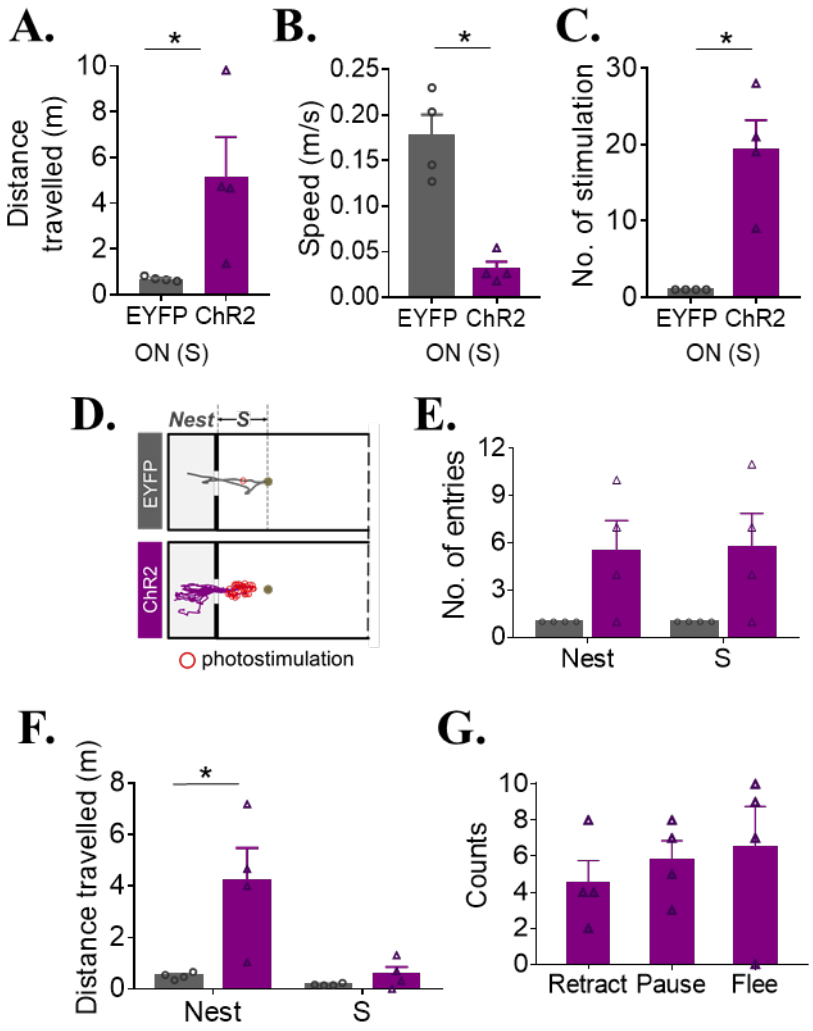


Figure 3.5. Locomotor data during the photostimulation with S distance pellet.
**(A)** The number of photostimulation during the stimulation session with S pellet. **(B)** Distance traveled during the stimulation session with S pellet. **(C)** The speed difference between groups during the stimulation session with S pellet. **(D)** Representative tracking data of EYFP- and ChR2-expressing rats. **(E)** The number of entries to Nest and S zones. **(F)** Distance traveled by zones during the stimulation session with S pellet. **(G)** Types of defensive behavior elicited by photostimulation. Data are presented as mean ± s.e.m. and individual data are represented as symbols. * $P < 0.05$ compared to EYFP.

## 3.4 DISCUSSION

Optogenetic stimulation of the BA successfully induced defensive behaviors. Moreover, we confirmed that these behaviors were as a result of photoexcitation of pyramidal neurons. These results specifically indicate that activity of pyramidal neurons in the BA is sufficient to elicit defensive behaviors. Indeed, despite the fact that there was no explicit threat, rats still showed defensive behaviors following photostimulation, suggesting that pyramidal cell stimulation served a similar role as the robot predator in chapter 2.

As mentioned in the introduction, the type of defensive behaviors expressed is determined by the environmental settings where amygdala stimulation happens, for example, either a small fear conditioning chamber or a large foraging area (E. J. Kim et al., 2013). Since the current study utilized the same foraging apparatus as the study from Kim et al., 2013, we also found that rats did not show freezing responses from BA stimulations. Rather, rats retracted their body, paused only during the stimulation or fled to the nest. These results, again, support the importance of the context in which the brain stimulation occurs.

The distance of the pellet also influenced the type of defensive behaviors expressed. When the rats were tested with the L-pellet, rats retracted their bodies or paused during the stimulation rather than fled to the nest. Most of the time, rats avoided the stimulation trigger zone (L zone in Figure 3.4D) but stayed in the foraging area closer to the nest (S and M zones in Figure 3.4D). Rats showed a higher percentage of fleeing responses when tested with S-pellet. Since the nest was relatively close compared to the L-pellet, rats fled to the nest easily and stayed longer in the nest. In terms of behaviors, one study showed that when a mouse was close to the nest, it showed flight rather than freezing responses to a visual looming stimulus over its head (Yilmaz & Meister,

2013). These results suggest that proximity to the safe area determines the selection of defensive behaviors.

Stimulation of the BA neurons was sufficient to trigger defensive behaviors, but it did not fully replace the robot predator. The number of stimulations refers to the number of attempts to procure the pellet. During the robot test, rats took the average of twelve minutest to make 10 attempts, which is equal to 2.5 attempts for three minutes. However, rats made the average of 24.4 attempts for the three-minute stimulation session. During the robot attack, unlike the brain stimulation, rats are facing visual, auditory, and sometimes tactile cues from the robot predator. Such multimodal cues will activate other brain regions in addition to the amygdala. Contrary to the interaction with the predator, there are no sensory cues that rats can utilize to interpret the situation during the stimulation. Apparently, the amygdala is essential to show defensive behaviors (Choi & Kim, 2010), but a full response to predatory threat requires harmonious brain activity not only from the amygdala but also from other brain regions.

To understand the functional heterogeneity of the amygdala, it is worth noting that there are two different neuronal populations; positive valence coding neurons and negative valence coding neurons in the amygdala (Belova, Paton, Morrison, & Salzman, 2007; Knapska, Radwanska, Werka, & Kaczmarek, 2007; Muramoto, Ono, Nishijo, & Fukuda, 1993; Paton et al., 2006). The two seemingly distinct populations are either intermingled (Gore et al., 2015; Paton et al., 2006) or spatially separated in the amygdala (J. Kim et al., 2016). The first claim was supported by the fact that two functionally different populations tagged by c-fos (immediate early gene indicates recent neuronal activity) expression were intermingled in the amygdala (Gore et al., 2015) and the second claim was supported by the fact that positive and negative valence coding neurons show differential genetic labelling and spatial segregation (J. Kim et al., 2016). Based on

this prewired view of amygdalar function, stimulation will activate not only fear-related neurons but also reward-related neurons. This, in turn, will lead to both reward-seeking behaviors and fear responses. However, in the current study, we only saw fear behaviors by the stimulation. From an evolutionary perspective, the primary function of fear is to ensure survival, which is accomplished in part by inhibiting other drives not relevant during a threatening scenario (Pellman & Kim, 2016). Therefore, one possible explanation for the obtained results is that activation of "fear" neurons overrides activation of "appetitive" neurons. Future studies can test the validity of this idea by stimulating only positive valence encoding neurons during predator interaction.

# Chapter 4. IMPACTS OF AMYGDALAR FUNCTION ON HIPPOCAMPAL PLACE CELLS

## 4.1 INTRODUCTION

Here, in chapter 4, the role of the amygdala on stability of the place cells in foraging behaviors was examined. Previously, we found that the amygdala lesion abolished adaptive foraging behaviors when confronted with the robot predator (Choi & Kim, 2010). From these results, we can conclude that having an intact amygdala in a risky foraging situation helps maintain optimal decision-making by ensuring the selection of appropriate behaviors; to approach food and avoid the predator. This conclusion raises another set of questions regarding the relationship between the amygdala and hippocampus in a risky foraging task. First, will failure to generate defensive behaviors to predatory threats not change spatial representations encoded before the robot interaction? Second, since we confirmed that optogenetic stimulation successfully induced defensive behaviors in chapter 3, will the optogenetic stimulation also sufficiently affect the stability of the place cells?

Many studies have reported that aversive experiences alter the spatial representation of place cells (E. J. Kim, Kim, Park, Cho, & Kim, 2012; E. J. Kim et al., 2015; J. J. Kim et al., 2007; Moita, Rosis, Zhou, LeDoux, & Blair, 2004; Okada, Igata, Sasaki, & Ikegaya, 2017; Wu, Haggerty, Kemere, & Ji, 2017). Reorganization of hippocampal place fields in response to aversive stimuli may be a neural mechanism of decision making in a risky environment dependent on cooperation with the amygdala.

From chapter 2, we found that hippocampal place cells that fired synchronously with Robot cells in the BA showed a greater degree of remapping than other cells that did not show

spike synchrony with Robot cells. Sustained activity of Robot cells was a key factor that affected the stability of place cells. To mimic the role of Robot cells in the BA, selective excitation of neurons in the BA using optogenetics can be utilized. If the artificially evoked neuronal activities in the BA induce remapping in the place cells, it is predicted that heightened activities of the amygdala are the source of remapping and defensive behaviors even without external, visible threat.

In this chapter, we tested the necessity and sufficiency of the amygdala in place cells' stability. To test the necessity of the amygdala, experiment 1 studied the effect of amygdalar lesion on place cells' remapping. Bilateral electrolytic lesion of the amygdala was performed to abolish the expression of the defensive behaviors completely. To test the sufficiency of the amygdala, experiment 2 investigated whether optogenetic stimulation of the amygdala produced remapping of place fields, especially the fields near the stimulation trigger zone, and induced prominent theta rhythm during the stimulation. Results from experiment 1 and 2 confirmed that the amygdala is essential for foraging behaviors in a risky situation by producing an adequate spatial representation.

## 4.2 Materials and Methods

*Subjects.*

Male Long-Evans rats (initially weighing 325-350 g) were individually housed in a climate-controlled vivarium (accredited by the Association for Assessment and Accreditation of Laboratory Animal Care) and maintained on a reversed 12-h light/dark cycle (lights on at 19:00 hours). Rats were placed on a standard food-deprivation schedule, with free access to water, to gradually reach and maintain ~ 85% of their normal weight. All experiments were conducted

during the dark phase of the cycle in strict compliance with University of Washington Institutional Animal Care and Use Committee guidelines.

*Surgery.*

*Experiment 1*. Under anesthesia, four rats were mounted in a stereotaxic instrument and bilateral amygdalar lesions were made by passing a constant current (1 mA, 10 Sec, Ugo Basile) through epoxy-insulated stainless steel insect pins (#00), except for ~ 0.5 mm at the tip [coordinates from bregma: 2.8 mm posterior, 4.0 (and 5.0) mm lateral, 7.6 (and 8.4) mm ventral]. After the lesions made, a microdrive of tetrode bundles was implanted into the dHPC (same coordinates as chapter 2). The microdrive was fixed by dental cement with anchoring screws. Behavioral experiments and recording session started after one week of recovery.

*Experiment 2.* Seven rats were anesthetized with the same cocktail of ketamine and xylazine described above and mounted in a stereotaxic. The virus described above (ChR2) was delivered into the right BA (n = 5) or bilateral BA (n = 2) (same coordinates as described in chapter 3) via a microinjection pump with a 33-gauge syringe (Figure 4.2B). Functional lateralization of the amygdala has been widely supported, with the right amygdala being closely linked to negative emotion (Baas, Aleman, & Kahn, 2004; Baker & Kim, 2004; Blair et al., 2005; Glascher & Adolphs, 2003; Lanteaume et al., 2007). Stimulation of the right amygdala successfully induced defensive behaviors, confirming this notion. The total volume was 0.5 µl per site, and the injection speed was 0.05 µl/min. The syringe was left in place for 10 minutes to prevent backflow. Following injection, optic fibers attached to ferrules (optic fiber:  0.22 NA, 200 µm core; ferrule diameter: 2.5 mm; Doric Lenses) were implanted into the right BA or bilateral BA (0.4 mm dorsal to the virus injection site). After the virus injection and the optic fiber implantation, a microdrive of

tetrode bundles (n = 5) or VersaDrive-8 (n = 2, Neuralynx) was implanted into the dHPC (same coordinates as chapter 2 experiment; Figure 4.2A). The optic fibers and electrodes were fixed by Metabond and dental cement with anchoring screws. Behavioral experiments and recording session started after 4–5 weeks of recovery and viral expression.

*Behavioral paradigms.*

Rats maintained their body weights at ~ 85% of normal weight throughout the experiment.

*Habituation.* Rats stayed in the nest for 30 min/day for 2 consecutive days with twenty food pellets to acclimate to the nest and experimental room.

*Experiment 1.* Baseline foraging procedure was the same as described for the experiment of chapter 2. When the rats learned to procure a pellet from the longest distance, the pellet distance was fixed at 125 cm, unit screening started. Rats underwent baseline foraging until place cells were detected. Place cells from the dHPC were recorded throughout the three sessions; pre-robot, robot, and post-robot (Figure 4.1A, B). The description of each session is the same as in chapter 2.

*Experiment 2.* Baseline foraging procedure was the same as the experiment of chapter 2. When the rat learned to procure a pellet from the longest distance, the pellet distance was fixed at 125 cm, unit screening started. Place cell activities from the dHPC were recorded throughout the three sessions; pre-stimulation, stimulation, and post-stimulation (Figure 4.2C). During the pre-stimulation session, 8-10 trials of foraging with a pellet placed at 125 cm from the nest were conducted to record baseline place cell activities. After the pre-stimulation session, the bilateral

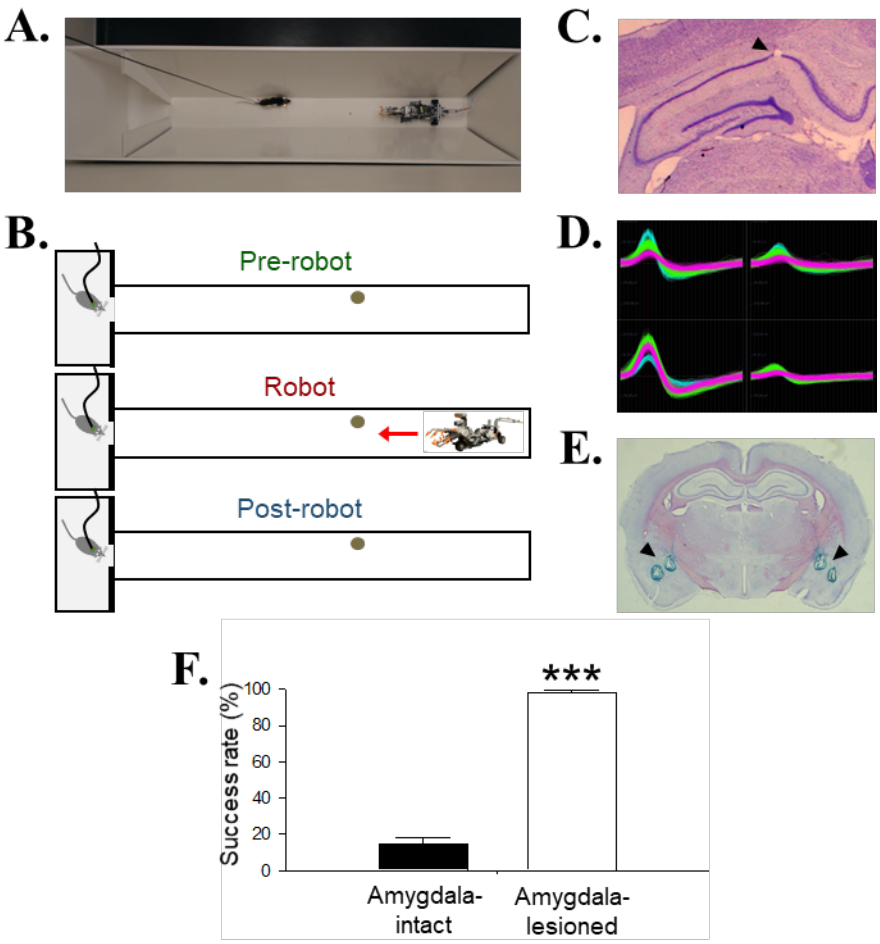


Figure 4.1. Hippocampal place cells with amygdala lesioned rats and the robot predator. **(A)** A photograph of the foraging apparatus of the experiment. **(B)** Illustrations of three sessions (pre-robot, robot, and post-robot). **(C)** A photomicrograph of tetrode tips in the dHPC (arrowhead). **(D)** Representative waveforms of place cells obtained from each channel of a tetrode. **(E)** A photomicrograph of amygdala bilateral lesion (arrowhead). **(F)** Amygdala-lesioned rats showed a higher success rate of procuring a pellet during the robot session compared to the amygdala-intact rats. Data are presented as mean ± s.e.m. *** $P < 0.0001$.

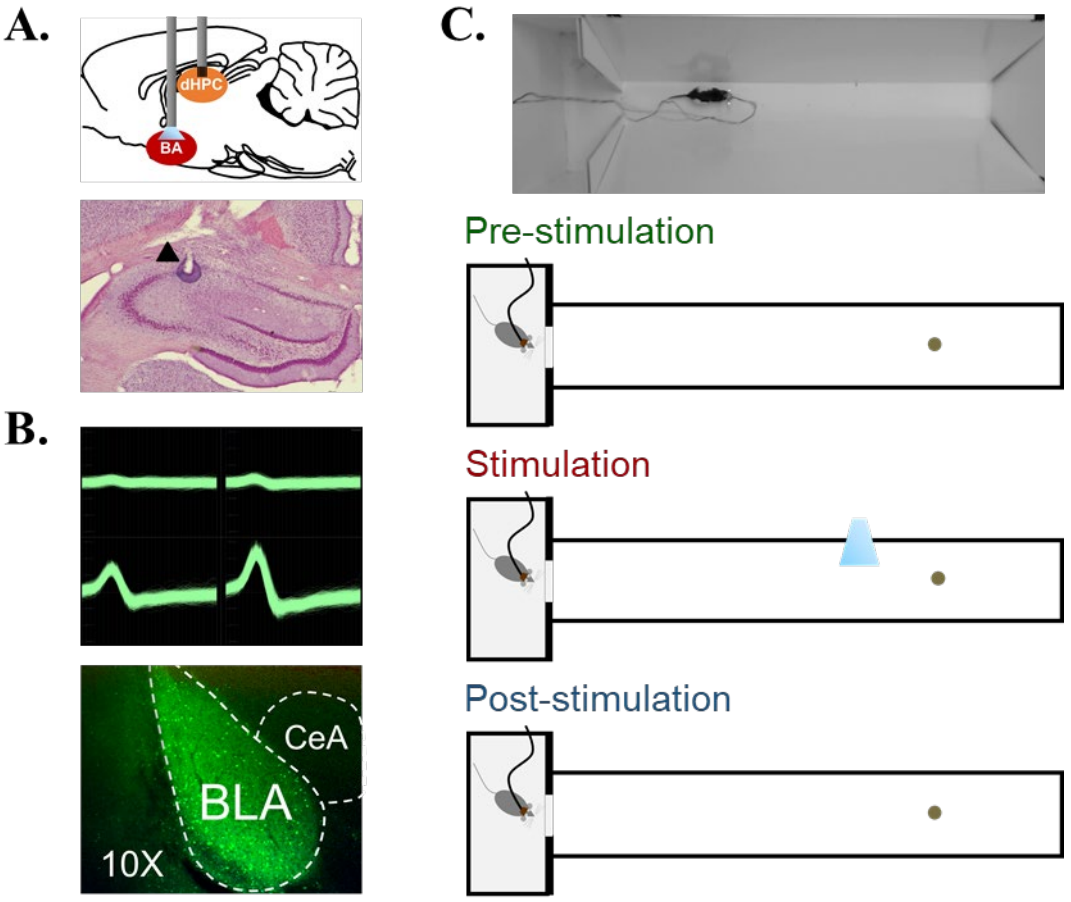


Figure 4.2. Optogenetic stimulation of the BA and recording from the dHPC in risky foraging situations.
**(A)** Schematic image of the experiment (top) and a photomicrograph of tetrode tips in the dHPC (arrowhead, bottom). **(B)** Representative waveforms of a place cell obtained from each channel of a tetrode (top) and a representative fluorescent microscopy image of viral expressions (bottom). **(C)** A photograph of the foraging apparatus of the experiment (top) and illustrations of three sessions (pre-stimulation, stimulation, and post-stimulation).

or unilateral BA were activated by the laser whenever the rats approached the vicinity of the pellet (~ 25 cm). The laser was connected to a pulse generator (A.M.P.I.) to deliver.

*Behavioral data acquisition and analyses.*

Behavioral data analyses were the same as the chapter 2 experiment. The ANY-maze and a webcam were used to analyze behavioral data.

*Unit recording and place cell analyses.*

The impedance of electrode tips was matched to 100-300 kΩ measured at 1 kHz through gold plating. After the postoperative recovery period, electrodes were gradually advanced (≤ 160 μm per day) until they reached the target regions. Unit isolation and cluster cutting procedures have been described in chapter 2. Place cell analyses were conducted the same as the experiment of chapter 2.

BA-simulation-evoked responses in the dHPC were also examined in experiment 2. All units' activities were aligned by photostimulations and were binned at 0.5 s. Photostimulation-evoked responses were defined when the activity change occurred during the laser delivery (2 s). To quantify neural responses to the stimulation, activities were normalized to 3 s before the stimulation. Units were classified as excited when at least one of the z-scores was greater than 3 during the stimulation period. Inhibited cells were defined when at least one of the z-scores was less than -1.5 during the stimulation.

*Histology.*

After the completion of the experiment, electrolytic currents (10 μA, 10 s) were applied to tips of each tetrode to confirm the placement of the electrodes. Histology procedure for experiment 1 was the same as the experiment of chapter 2. Histology procedure for experiment 2 was the same as the experiments of chapter 3 to verify viral expressions.

*Statistical Analyses.*

Statistical significance was determined with repeated measures ANOVA, two-way ANOVA, linear regression, Pearson's *r*, unpaired *t* test, or Friedman test using Bonferroni *post hoc* or Dunn's multiple comparisons tests (SPSS or Prism). The detailed information is described in each figure legend. Kolmogorov-Smirnov normality test also was used to determine the application of parametric or nonparametric tests. Statistical significance was set at $P < 0.05$. Graphs were made using GraphPad Prism (version 8).

## 4.3 RESULTS

*Experiment 1: Hippocampal place cells with the amygdala lesion.*

Previous studies have shown that amygdala lesion and inactivation abolished the foraging rats' fear of the looming robot (Choi & Kim, 2010), whereas amygdalar stimulation evoked the same fleeing response in naive rats in absence of the robot (E. J. Kim et al., 2013). To test whether the robot-induced instability of place fields around the source of threat is mediated via the amygdala-fear system, we recorded place cells in amygdala-lesioned rats (Figure 4.1C-E). These rats easily obtained the pellets despite the surging robot (Figure 4.1F), and the pixel-by-pixel correlation analysis showed that place fields in the distal area remained stable across all

recording sessions (Figure 4.3A and B). Place fields were comparable to the nest and proximal place fields (one-way ANOVA, $F < 2.19$, $P > 0.12$). No reliable correlation was observed between the peak X position during the pre-robot session and the spatial correlation across sessions ($r < 0.213$, $P > 0.08$; Figure 4.3C). Similarly, there was no difference between the cell types in the peak distance across sessions ($\chi^2 < 1.778$, $P > 0.411$; Figure 4.4A). In addition, the theta power of distal cells in amygdala-lesioned rats (Figure 4.4B, C) did not differ across sessions ($F_{2, 22} = 0.279$, $P = 0.759$; Figure 4.3C). Table 4.1 displays the characteristics of place cells that were recorded from the experiment.

*Experiment 2: Optogenetic stimulation of the BA and place cells in dHPC.*

Experiment 2 examined whether optogenetic stimulation of the amygdala is sufficient to alter the stability of hippocampal place cells. We hypothesized that defensive behaviors induced by the BA stimulation is sufficient to disrupt the stability of place cells.

There were two groups of rats; one group showed behavioral effects to the photostimulations (n = 17 recording sessions, labeled purple; Figure 4.5A-C) and the other group did not show behavioral effects to the photostimulations (n = 6 recording sessions, labeled grey, Figure 4.5F-H). Behavioral effects by the photostimulations included the defensive behaviors mentioned in Figure 3.4G. No response to the photostimulation was due to mistargeting of the optic fibers or low intensities of the laser.

Rats with behavioral effects made multiple attempts to retrieve a pellet (representative trajectory plots during the three sessions are shown in Figure 4.5A), yet the success rate was significantly lower during the stimulation session compared to pre- and post-stimulation sessions (Friedman test, $P < 0.001$, Figure 4.5B). Rats without behavioral effects, however, did not make

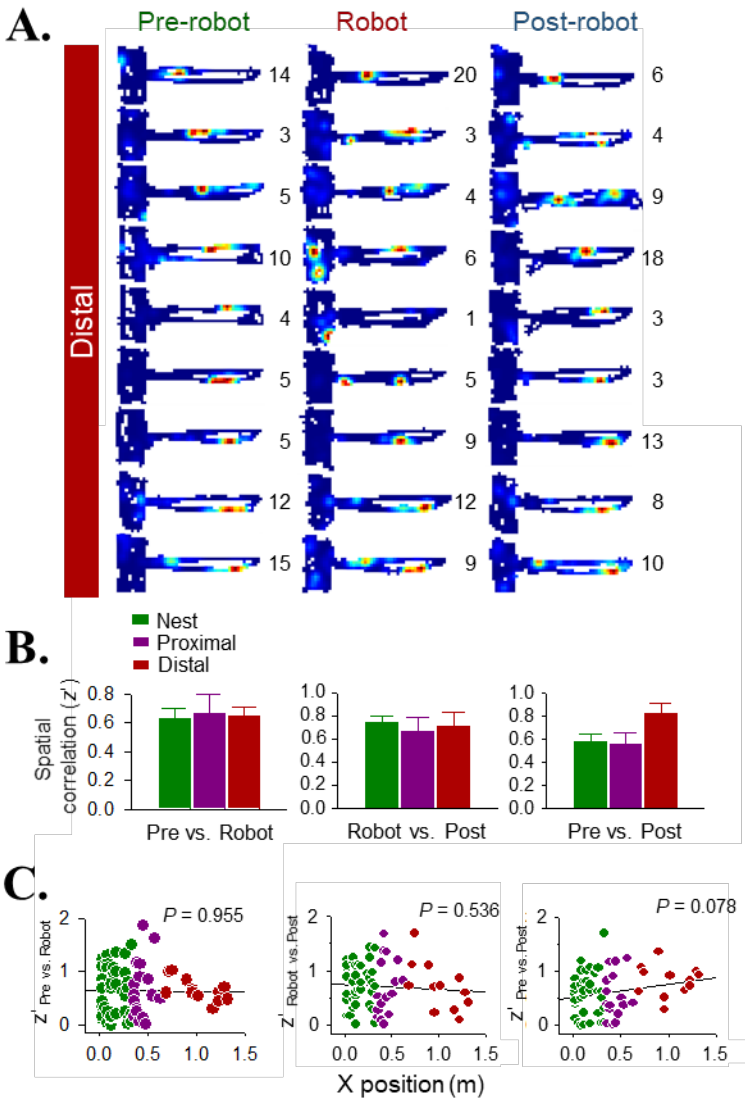


Figure 4.3. Hippocampal place cells from amygdala-lesioned rats and the robot predator. **(A)** Examples of distal cells' place fields during each session. **(B)** Differences in the pixel-by-pixel spatial correlations (Z') value between sessions. **(C)** Scatter plots displaying X positions of peak firing during the pre-robot session vs. differences of Z' between sessions. Data are presented as mean ± s.e.m.

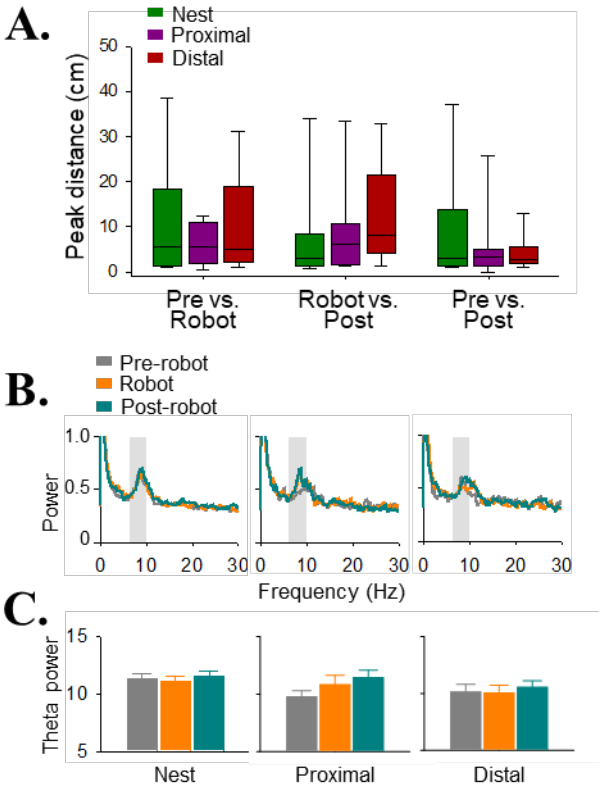


Figure 4.4. Differences of the peak distances and the theta power between sessions from amygdala-lesioned rats.
**(A)** Differences in peak distance between sessions. **(B)** The population-averaged power spectrums of the nest, proximal, and distal cells in the amygdala-lesioned rats.
**(C)** Comparisons of the theta band (6–10 Hz; gray sections in B) across the pre-robot, robot, and post-robot sessions. Data are represented as mean ± s.e.m.

Table 4.1. Firing properties of place cells during the pre-robot, robot, and post-robot sessions from rats with the amygdala lesion.

| Properties | | Pre-robot | Robot | Post-robot |
|---|---|---|---|---|
| Average firing rate (Hz) | Nest | 0.52 (0.21, 1.00) | 0.38 (0.24, 1.21) | 0.42 (0.24, 0.90) |
| | Proximal | 0.28 (0.18, 0.42) * | 0.29 (0.16, 0.62) | 0.27 (0.17, 0.52) |
| | Distal | 0.31 (0.20, 0.57) | 0.36 (0.14, 0.44) | 0.36 (0.21, 0.48) |
| Field size ($cm^2$) | Nest | 427.73 ± 28.09 | 420.53 ± 28.13 | 455.63 ± 29.30 |
| | Proximal | 398.12 ± 55.47 | 360.53 ± 52.55 | 310.76 ± 35.18 |
| | Distal | 588.75 ± 54.53 * # | 474.00 ± 53.71 | 551.25 ± 61.20 * ## |
| Peak rate (Hz) | Nest | 9.17 (4.00, 18.06) | 6.88 (2.67, 15.64) | 7.21 (3.06, 12.19) |
| | Proximal | 4.66 (2.87, 13.09) | 2.75 (0.87, 21.29) | 4.07 (1.84, 10.85) |
| | Distal | 8.38 (4.73, 13.18) ** # | 9.02 (4.28, 24.76) | 9.57 (4.65, 18.18) |
| Spatial info (bits/s) | Nest | 10.64 (5.30, 17.03) | 9.54 (5.29, 14.01) | 10.70 (4.65, 19.37) |
| | Proximal | 8.17 (3.26, 13.82) | 15.77 (3.80, 31.30) | 15.76 (8.65, 20.08) |
| | Distal | 1.06 (0.86, 2.01) ** ### | 1.23 (0.74, 3.69) ** ### | 1.60 (1.03, 2.74) ** ### |
| Running speed (cm/s) | Nest | 5.75 (4.55, 6.37) | 5.08 (3.50, 9.32) | 4.21 (3.30, 5.47) |
| | Proximal | 20.95 (20.16, 22.60)** | 21.22 (20.12, 22.45)** | 19.29 (17.34, 20.31)** |
| | Distal | 41.14 (38.28, 46.94) ** ### | 32.65 (28.58, 35.86) ** ### | 41.10 (32.64, 43.81) ** ### |

* $P < 0.05$; ** $P < 0.01$ compared to the nest cells. # $P < 0.05$; ## $P < 0.01$; ### $P < 0.001$ compared to the proximal cells.

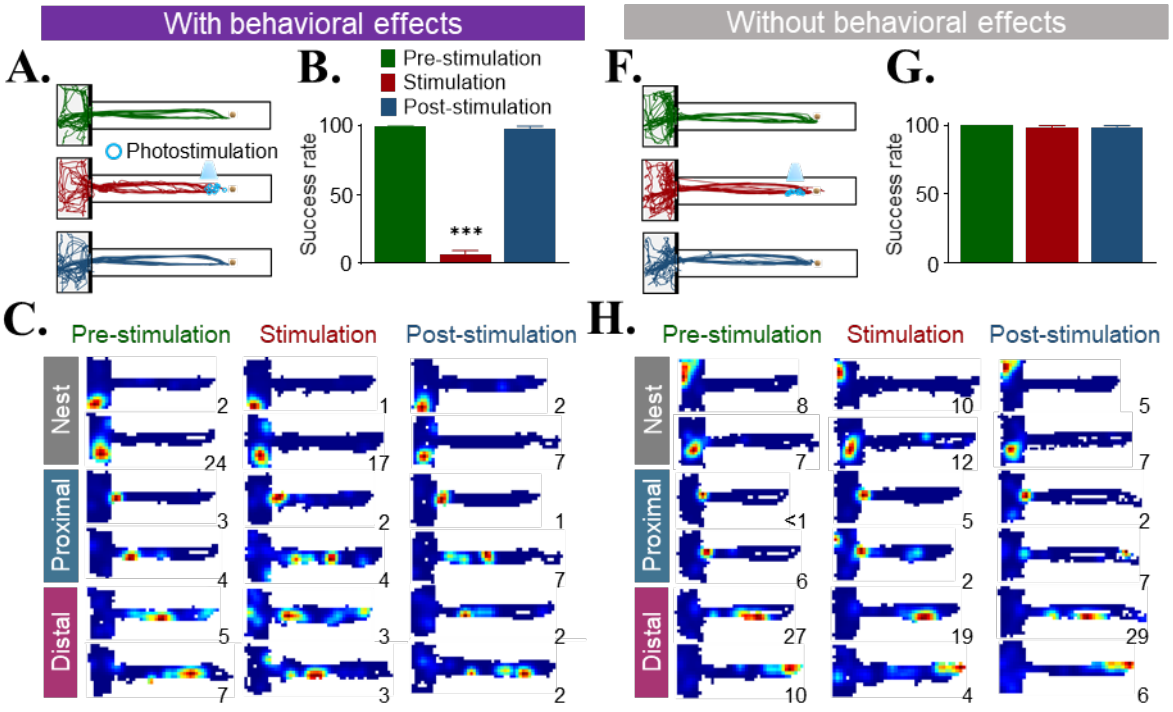


Figure 4.5. The effects of the optogenetic BA stimulation on behavior and place fields. **(A, F)** Representative trajectories during each session from a rat with behavioral effects **(A)** and from a rat without behavioral effects **(F)**. **(B, G)** Success rates of pellet retrieval during the stimulation session significantly decreased when rats showed behavioral effects to photostimulation **(B)** but not when rats did not show behavioral effects to photostimulation **(G)**. **(C, H)** Examples of place fields (with behavioral effects, **C**; without behavioral effects, **H**) from the nest, proximal, and distal cells during each session. The numerical value represents the peak firing rate for each session. *** $P < 0.001$.

multiple attempts to acquire a pellet because they succeeded in pellet retrieval (representative trajectory plots in Figure 4.5F). The success rates from all three sessions were not different in this group (Friedman test, $P > 0.999$; Figure 4.5G).

Hippocampal place cells were classified into three types; nest, proximal, and distal cells. Examples of place maps from rats with behavioral effects or without behavioral effects during each session are shown in Figure 4.5C and Figure 4.5H, respectively. Spatial correlations between the pre-stimulation and the stimulation sessions were decreased only in distal cells when the optogenetic manipulations worked (one-way ANOVA, $F_{2,250} = 3.559$, $P = 0.030$ using Bonferroni *post hoc* test; Figure 4.6A). On the other hand, rats without behavioral effects did not show difference in Z' between all cell types (one-way ANOVA, $F_{2,68} = 0.8399$, $P = 0.4362$; Figure 4.7A). Peak distances between the pre- and stimulation sessions were also significantly longer in distal cells when the rats responded to photostimulations (Kruskal-Wallis test, $P = 0.018$ using Dunn's multiple comparisons test; Figure 4.6B). In rats without behavioral effects, there was no difference in peak distance between the two sessions (one-way ANOVA, $F_{2,68} = 0.05118$, $P = 0.950$; Figure 4.7B). Figure 4.6C and Figure 4.7C show scatter plots displaying differences of Z' between sessions as a function of X positions of peak firing during the pre-stimulation session. The data from rats with behavioral effects indicates that differences in $Z'_{\text{pre vs. Robot}}$ are negatively correlated with the distances from the nest ($r = -0.1320$, $P = 0.0359$). However, this negative correlation was not found in rats without behavioral effects ($r = 0.06348$, $P = 0.5963$). Spatial correlations, peak distance, and scatter plots of distal cells from both groups were not different from the nest and proximal cells when they were compared between stimulation vs. post-stimulation or pre- vs. post-stimulation sessions. Other properties of place cells from rats with behavioral effects and from rats without behavioral effects are shown in

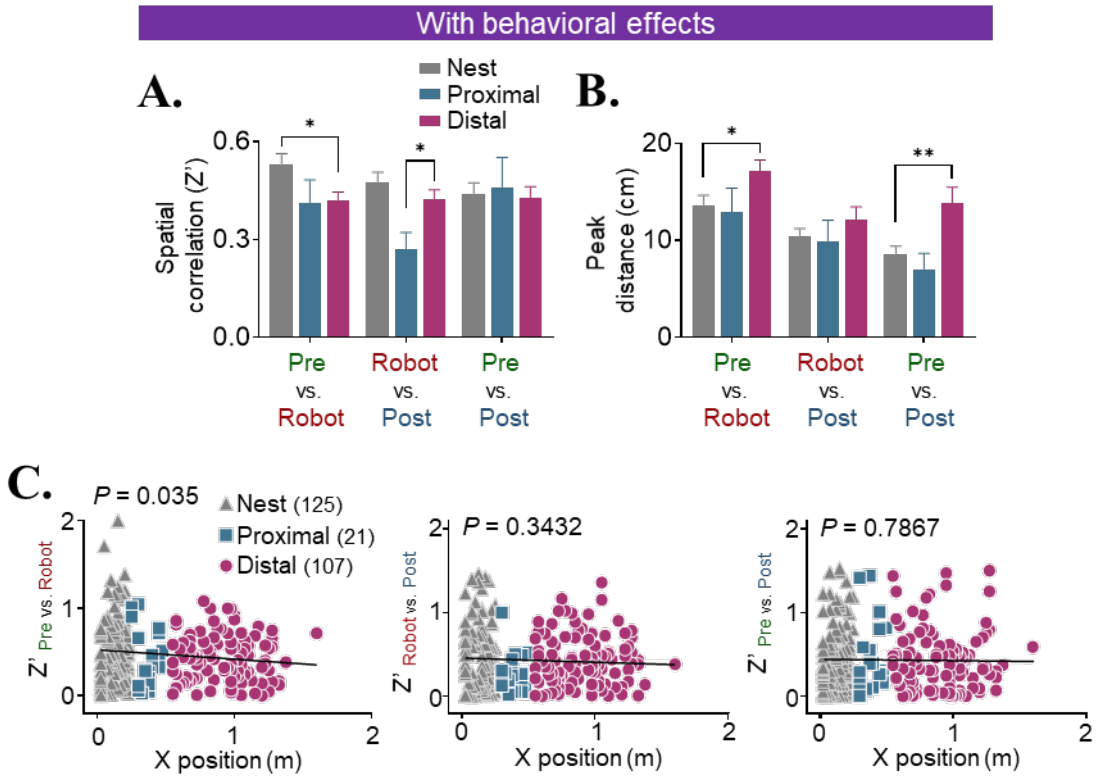


Figure 4.6. The effects of the optogenetic BA stimulation onto the place cells' stabilities in rats with behavioral responses.
**(A)** Differences in the pixel-by-pixel spatial correlations (Z') value between sessions. **(B)** Differences in peak distance between sessions. **(C)** Scatter plots displaying X positions of peak firing during the pre-robot session vs. differences of Z' between sessions. Data are presented as mean ± s.e.m. * $P < 0.05$; ** $P < 0.01$.

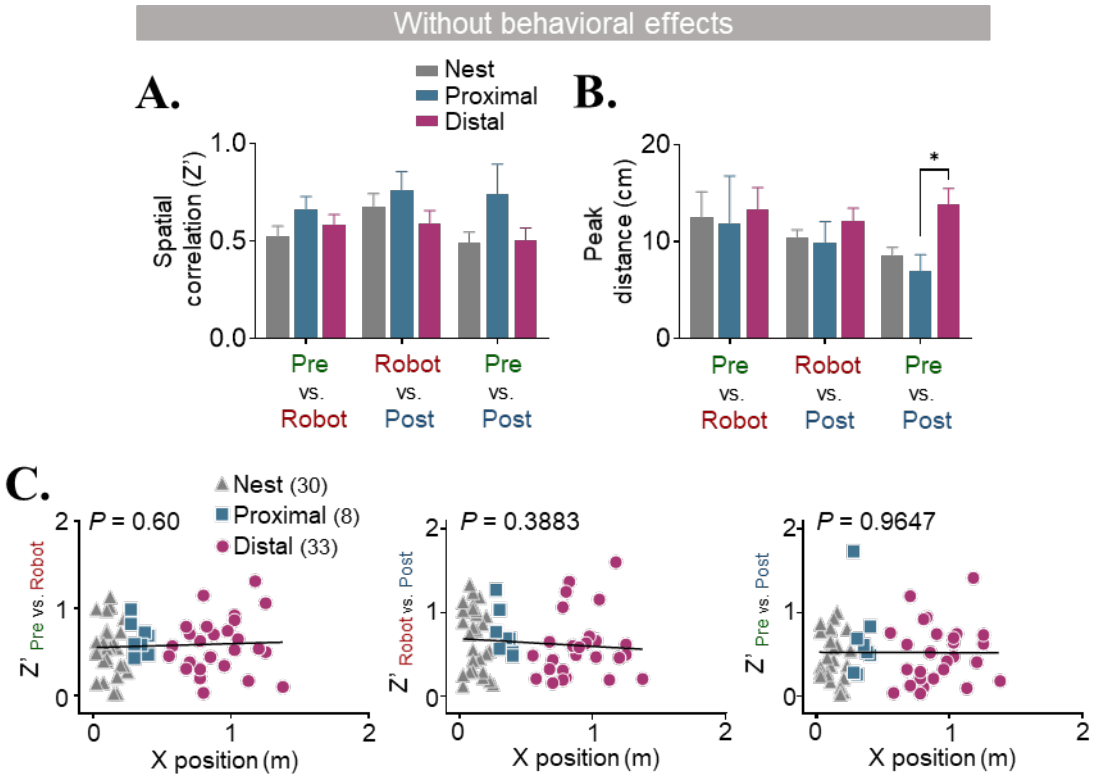


Figure 4.7. The effects of the optogenetic BA stimulation on the place cells' stabilities in rats without behavioral responses.
**(A)** Differences in the pixel-by-pixel spatial correlations (Z') value between sessions.
**(B)** Differences in peak distance between sessions. **(C)** Scatter plots displaying X positions of peak firing during the pre-robot session vs. differences of Z' between sessions. Data are presented as mean ± s.e.m. * $P < 0.05$.

Table 4.2 and Table 4.3, respectively. Therefore, it is concluded that the optogenetic stimulation was sufficient to induce remapping of the place cells only near the stimulation trigger zone.

*Optogenetic stimulation of the BA and LFPs in dHPC.*

To further investigate whether optogenetic stimulation induces different effects on LFPs in relation to behavioral responses, event-evoked LFP differences between rats with behavioral responses and rats without behavioral responses were compared. First, PSD was used to quantify the increased theta power during the stimulation session. When PSD was calculated to include the whole session (pre-stimulation, stimulation, and post-stimulation), there was a higher peak in the theta range during the stimulation session than during pre- and post-stimulation sessions only in rats with behavioral effects (peak at 8 Hz, Friedman test, $P < 0.001$ using Dunn's multiple comparisons test; Figure 4.8A). The sum of the percentage of theta was more during the stimulation session than the other two sessions (Friedman test, $P = 0.007$ using Dunn's multiple comparisons test; Figure 4.8A inserted bar graph). Conversely, rats without behavioral effects did not show a clear peak of the percentage in the theta range. The highest percentage in the theta range was at 6 Hz where the pre-stimulation had a significantly higher percentage than the other two sessions (repeated measures ANOVA, $F_{2,62} = 16.46$, $P < 0.001$ using Bonferroni *post hoc* test; Figure 4.8B). Total theta percentage was significantly higher in the pre-stimulation session when it compared to the post-stimulation session. There was no elevated percentage during the stimulation session (repeated measures ANOVA, $F_{2,62} = 6.620$, $P = 0.002$ using Bonferroni *post hoc* test; Figure 4.8B inserted bar graph).

Next, we focused our examination on the optogenetic stimulation effects of PSD only including 5 seconds after each stimulation. During this period, rats with behavioral effects

Table 4.2. Firing properties of place cells during the pre-stimulation, stimulation, and post-stimulation sessions from rats with behavioral effects.

| Properties | | Pre-robot | Robot | Post-robot |
|---|---|---|---|---|
| Average firing rate (Hz) | Nest | 0.76 (0.39, 1.41) | 0.42 (0.23, 0.89) | 0.40 (0.13, 0.78) |
| | Proximal | 0.59 (0.27, 1.36) | 0.43 (0.22, 0.72) | 0.26 (0.17, 0.94) |
| | Distal | 0.58 (0.31, 1.01) | 0.52 (0.33, 1.13) | 0.34 (0.17, 0.78) |
| Field size ($cm^2$) | Nest | 486 (378, 594) | 540 (423, 657) | 405 (288, 567) |
| | Proximal | 450 (261, 567) | 477 (333, 567) | 396 (315, 522) |
| | Distal | 567 (445.5, 688.5) ** # | 603 (477, 688.5) # | 540 (382.5, 679.5) *** # |
| Peak rate (Hz) | Nest | 6.03 (3.28, 11.37) | 4.94 (2.57, 9.56) | 4.39 (1.51, 7.31) |
| | Proximal | 4.51 (1.71, 8.37) | 3.39 (2.19, 6.11) | 3.45 (1.53, 9.42) |
| | Distal | 7.37 (3.55, 13.13) | 4.33 (2.54, 9.62) | 4.19 (2.03, 9.46) |
| Spatial info (bits/s) | Nest | 6.78 (4.00, 11.40) | 5.30 (3.45, 7.98) | 7.10 (4.25, 11.07) |
| | Proximal | 7.12 (3.71, 14.74) | 5.71 (3.96, 10.22) | 6.87 (5.33, 12.99) |
| | Distal | 2.62 (1.40, 5.16) *** ### | 4.77 (3.38, 6.90) | 4.01 (2.18, 7.74) *** ## |
| Running speed (cm/s) | Nest | 14.55 (12.66, 16.91) | 16.70 (12.83, 20.86) | 13.47 (11.04, 15.78) |
| | Proximal | 15.86 (13.54, 17.95) | 17.06 (12.86, 22.53) | 13.47 (11.85, 15.78) |
| | Distal | 15.41 (12.66, 16.26) | 17.06 (12.83, 21.82) | 13.47 (10.67, 16.61) |

** $P < 0.01$; *** $P < 0.001$ compared to the nest cells. # $P < 0.05$; ## $P < 0.01$; ### $P < 0.001$ compared to the proximal cells.

Table 4.3. Firing properties of place cells during the pre-stimulation, stimulation, and post-stimulation sessions from rats without behavioral effects.

| Properties | | Pre-robot | Robot | Post-robot |
|---|---|---|---|---|
| Average firing rate (Hz) | Nest | 0.55 (0.27, 0.97) | 0.62 (0.43, 1.55) | 0.70 (0.35, 1.17) |
| | Proximal | 0.54 (0.26, 0.82) | 0.62 (0.50, 0.79) | 0.70 (0.52, 0.96) |
| | Distal | 0.46 (0.34, 0.83) | 0.59 (0.30, 1.01) | 0.75 (0.35, 1.07) |
| Field size ($cm^2$) | Nest | 342 (175, 504) | 400.5 (256.5, 571.5) | 423 (270, 603) |
| | Proximal | 252 (189, 463) | 445.5 (272.25, 564.75) | 247.5 (229.5, 321.75) |
| | Distal | 486 (400.5, 711) * | 594 (400.5, 675) | 558 (346.5, 720) # |
| Peak rate (Hz) | Nest | 4.03 (1.53, 6.41) | 7.26 (3.96, 9.50) | 7.40 (3.96, 9.50) |
| | Proximal | 3.60 (2.59, 6.28) | 5.09 (2.41, 5.93) | 3.28 (2.28, 4.32) |
| | Distal | 4.94 (3.47, 8.02) *** # | 5.06 (3.44, 9.00) | 4.95 (3.31, 11.42) # |
| Spatial info (bits/s) | Nest | 11.93 (5.64, 21.33) | 6.21 (3.34, 12.68) | 6.56 (3.37, 15.44) |
| | Proximal | 17.39 (4.98, 23.18) | 12.02 (6.28, 19.04) | 23.96 (14.50, 35.41) |
| | Distal | 2.83 (1.53, 5.96) | 3.19 (2.11, 6.37) | 3.84 (1.65, 8.15) |
| Running speed (cm/s) | Nest | 15.17 (14.02, 16.03) | 13.51 (13.14, 13.79) | 11.63 (11.40, 11.83) |
| | Proximal | 15.72 (15.30, 15.80) | 13.79 (13.63, 13.96) | 11.83 (11.72, 12.22) |
| | Distal | 14.61 (13.47, 15.72) | 13.73 (13.51, 13.79) | 11.83 (11.63, 12.73) |

* $P < 0.05$; *** $P < 0.001$ compared to the nest cells. # $P < 0.05$ compared to the proximal cells.

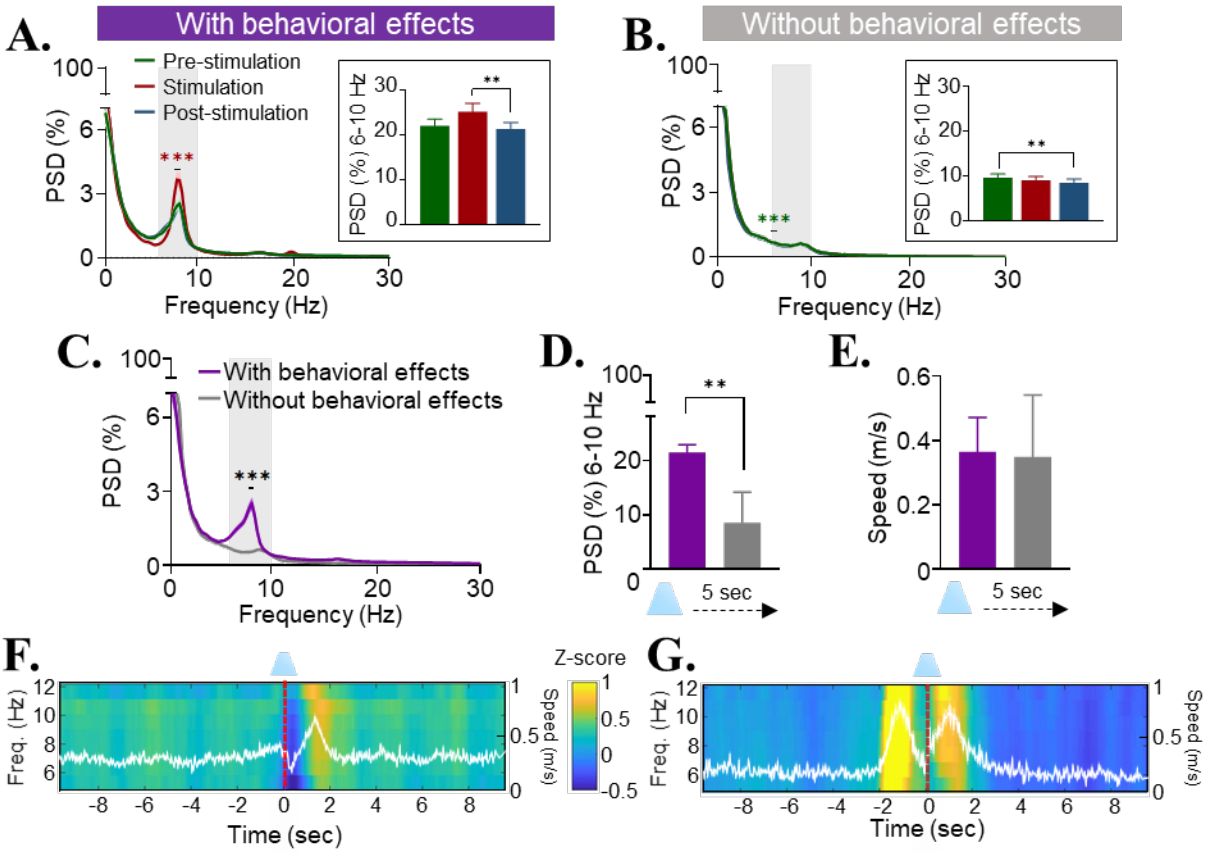


Figure 4.8. dHPC LFP responses changed by optogenetic stimulation of the BA.
**(A, B)** PSD of different frequency bands (1 - 30 Hz) was compared during each session (shown as % of total PSD) from rats with behavioral effects **(A)** or rats without behavioral effects **(B)**. The whole sessions were included. **(C)** PSD of different frequency bands was compared between rats with behavioral effects and without effects during 5 seconds after photostimulation. **(D)** The summed PSD percentages of the theta band were larger in rats with behavioral effects than in rats without behavioral effects. **(E)** During 5 seconds after each photostimulation, there was no difference in running speed between the two groups of rats. **(F, G)** Spectrograms of z-scored power in the theta bands during stimulation session from rats with behavioral effects **(F)** or without behavioral effects **(G)**. Data are presented as mean ± s.e.m. ** $P < 0.01$; *** $P < 0.001$.

showed a peak within the theta range, but rats without behavioral effects did not show stimulation effects in PSD (peak at 8 Hz; rats with effects, 2.504 ± 0.221%; rats without effects, 0.534 ± 0.054%; Unpaired *t* test, $t_{146} = 4.649$, $P < 0.001$; Figure 4.8C). A total percentage of theta was significantly higher in rats with behavioral effects (Unpaired *t* test, $t_{146} = 3.222$, $P = 0.002$; Figure 4.8D). Increased theta was not a side effect of running speed because the speed during the same period was not different between the two groups (Unpaired *t* test, $t_{296} = 0.07361$, $P = 0.941$; Figure 4.8E).

Figure 4.8F and G show spectrograms of z-scored power in the theta band during the stimulation session with rats showing behavioral effects and rats not showing behavioral effects, respectively (t = 0, stimulations). From both groups, increased running speed led to increased theta power. Overall (pre-10 s and post-10 s of the photostimulations), elevated theta power was observed in rats with behavioral effects compared to the rats without effects (averaged z-score, rats with effects, 0.274; rats without effects, 0.143). Interestingly, optogenetic stimulation in rats with behavioral effects also evoked a transient decrease of the LFPs in a short period of time, which was matched to the duration of the photostimulation. Decreased LFPs after the stimulations were not found in rats without behavioral effects. In summary, these results indicate that BA stimulation alters LFP activities in the dHPC.

*Optogenetic stimulation-evoked responses in place cells.*

To see more direct effects of BA stimulation on the place cells, we subsequently investigated whether BA stimulation evokes neuronal firing changes in dHPC place cells. Stimulation-evoked responses were identified by aligning activities to the stimulation events. Among 253 recorded place cells, 11% showed excited responses (n = 29) and 19% showed

inhibited responses to the photostimulations (n = 48). Six percent of the cells showed excitation and inhibition during the stimulations (bi-phasic, n = 14) (Figure 4.9A). Those responsive cell types (excitation, inhibition, or bi-phasic) showed significantly different z-scored firing rates compared to non-responsive cells (Kruskal-Wallis test, $P < 0.001$ using Dunn's multiple comparisons test; Figure 4.9B). Figure 4.9C displays representative cells that showed excitation (top row) and inhibition (bottom row) during the photostimulations. During the stimulation session, these cells also showed remapping compared to the pre-stimulation session. These results indicate that BA activation directly alters place cell firing.

Next, we tested whether stimulations evoked different responses among different place cell types. Interestingly, distal cells seemed to be affected more by the photostimulation than nest cells. Among excitation and inhibition cells, 52% and 65% were distal cells, respectively (excitation: nest, n = 14; proximal, n = 0; distal, n = 15; inhibition: nest, n = 14; proximal, n = 3; distal, n = 32; Figure 4.9D). These differences were reflected in the peak firing rate and the mean firing rate of each cell type. BA stimulation led to decreases in the peak firing rate of both nest and distal cells with a stronger effect in distal cells (nest: Wilcoxon matched-pairs signed rank test, $P = 0.021$; distal: Wilcoxon matched-pairs signed rank test, $P < 0.001$). However, in nest cells, a decrease of the peak firing rate also led to a decrease of the mean firing rate (Wilcoxon matched-pairs signed rank test, $P < 0.001$). This can be explained by the fact that BA stimulation produced rate remapping of nest cells. In distal cells, on the other hand, a reduced peak firing rate was not accompanied by a decrease of the mean firing rate. Speculatively, the cause of this effect is by increased firing rates other than the peak location, which can also be explained by disrupted place maps (global remapping).

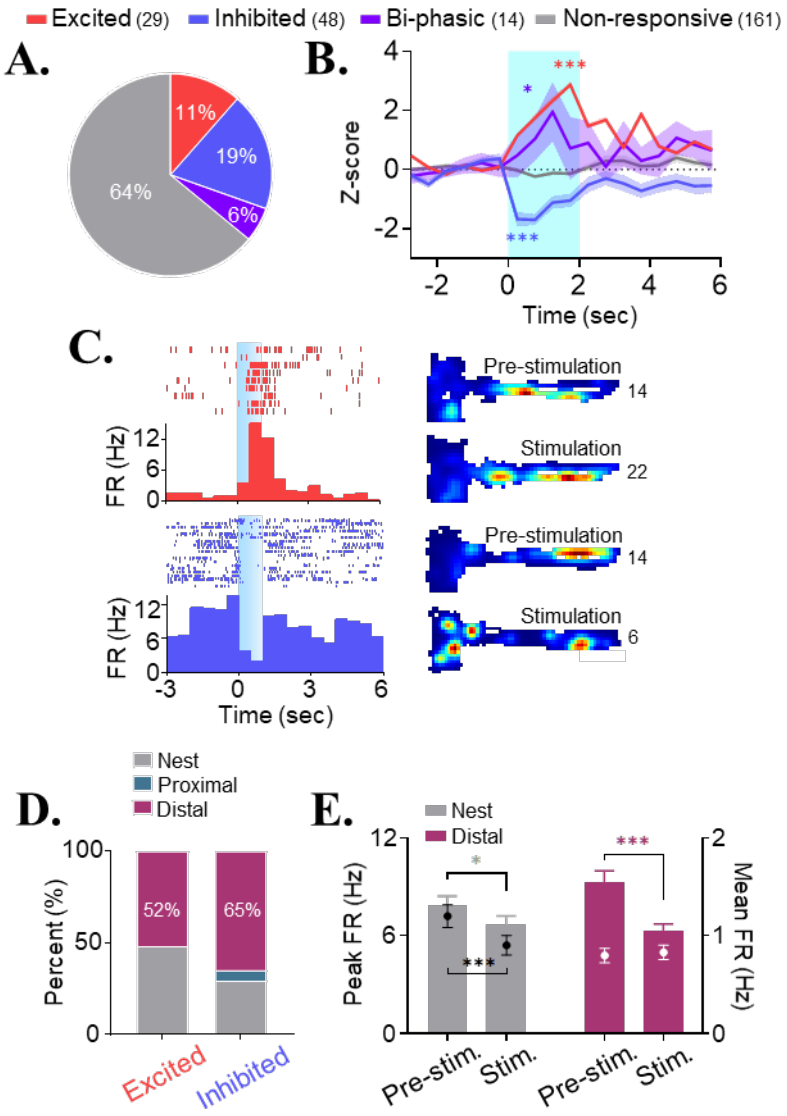


Figure 4.9. Optogenetic stimulation-evoked responses in place cells when the rats showed behavioral effects.
**(A)** Percentages of each responsive cell type. **(B)** Z-scored activities of each type of cells. **(C)** Representative excited (top row) and inhibited (bottom row) cells by photostimulations. Raster plots and peri event histograms (left column) and place fields (right column) during the pre-stimulation and stimulation sessions. Blue shaded area indicates photostimulation and the numerical value represents the peak firing rate for each session. **(D)** The number of the nest, proximal, and distal cells showed excitation or inhibition by the stimulations. **(E)** Showing peak firing rates (bar) and mean firing rates (circle) of the nest and distal cells during the pre-stimulation and stimulation sessions. Data are presented as mean ± s.e.m. * $P < 0.05$; *** $P < 0.001$.

## 4.4 DISCUSSION

Findings from chapter 4 indicate that having an intact amygdala is crucial for selecting adequate foraging behaviors in a risky situation as it helps to determine normal representations of a safety-danger boundary in the hippocampus. Absence of the amygdala led to expressions of inappropriate foraging behaviors when rats faced the robot predator and produced a failure of the dorsal hippocampus to change the representation of the context as well as increase theta oscillation selectively in distal cells. Furthermore, heightened activity of the amygdala induced defensive behaviors even without external threats. It also produced instability of place fields, especially near the stimulation zone, along with an increase of theta rhythms seen in LFPs. To cause instability in distal cells and increases in theta oscillations, the amygdala has to be activated enough to generate defensive behaviors. For instance, when the amygdala was stimulated under the threshold to show fleeing responses, there was no change in spatial representations during the stimulation session.

Previously, we reported that amygdala electrical stimulations induced remapping by the hippocampal place cells (E. J. Kim et al., 2012). The current study also found that the optogenetic stimulation of the amygdala induced remapping by place cells. However, there are fundamental differences in findings between the two studies attributed to different experimental procedures. From the Kim et al., 2012 study, rats were tested on open-field platforms, which were not divided into the nest and foraging zones. For electrical amygdala stimulation, rats were placed in an operant chamber and place cells were not recorded due to electrical interference of neural signals. These procedures, unfortunately, were unable to capture the real time changes caused by amygdala stimulation. To overcome these limitations, the current study used optogenetic stimulations that do not interfere with the neural signals. Using these techniques, the current study showed that a greater degree of remapping occurred in distal cells, which had place fields near the stimulation

trigger zone, than in nest cells, which had place fields in a safe area. This data suggests that BA stimulation causes remapping by the place cells that reflected a gradient of fear.

As we discussed in chapter 3, behavioral differences were observed when the rats interact with the robot predator and when only the BA is stimulated. There are also differences in spatial representations in dHPC; spatial correlations between the pre- and post-stimulation were decreased in all three cell types (Figure 2.6B vs. Figure 4.6A). These data indicate that remapping happened in dHPC during the post-stimulation session. The first possible reason is that there were differences in experimental contexts between the post-robot and post-stimulation sessions. During the post-robot session, the absence of the robot predator gives rats a visual cue that there will be no threat in contrast to the robot session. Physical differences of experimental settings between the robot and post-robot sessions enable different representations of the surrounding environments. However, during the post-stimulation session, spatial characteristics such as the testing apparatus were identical to the stimulation session. In this case, rats cannot predict whether they will receive another set of BA stimulation, and therefore spatial representation of the post-stimulation session seems to be a continuation of the stimulation session.

The second possible explanation is that repeated stimulations of the amygdala reset the representations of the space where the rats were previously. This interpretation becomes plausible because in some cases, repeated stimulations of the BA led to an occurrence of a seizure. This is indicative of a 'kindling effect', which is a phenomenon characterized by a gradual increase in seizure susceptibility due to the repeated application of sub-convulsant stimuli to specific brain regions (Bertram, 2007; Kalynchuk, 2000). Consistent with the amygdala being known as a source of seizure initiation (Meldrum, 1988), repeated BA stimulations in the current study provoked seizures in some rats. Kindling process accompanies not only behavioral effects such as

convulsion but also long-lasting modifications in neuronal structures and function (Goddard, 1983; Goddard et al., 1969). In the current study, even though rats that had seizures did not demonstrate seizures during stimulation testing, it cannot be ruled out that previous seizures induced long-lasting changes in neural functioning that persisted into stimulation testing, and that such changes affected the stability of place cells during the stimulation and post-stimulation sessions.

BA stimulation directly affects neuronal activities in dHPC. However, when we consider the latency of the responses in excited cells, we cannot conclude that only BA neurons directly projecting to the dHPC were stimulated. Among a total of 29 excited neurons, 21 neurons showed significant increases in firing rate at the second or later bin. This suggests that the response latency was over 0.5 s to the BA stimulation (data were binned at 0.5 s). This is too slow for monosynaptic connection because a delay between monosynaptically connected neurons is less than 15 ms (Fukuhara et al., 2013; Gonzalez-Burgos, Barrionuevo, & Lewis, 2000). One possible explanation is that the stimulation of the BA activates some other brain region(s) whose output arrives later at dHPC. Ventral hippocampus is a great candidate for a relay station. First, amygdala and vHPC share vigorous reciprocal connections (Pikkarainen, Ronkko, Savander, Insausti, & Pitkanen, 1999) and when it comes to formation of fear memory, the amygdala receives direct hippocampal input from the vHPC (Maren & Fanselow, 1995). Secondly, amygdala-vHPC connections modulate anxiety-related behaviors (Allsop et al., 2014; Beyeler et al., 2018; Felix-Ortiz et al., 2013). Combining these findings, stimulation of the amygdala excites vHPC which then leads to an increase of firing rate in dHPC.

BA stimulation-evoked inhibited cells showed a faster latency than excited cells but there are still possibilities that the inhibition was from di- or polysynaptic connections. In this case,

either direct or indirect inputs from the BA presumably reach interneurons in the dHPC to complete local inhibition.

As we found, stimulation of the BA produced two different types of remapping; rate remapping and global remapping (Colgin et al., 2008; Leutgeb et al., 2005). In nest cells, BA stimulation caused a decrease of both the peak and average firing rates but with the high spatial correlations, which manifests as rate remapping. Rate remapping is defined as when place cells substantially alter their firing rates, but the preferred locations remain unchanged. On the other hand, BA stimulation caused global remapping in distal cells, reflected in a decrease of spatial correlations. Global remapping refers to arbitrary changes in both firing rates and preferred locations of place cells.

Interestingly, BA stimulation decreased peak firing rates in both nest and distal cells. Thus, this indicates that heightened amygdalar activity reduces general responsiveness of place cells due to changes in internal state since there was no change in spatial configurations. Internal contextual cues can be shifted by negative events such as predatory threats, shocks, or electrical stimulation of the amygdala, which lead to remapping of the place cells (E. J. Kim et al., 2012; E. J. Kim et al., 2015; Moita et al., 2004; Wu et al., 2017). These results suggest that the hippocampus encodes not only spatial information including geometry and features (Anderson & Jeffery, 2003; R. U. Muller & Kubie, 1987), but also spatial ‘context’ information such as motivational/emotional valence and adaptive behaviors that are associated with that space.

# Chapter 5. GENERAL CONCLUSIONS

*Summary of results.*

The studies presented in this dissertation investigated whether the amygdala and hippocampus communicate while rats forage for food in a risky situation by encoding the safety-danger boundary. In chapter 2, we found that the amygdala neurons, especially the BA neurons, showed robust responses to either the pellet or the robot predator. Showing different neuronal activities to the threat or reward suggests that the BA encodes the valence of the events, not the movement velocity (Amir et al., 2015; Pare & Quirk, 2017). The amygdala also showed significantly increased theta and gamma power in response to the predator, which implicates a role for these rhythms in enhanced attention and arousal (Amir et al., 2018; Stujenske et al., 2014). Hippocampal place fields showed a different degree of remapping based on the distance from the threat source. During the robot session, place fields near the predator were remapped more than place fields inside the nest. This confirms that the hippocampus builds spatial representations that reflect a distance gradient of fear (E. J. Kim et al., 2015). Increased theta power was found in all three sessions, but the increased theta during the pre- and post-robot sessions were explained by the increased running speed. On the contrary, the increased theta during the robot session was not the outcome of increased running speed. Next, we found that the amygdala and hippocampus communicate with each other via spike synchrony at the time of robot interaction. Especially, distal place fields that showed spike synchrony with Robot cells tended to be remapped to a greater degree than any other cell type including nest cells and distal cells that did not show spike synchrony with Robot cells. These results suggest that the amygdala and hippocampus simultaneously process information relevant to situations where the rats need to exhibit optimal behavior during risky foraging.

In chapter 3, we studied whether the expression of defensive behaviors to the robot predator was due to the heightened activity of the amygdala. The heightened activity was generated by selective stimulation of the neurons in the BA using optogenetics. This resulted in pyramidal neurons in the BA excited by the photostimulation successfully inducing defensive behaviors including fleeing responses even without the explicit threat. These data suggest that the enhanced activity of the amygdala, which imitates the role of the predator in chapter 2, is necessary for the expression of defensive behaviors.

In chapter 4, we examined whether altered activity in the amygdala is necessary and sufficient to cause instability of the hippocampal place cells. Firstly, amygdala lesion led to no fear responses to the predator, remapping of the distal place fields, nor increased theta power by the predator. These results suggest that the amygdala is necessary to induce instability of place cells and theta increase. Secondly, we used optogenetics to artificially induce heighten activity in the amygdala, which successfully generated defensive behaviors without external threats. Selective stimulation of the BA also imitates the role of Robot cells. Our results showed that optogenetic stimulation produced instability of place fields, especially near the stimulation trigger zone, and an increase of the theta rhythms in LFPs. Interestingly, BA stimulation did not directly cause place fields instability because rats without behavioral effects to the BA stimulation did not show remapping of place fields. From these data, we can conclude that the amygdala stimulation was sufficient to induce instability of the place fields but only when it is stimulated at a high enough level to generate defensive behaviors.

*The safety-danger boundary by the amygdala and hippocampus*

Findings from this dissertation posit that the BA-dHPC pathway provides for safety-danger transitions in a risky foraging situation. The proposed model is shown in Figure 5.1.

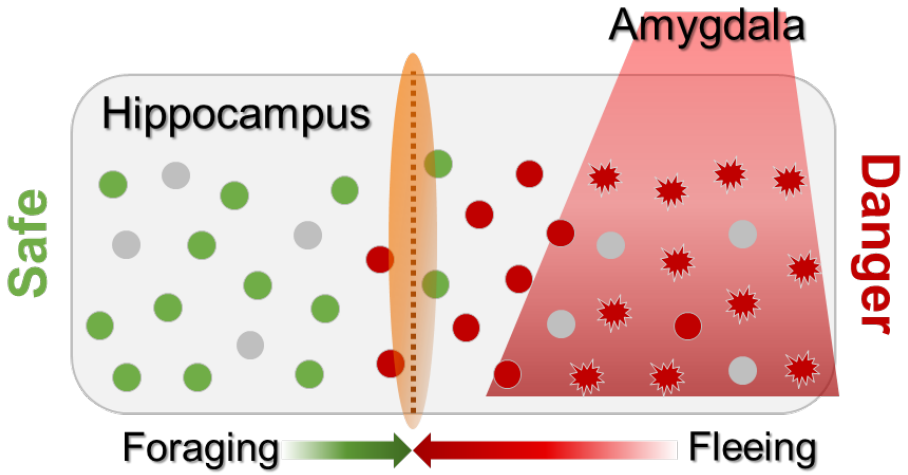


Figure 5.1. The model of the safety-danger boundary coded by the amygdala and hippocampus.

According to this model, the dHPC builds a spatial representation of the context through place cells activities. Without any threats, place cells have stable place fields (green). However, when the rat is confronted with the predator, some spatial representations become unstable (red). Under the threat, the amygdala sends fear signals directly (Rei et al., 2015) or indirectly (Pitkanen et al., 2000) to the hippocampus (red shaded area) to alter the spatial representation. The spatial representation has two zones; safe area (i.e., nest) and dangerous area (i.e., robot predator trigger zone). Place fields in the safe area do not receive input from the amygdala, so they remain stable. On the other hand, place fields in the dangerous area become unstable, and cells that receive direct amygdalar inputs become even more unstable.

In conclusion, the hippocampus sets a safety-danger boundary (orange line and shaded area) utilizing the fear signal that comes from the amygdala. This boundary allows an organism to

select optimal behavior during risky foraging situations, and this is the how the amygdala and the hippocampus will normally interact. However, when the amygdala and hippocampus are dysfunctional, this boundary becomes blurry, perhaps explaining why patients with fear disorders tend to exhibit fear even when in safe situations. Conversely, it follows that not having a clear safety-danger boundary produces maladaptive fear behavior.

# BIBLIOGRAPHY

Allikmets, L. (1966). [Behavioral responses to electric stimulation of the amygdaloid complex of the forebrain in cats]. *Zh Vyssh Nerv Deiat Im I P Pavlova, 16*(6), 1082-1091.

Allsop, S. A., Vander Weele, C. M., Wichmann, R., & Tye, K. M. (2014). Optogenetic insights on the relationship between anxiety-related behaviors and social deficits. *Front Behav Neurosci, 8*, 241. doi:10.3389/fnbeh.2014.00241

Amano, T., Duvarci, S., Popa, D., & Pare, D. (2011). The fear circuit revisited: contributions of the basal amygdala nuclei to conditioned fear. *J Neurosci, 31*(43), 15481-15489. doi:10.1523/JNEUROSCI.3410-11.2011

Amir, A., Headley, D. B., Lee, S. C., Haufler, D., & Pare, D. (2018). Vigilance-Associated Gamma Oscillations Coordinate the Ensemble Activity of Basolateral Amygdala Neurons. *Neuron, 97*(3), 656-669 e657. doi:10.1016/j.neuron.2017.12.035

Amir, A., Lee, S. C., Headley, D. B., Herzallah, M. M., & Pare, D. (2015). Amygdala Signaling during Foraging in a Hazardous Environment. *J Neurosci, 35*(38), 12994-13005. doi:10.1523/JNEUROSCI.0407-15.2015

Amorapanth, P., LeDoux, J. E., & Nader, K. (2000). Different lateral amygdala outputs mediate reactions and actions elicited by a fear-arousing stimulus. *Nat Neurosci, 3*(1), 74-79. doi:10.1038/71145

Anderson, M. I., & Jeffery, K. J. (2003). Heterogeneous modulation of place cell firing by changes in context. *J Neurosci, 23*(26), 8827-8835.

Anglada-Figueroa, D., & Quirk, G. J. (2005). Lesions of the basal amygdala block expression of conditioned fear but not extinction. *J Neurosci, 25*(42), 9680-9685. doi:10.1523/JNEUROSCI.2600-05.2005

Baas, D., Aleman, A., & Kahn, R. S. (2004). Lateralization of amygdala activation: a systematic review of functional neuroimaging studies. *Brain Res Brain Res Rev, 45*(2), 96-103. doi:10.1016/j.brainresrev.2004.02.004

Baker, K. B., & Kim, J. J. (2004). Amygdalar lateralization in fear conditioning: evidence for greater involvement of the right amygdala. *Behav Neurosci, 118*(1), 15-23. doi:10.1037/0735-7044.118.1.15

Bannerman, D. M., Grubb, M., Deacon, R. M. J., Yee, B. K., Feldon, J., & Rawlins, J. N. P. (2003). Ventral hippocampal lesions affect anxiety but not spatial learning. *Behavioural Brain Research, 139*(1-2), 197-213. doi:10.1016/s0166-4328(02)00268-1

Bazelot, M., Bocchio, M., Kasugai, Y., Fischer, D., Dodson, P. D., Ferraguti, F., & Capogna, M. (2015). Hippocampal Theta Input to the Amygdala Shapes Feedforward Inhibition to

Gate Heterosynaptic Plasticity. *Neuron, 87*(6), 1290-1303. doi:10.1016/j.neuron.2015.08.024

Belova, M. A., Paton, J. J., Morrison, S. E., & Salzman, C. D. (2007). Expectation modulates neural responses to pleasant and aversive stimuli in primate amygdala. *Neuron, 55*(6), 970-984. doi:10.1016/j.neuron.2007.08.004

Bertram, E. (2007). The relevance of kindling for human epilepsy. *Epilepsia, 48 Suppl 2*, 65-74.

Beyeler, A., Chang, C. J., Silvestre, M., Leveque, C., Namburi, P., Wildes, C. P., & Tye, K. M. (2018). Organization of Valence-Encoding and Projection-Defined Neurons in the Basolateral Amygdala. *Cell Rep, 22*(4), 905-918. doi:10.1016/j.celrep.2017.12.097

Bissiere, S., Humeau, Y., & Luthi, A. (2003). Dopamine gates LTP induction in lateral amygdala by suppressing feedforward inhibition. *Nat Neurosci, 6*(6), 587-592. doi:10.1038/nn1058

Blair, H. T., Huynh, V. K., Vaz, V. T., Van, J., Patel, R. R., Hiteshi, A. K., . . . Tarpley, J. W. (2005). Unilateral storage of fear memories by the amygdala. *J Neurosci, 25*(16), 4198-4205. doi:10.1523/JNEUROSCI.0674-05.2005

Blanchard, D. C., Blanchard, R. J., Lee, E. M. C., & Fukunaga, K. K. (1977). Movement arrest and the hippocampus. *Physiological Psychology, 5*(3), 5. doi:https://doi.org/10.3758/BF03335340

Blanchard, R. J., & Blanchard, D. C. (1972). Effects of hippocampal lesions on the rat's reaction to a cat. *J Comp Physiol Psychol, 78*(1), 77-82.

Blanchard, R. J., & Blanchard, D. C. (1989). Attack and defense in rodents as ethoexperimental models for the study of emotion. *Prog Neuropsychopharmacol Biol Psychiatry, 13 Suppl*, S3-14.

Blanchard, R. J., Blanchard, D. C., Rodgers, J., & Weiss, S. M. (1990). The characterization and modelling of antipredator defensive behavior. *Neurosci Biobehav Rev, 14*(4), 463-472.

Burgos-Robles, A., Vidal-Gonzalez, I., & Quirk, G. J. (2009). Sustained conditioned responses in prelimbic prefrontal neurons are correlated with fear expression and extinction failure. *J Neurosci, 29*(26), 8474-8482. doi:10.1523/JNEUROSCI.0378-09.2009

Choi, J. S., & Kim, J. J. (2010). Amygdala regulates risk of predation in rats foraging in a dynamic fear environment. *Proc Natl Acad Sci U S A, 107*(50), 21773-21777. doi:10.1073/pnas.1010079108

Ciocchi, S., Herry, C., Grenier, F., Wolff, S. B., Letzkus, J. J., Vlachos, I., . . . Luthi, A. (2010). Encoding of conditioned fear in central amygdala inhibitory circuits. *Nature, 468*(7321), 277-282. doi:10.1038/nature09559

Colgin, L. L., Moser, E. I., & Moser, M. B. (2008). Understanding memory through hippocampal remapping. *Trends Neurosci, 31*(9), 469-477. doi:10.1016/j.tins.2008.06.008

Collins, D. R., & Pare, D. (2000). Differential fear conditioning induces reciprocal changes in the sensory responses of lateral amygdala neurons to the CS(+) and CS(-). *Learn Mem, 7*(2), 97-103.

Corcoran, K. A., & Maren, S. (2001). Hippocampal inactivation disrupts contextual retrieval of fear memory after extinction. *J Neurosci, 21*(5), 1720-1726.

Deisseroth, K., Feng, G., Majewska, A. K., Miesenbock, G., Ting, A., & Schnitzer, M. J. (2006). Next-generation optical technologies for illuminating genetically targeted brain circuits. *J Neurosci, 26*(41), 10380-10386. doi:10.1523/JNEUROSCI.3863-06.2006

Depaulis, A., Keay, K. A., & Bandler, R. (1992). Longitudinal neuronal organization of defensive reactions in the midbrain periaqueductal gray region of the rat. *Exp Brain Res, 90*(2), 307-318.

Di Ciano, P., & Everitt, B. J. (2004). Direct interactions between the basolateral amygdala and nucleus accumbens core underlie cocaine-seeking behavior by rats. *J Neurosci, 24*(32), 7167-7173. doi:10.1523/JNEUROSCI.1581-04.2004

Do-Monte, F. H., Manzano-Nieves, G., Quinones-Laracuente, K., Ramos-Medina, L., & Quirk, G. J. (2015). Revisiting the role of infralimbic cortex in fear extinction with optogenetics. *J Neurosci, 35*(8), 3607-3615. doi:10.1523/JNEUROSCI.3137-14.2015

Duvarci, S., & Pare, D. (2014). Amygdala microcircuits controlling learned fear. *Neuron, 82*(5), 966-980. doi:10.1016/j.neuron.2014.04.042

Duvarci, S., Popa, D., & Pare, D. (2011). Central amygdala activity during fear conditioning. *J Neurosci, 31*(1), 289-294. doi:10.1523/JNEUROSCI.4985-10.2011

Everitt, B. J., Parkinson, J. A., Olmstead, M. C., Arroyo, M., Robledo, P., & Robbins, T. W. (1999). Associative processes in addiction and reward. The role of amygdala-ventral striatal subsystems. *Ann N Y Acad Sci, 877*, 412-438.

Fanselow, M. S., & Dong, H. W. (2010). Are the dorsal and ventral hippocampus functionally distinct structures? *Neuron, 65*(1), 7-19. doi:10.1016/j.neuron.2009.11.031

Felix-Ortiz, A. C., Beyeler, A., Seo, C., Leppla, C. A., Wildes, C. P., & Tye, K. M. (2013). BLA to vHPC inputs modulate anxiety-related behaviors. *Neuron, 79*(4), 658-664. doi:10.1016/j.neuron.2013.06.016

Fenton, A. A., Kao, H. Y., Neymotin, S. A., Olypher, A., Vayntrub, Y., Lytton, W. W., & Ludvig, N. (2008). Unmasking the CA1 ensemble place code by exposures to small and large environments: more place cells and multiple, irregularly arranged, and expanded place fields in the larger space. *J Neurosci, 28*(44), 11250-11262. doi:10.1523/JNEUROSCI.2862-08.2008

Ferrero, D. M., Lemon, J. K., Fluegge, D., Pashkovski, S. L., Korzan, W. J., Datta, S. R., . . . Liberles, S. D. (2011). Detection and avoidance of a carnivore odor by prey. *Proc Natl Acad Sci U S A, 108*(27), 11235-11240. doi:10.1073/pnas.1103317108

Fukuhara, K., Imai, F., Ladle, D. R., Katayama, K., Leslie, J. R., Arber, S., . . . Yoshida, Y. (2013). Specificity of monosynaptic sensory-motor connections imposed by repellent Sema3E-PlexinD1 signaling. *Cell Rep, 5*(3), 748-758. doi:10.1016/j.celrep.2013.10.005

Gale, G. D., Anagnostaras, S. G., Godsil, B. P., Mitchell, S., Nozawa, T., Sage, J. R., . . . Fanselow, M. S. (2004). Role of the basolateral amygdala in the storage of fear memories across the adult lifetime of rats. *J Neurosci, 24*(15), 3810-3815. doi:10.1523/JNEUROSCI.4100-03.2004

Geisler, C., Robbe, D., Zugaro, M., Sirota, A., & Buzsaki, G. (2007). Hippocampal place cell assemblies are speed-controlled oscillators. *Proc Natl Acad Sci U S A, 104*(19), 8149-8154. doi:10.1073/pnas.0610121104

Gewirtz, J. C., McNish, K. A., & Davis, M. (2000). Is the hippocampus necessary for contextual fear conditioning? *Behav Brain Res, 110*(1-2), 83-95.

Glascher, J., & Adolphs, R. (2003). Processing of the arousal of subliminal and supraliminal emotional stimuli by the human amygdala. *J Neurosci, 23*(32), 10274-10282.

Goddard, G. V. (1983). The kindling model of epilepsy. *Trendsin Neurosciences, 6*, 5. doi:https://doi.org/10.1016/0166-2236(83)90118-2

Goddard, G. V., McIntyre, D. C., & Leech, C. K. (1969). A permanent change in brain function resulting from daily electrical stimulation. *Exp Neurol, 25*(3), 295-330.

Gonzalez-Burgos, G., Barrionuevo, G., & Lewis, D. A. (2000). Horizontal synaptic connections in monkey prefrontal cortex: an in vitro electrophysiological study. *Cereb Cortex, 10*(1), 82-92.

Goosens, K. A., & Maren, S. (2001). Contextual and auditory fear conditioning are mediated by the lateral, basal, and central amygdaloid nuclei in rats. *Learn Mem, 8*(3), 148-155. doi:10.1101/lm.37601

Goosens, K. A., & Maren, S. (2003). Pretraining NMDA receptor blockade in the basolateral complex, but not the central nucleus, of the amygdala prevents savings of conditional fear. *Behav Neurosci, 117*(4), 738-750.

Gore, F., Schwartz, E. C., Brangers, B. C., Aladi, S., Stujenske, J. M., Likhtik, E., . . . Axel, R. (2015). Neural Representations of Unconditioned Stimuli in Basolateral Amygdala Mediate Innate and Learned Responses. *Cell, 162*(1), 134-145. doi:10.1016/j.cell.2015.06.027

Goshen, I., Brodsky, M., Prakash, R., Wallace, J., Gradinaru, V., Ramakrishnan, C., & Deisseroth, K. (2011). Dynamics of retrieval strategies for remote memories. *Cell, 147*(3), 678-689. doi:10.1016/j.cell.2011.09.033

Gray, T. S., & Magnuson, D. J. (1992). Peptide immunoreactive neurons in the amygdala and the bed nucleus of the stria terminalis project to the midbrain central gray in the rat. *Peptides, 13*(3), 451-460.

Gupta, A. S., van der Meer, M. A., Touretzky, D. S., & Redish, A. D. (2012). Segmentation of spatial experience by hippocampal theta sequences. *Nat Neurosci, 15*(7), 1032-1039. doi:10.1038/nn.3138

Hampson, R. E., Heyser, C. J., & Deadwyler, S. A. (1993). Hippocampal cell firing correlates of delayed-match-to-sample performance in the rat. *Behav Neurosci, 107*(5), 715-739.

Hasselmo, M. E. (2005). What is the function of hippocampal theta rhythm?--Linking behavioral data to phasic properties of field potential and unit recording data. *Hippocampus, 15*(7), 936-949. doi:10.1002/hipo.20116

Haubensak, W., Kunwar, P. S., Cai, H., Ciocchi, S., Wall, N. R., Ponnusamy, R., . . . Anderson, D. J. (2010). Genetic dissection of an amygdala microcircuit that gates conditioned fear. *Nature, 468*(7321), 270-276. doi:10.1038/nature09553

Herry, C., Ciocchi, S., Senn, V., Demmou, L., Muller, C., & Luthi, A. (2008). Switching on and off fear by distinct neuronal circuits. *Nature, 454*(7204), 600-606. doi:10.1038/nature07166

Hill, A. J., & Best, P. J. (1981). Effects of deafness and blindness on the spatial correlates of hippocampal unit activity in the rat. *Exp Neurol, 74*(1), 204-217.

Huberman, A. D., Wei, W., Elstrott, J., Stafford, B. K., Feller, M. B., & Barres, B. A. (2009). Genetic identification of an On-Off direction-selective retinal ganglion cell subtype reveals a layer-specific subcortical map of posterior motion. *Neuron, 62*(3), 327-334. doi:10.1016/j.neuron.2009.04.014

Huff, M. L., Miller, R. L., Deisseroth, K., Moorman, D. E., & LaLumiere, R. T. (2013). Posttraining optogenetic manipulations of basolateral amygdala activity modulate consolidation of inhibitory avoidance memory in rats. *Proc Natl Acad Sci U S A, 110*(9), 3597-3602. doi:10.1073/pnas.1219593110

Johansen, J. P., Hamanaka, H., Monfils, M. H., Behnia, R., Deisseroth, K., Blair, H. T., & LeDoux, J. E. (2010). Optical activation of lateral amygdala pyramidal cells instructs associative fear learning. *Proc Natl Acad Sci U S A, 107*(28), 12692-12697. doi:10.1073/pnas.1002418107

Jung, M. W., Wiener, S. I., & McNaughton, B. L. (1994). Comparison of spatial firing characteristics of units in dorsal and ventral hippocampus of the rat. *J Neurosci, 14*(12), 7347-7356.

Kalynchuk, L. E. (2000). Long-term amygdala kindling in rats as a model for the study of interictal emotionality in temporal lobe epilepsy. *Neurosci Biobehav Rev, 24*(7), 691-704.

Kemp, I. R., & Kaada, B. R. (1975). The relation of hippocampal theta activity to arousal, attentive behaviour and somato-motor movements in unrestrained cats. *Brain Res, 95*(2-3), 323-342.

Kheirbek, M. A., Drew, L. J., Burghardt, N. S., Costantini, D. O., Tannenholz, L., Ahmari, S. E., . . . Hen, R. (2013). Differential control of learning and anxiety along the dorsoventral axis of the dentate gyrus. *Neuron, 77*(5), 955-968. doi:10.1016/j.neuron.2012.12.038

Kim, E. J., Horovitz, O., Pellman, B. A., Tan, L. M., Li, Q., Richter-Levin, G., & Kim, J. J. (2013). Dorsal periaqueductal gray-amygdala pathway conveys both innate and learned fear responses in rats. *Proc Natl Acad Sci U S A, 110*(36), 14795-14800. doi:10.1073/pnas.1310845110

Kim, E. J., Kim, E. S., Park, M., Cho, J., & Kim, J. J. (2012). Amygdalar stimulation produces alterations on firing properties of hippocampal place cells. *J Neurosci, 32*(33), 11424-11434. doi:10.1523/JNEUROSCI.1108-12.2012

Kim, E. J., Kong, M. S., Park, S. G., Mizumori, S. J. Y., Cho, J., & Kim, J. J. (2018). Dynamic coding of predatory information between the prelimbic cortex and lateral amygdala in foraging rats. *Sci Adv, 4*(4), eaar7328. doi:10.1126/sciadv.aar7328

Kim, E. J., Park, M., Kong, M. S., Park, S. G., Cho, J., & Kim, J. J. (2015). Alterations of hippocampal place cells in foraging rats facing a "predatory" threat. *Curr Biol, 25*(10), 1362-1367. doi:10.1016/j.cub.2015.03.048

Kim, J., Pignatelli, M., Xu, S., Itohara, S., & Tonegawa, S. (2016). Antagonistic negative and positive neurons of the basolateral amygdala. *Nat Neurosci, 19*(12), 1636-1646. doi:10.1038/nn.4414

Kim, J. J., & Fanselow, M. S. (1992). Modality-specific retrograde amnesia of fear. *Science, 256*(5057), 675-677.

Kim, J. J., Lee, H. J., Welday, A. C., Song, E., Cho, J., Sharp, P. E., . . . Blair, H. T. (2007). Stress-induced alterations in hippocampal plasticity, place cells, and spatial memory. *Proc Natl Acad Sci U S A, 104*(46), 18297-18302. doi:10.1073/pnas.0708644104

Kim, J. J., Rison, R. A., & Fanselow, M. S. (1993). Effects of amygdala, hippocampus, and periaqueductal gray lesions on short- and long-term contextual fear. *Behav Neurosci, 107*(6), 1093-1098.

Kim, N., Kong, M. S., Jo, K. I., Kim, E. J., & Choi, J. S. (2015). Increased tone-offset response in the lateral nucleus of the amygdala underlies trace fear conditioning. *Neurobiol Learn Mem, 126*, 7-17. doi:10.1016/j.nlm.2015.10.010

Kjelstrup, K. G., Tuvnes, F. A., Steffenach, H. A., Murison, R., Moser, E. I., & Moser, M. B. (2002). Reduced fear expression after lesions of the ventral hippocampus. *Proc Natl Acad Sci U S A, 99*(16), 10825-10830. doi:10.1073/pnas.152112399

Klimesch, W. (1999). EEG alpha and theta oscillations reflect cognitive and memory performance: a review and analysis. *Brain Res Brain Res Rev, 29*(2-3), 169-195.

Klüver, H., & Bucy, P. C. (1937). "Psychic blindness" and other symptoms following bilateral temporal lobectomy in Rhesus monkeys. *American Journal of Physiology, 119*, 2.

Knapska, E., Radwanska, K., Werka, T., & Kaczmarek, L. (2007). Functional internal complexity of amygdala: focus on gene activity mapping after behavioral training and drugs of abuse. *Physiol Rev, 87*(4), 1113-1173. doi:10.1152/physrev.00037.2006

Krettek, J. E., & Price, J. L. (1978). A description of the amygdaloid complex in the rat and cat with observations on intra-amygdaloid axonal connections. *J Comp Neurol, 178*(2), 255-280. doi:10.1002/cne.901780205

Lalumiere, R. T. (2014). Optogenetic dissection of amygdala functioning. *Front Behav Neurosci, 8*, 107. doi:10.3389/fnbeh.2014.00107

Lanteaume, L., Khalfa, S., Regis, J., Marquis, P., Chauvel, P., & Bartolomei, F. (2007). Emotion induction after direct intracerebral stimulations of human amygdala. *Cereb Cortex, 17*(6), 1307-1313. doi:10.1093/cercor/bhl041

Lavond, D. G., Kim, J. J., & Thompson, R. F. (1993). Mammalian brain substrates of aversive classical conditioning. *Annu Rev Psychol, 44*, 317-342. doi:10.1146/annurev.ps.44.020193.001533

LeDoux, J. E. (2000). Emotion circuits in the brain. *Annu Rev Neurosci, 23*, 155-184. doi:10.1146/annurev.neuro.23.1.155

Letzkus, J. J., Wolff, S. B., Meyer, E. M., Tovote, P., Courtin, J., Herry, C., & Luthi, A. (2011). A disinhibitory microcircuit for associative fear learning in the auditory cortex. *Nature, 480*(7377), 331-335. doi:10.1038/nature10674

Leutgeb, S., Leutgeb, J. K., Barnes, C. A., Moser, E. I., McNaughton, B. L., & Moser, M. B. (2005). Independent codes for spatial and episodic memory in hippocampal neuronal ensembles. *Science, 309*(5734), 619-623. doi:10.1126/science.1114037

Lu, X., & Bilkey, D. K. (2010). The velocity-related firing property of hippocampal place cells is dependent on self-movement. *Hippocampus, 20*(5), 573-583. doi:10.1002/hipo.20666

Maren, S., & Fanselow, M. S. (1995). Synaptic plasticity in the basolateral amygdala induced by hippocampal formation stimulation in vivo. *J Neurosci, 15*(11), 7548-7564.

Maren, S., & Fanselow, M. S. (1997). Electrolytic lesions of the fimbria/fornix, dorsal hippocampus, or entorhinal cortex produce anterograde deficits in contextual fear conditioning in rats. *Neurobiol Learn Mem, 67*(2), 142-149. doi:10.1006/nlme.1996.3752

Maren, S., & Quirk, G. J. (2004). Neuronal signalling of fear memory. *Nat Rev Neurosci, 5*(11), 844-852. doi:10.1038/nrn1535

Maren, S., Yap, S. A., & Goosens, K. A. (2001). The amygdala is essential for the development of neuronal plasticity in the medial geniculate nucleus during auditory fear conditioning in rats. *J Neurosci, 21*(6), RC135.

Markus, E. J., Barnes, C. A., McNaughton, B. L., Gladden, V. L., & Skaggs, W. E. (1994). Spatial information content and reliability of hippocampal CA1 neurons: effects of visual input. *Hippocampus, 4*(4), 410-421. doi:10.1002/hipo.450040404

Maurer, A. P., Burke, S. N., Lipa, P., Skaggs, W. E., & Barnes, C. A. (2012). Greater running speeds result in altered hippocampal phase sequence dynamics. *Hippocampus, 22*(4), 737-747. doi:10.1002/hipo.20936

McAllister, W. R., McAllister, D. E., Scoles, M. T., & Hampton, S. R. (1986). Persistence of fear-reducing behavior: relevance for the conditioning theory of neurosis. *J Abnorm Psychol, 95*(4), 365-372.

McDonald, A. J. (1982). Neurons of the lateral and basolateral amygdaloid nuclei: a Golgi study in the rat. *J Comp Neurol, 212*(3), 293-312. doi:10.1002/cne.902120307

McNaughton, N., & Corr, P. J. (2004). A two-dimensional neuropsychology of defense: fear/anxiety and defensive distance. *Neurosci Biobehav Rev, 28*(3), 285-305. doi:10.1016/j.neubiorev.2004.03.005

Meldrum, B. S. F., J.A.; Weiser H.G. (1988). *Anatomy of epileptogenesis* (Vol. 6): John Libbey.

Mizumori, S. J. Y. (2008). *Hippocampal place fields: relavance to learning and memory*: Oxford scholarship online.

Moita, M. A., Rosis, S., Zhou, Y., LeDoux, J. E., & Blair, H. T. (2004). Putting fear in its place: remapping of hippocampal place cells during fear conditioning. *J Neurosci, 24*(31), 7015-7023. doi:10.1523/JNEUROSCI.5492-03.2004

Muller, J., Corodimas, K. P., Fridel, Z., & LeDoux, J. E. (1997). Functional inactivation of the lateral and basal nuclei of the amygdala by muscimol infusion prevents fear conditioning to an explicit conditioned stimulus and to contextual stimuli. *Behav Neurosci, 111*(4), 683-691.

Muller, R. U., & Kubie, J. L. (1987). The effects of changes in the environment on the spatial firing of hippocampal complex-spike cells. *J Neurosci, 7*(7), 1951-1968.

Muller, R. U., Kubie, J. L., & Saypoff, R. (1991). The hippocampus as a cognitive graph (abridged version). *Hippocampus, 1*(3), 243-246. doi:10.1002/hipo.450010306

Munch, T. A., da Silveira, R. A., Siegert, S., Viney, T. J., Awatramani, G. B., & Roska, B. (2009). Approach sensitivity in the retina processed by a multifunctional neural circuit. *Nat Neurosci, 12*(10), 1308-1316. doi:10.1038/nn.2389

Muramoto, K., Ono, T., Nishijo, H., & Fukuda, M. (1993). Rat amygdaloid neuron responses during auditory discrimination. *Neuroscience, 52*(3), 621-636.

Nader, K., Majidishad, P., Amorapanth, P., & LeDoux, J. E. (2001). Damage to the lateral and central, but not other, amygdaloid nuclei prevents the acquisition of auditory fear conditioning. *Learn Mem, 8*(3), 156-163. doi:10.1101/lm.38101

O'Keefe, J. (1976). Place units in the hippocampus of the freely moving rat. *Exp Neurol, 51*(1), 78-109.

O'Keefe, J., Burgess, N., Donnett, J. G., Jeffery, K. J., & Maguire, E. A. (1998). Place cells, navigational accuracy, and the human hippocampus. *Philos Trans R Soc Lond B Biol Sci, 353*(1373), 1333-1340. doi:10.1098/rstb.1998.0287

O'Keefe, J., & Dostrovsky, J. (1971). The hippocampus as a spatial map. Preliminary evidence from unit activity in the freely-moving rat. *Brain Res, 34*(1), 171-175.

O'Keefe, J., & Nadel, L. (1987). *The hippocampus as a cognitive map*: Clarendon press.

Okada, S., Igata, H., Sasaki, T., & Ikegaya, Y. (2017). Spatial Representation of Hippocampal Place Cells in a T-Maze with an Aversive Stimulation. *Front Neural Circuits, 11*, 101. doi:10.3389/fncir.2017.00101

Orsini, C. A., Kim, J. H., Knapska, E., & Maren, S. (2011). Hippocampal and prefrontal projections to the basal amygdala mediate contextual regulation of fear after extinction. *J Neurosci, 31*(47), 17269-17277. doi:10.1523/JNEUROSCI.4095-11.2011

Pape, H. C., & Pare, D. (2010). Plastic synaptic networks of the amygdala for the acquisition, expression, and extinction of conditioned fear. *Physiol Rev, 90*(2), 419-463. doi:10.1152/physrev.00037.2009

Papes, F., Logan, D. W., & Stowers, L. (2010). The vomeronasal organ mediates interspecies defensive behaviors through detection of protein pheromone homologs. *Cell, 141*(4), 692-703. doi:10.1016/j.cell.2010.03.037

Pare, D., & Quirk, G. J. (2017). When Scientific Paradigms Lead to Tunnel Vision: Lessons from the Study of Fear. *NPJ Sci Learn, 2*.

Pare, D., Royer, S., Smith, Y., & Lang, E. J. (2003). Contextual inhibitory gating of impulse traffic in the intra-amygdaloid network. *Ann N Y Acad Sci, 985*, 78-91.

Pare, D., Smith, Y., & Pare, J. F. (1995). Intra-amygdaloid projections of the basolateral and basomedial nuclei in the cat: Phaseolus vulgaris-leucoagglutinin anterograde tracing at the light and electron microscopic level. *Neuroscience, 69*(2), 567-583.

Paton, J. J., Belova, M. A., Morrison, S. E., & Salzman, C. D. (2006). The primate amygdala represents the positive and negative value of visual stimuli during learning. *Nature, 439*(7078), 865-870. doi:10.1038/nature04490

Pellman, B. A., & Kim, J. J. (2016). What Can Ethobehavioral Studies Tell Us about the Brain's Fear System? *Trends Neurosci, 39*(6), 420-431. doi:10.1016/j.tins.2016.04.001

Pendyam, S., Bravo-Rivera, C., Burgos-Robles, A., Sotres-Bayon, F., Quirk, G. J., & Nair, S. S. (2013). Fear signaling in the prelimbic-amygdala circuit: a computational modeling and recording study. *J Neurophysiol, 110*(4), 844-861. doi:10.1152/jn.00961.2012

Phillips, R. G., & LeDoux, J. E. (1994). Lesions of the dorsal hippocampal formation interfere with background but not foreground contextual fear conditioning. *Learn Mem, 1*(1), 34-44.

Pikkarainen, M., Ronkko, S., Savander, V., Insausti, R., & Pitkanen, A. (1999). Projections from the lateral, basal, and accessory basal nuclei of the amygdala to the hippocampal formation in rat. *J Comp Neurol, 403*(2), 229-260.

Pitkanen, A., Pikkarainen, M., Nurminen, N., & Ylinen, A. (2000). Reciprocal connections between the amygdala and the hippocampal formation, perirhinal cortex, and postrhinal cortex in rat. A review. *Ann N Y Acad Sci, 911*, 369-391.

Pitkanen, A., Savander, V., & LeDoux, J. E. (1997). Organization of intra-amygdaloid circuitries in the rat: an emerging framework for understanding functions of the amygdala. *Trends Neurosci, 20*(11), 517-523.

Poucet, B., Thinus-Blanc, C., & Muller, R. U. (1994). Place cells in the ventral hippocampus of rats. *Neuroreport, 5*(16), 2045-2048.

Quirk, G. J., Muller, R. U., & Kubie, J. L. (1990). The firing of hippocampal place cells in the dark depends on the rat's recent experience. *J Neurosci, 10*(6), 2008-2017.

Quirk, G. J., Repa, C., & LeDoux, J. E. (1995). Fear conditioning enhances short-latency auditory responses of lateral amygdala neurons: parallel recordings in the freely behaving rat. *Neuron, 15*(5), 1029-1039.

Rei, D., Mason, X., Seo, J., Graff, J., Rudenko, A., Wang, J., . . . Tsai, L. H. (2015). Basolateral amygdala bidirectionally modulates stress-induced hippocampal learning and memory deficits through a p25/Cdk5-dependent pathway. *Proc Natl Acad Sci U S A, 112*(23), 7291-7296. doi:10.1073/pnas.1415845112

Repa, J. C., Muller, J., Apergis, J., Desrochers, T. M., Zhou, Y., & LeDoux, J. E. (2001). Two different lateral amygdala cell populations contribute to the initiation and storage of memory. *Nat Neurosci, 4*(7), 724-731. doi:10.1038/89512

Richardson, M. P., Strange, B. A., & Dolan, R. J. (2004). Encoding of emotional memories depends on amygdala and hippocampus and their interactions. *Nat Neurosci, 7*(3), 278-285. doi:10.1038/nn1190

Romanski, L. M., Clugnet, M. C., Bordi, F., & LeDoux, J. E. (1993). Somatosensory and auditory convergence in the lateral nucleus of the amygdala. *Behav Neurosci, 107*(3), 444-450.

Rosen, J. B., Asok, A., & Chakraborty, T. (2015). The smell of fear: innate threat of 2,5-dihydro-2,4,5-trimethylthiazoline, a single molecule component of a predator odor. *Front Neurosci, 9*, 292. doi:10.3389/fnins.2015.00292

Royer, S., Sirota, A., Patel, J., & Buzsaki, G. (2010). Distinct representations and theta dynamics in dorsal and ventral hippocampus. *J Neurosci, 30*(5), 1777-1787. doi:10.1523/JNEUROSCI.4681-09.2010

Samson, R. D., & Pare, D. (2005). Activity-dependent synaptic plasticity in the central nucleus of the amygdala. *J Neurosci, 25*(7), 1847-1855. doi:10.1523/JNEUROSCI.3713-04.2005

See, R. E., Fuchs, R. A., Ledford, C. C., & McLaughlin, J. (2003). Drug addiction, relapse, and the amygdala. *Ann N Y Acad Sci, 985*, 294-307.

Seidenbecher, T., Laxmi, T. R., Stork, O., & Pape, H. C. (2003). Amygdalar and hippocampal theta rhythm synchronization during fear memory retrieval. *Science, 301*(5634), 846-850. doi:10.1126/science.1085818

Selden, N. R., Everitt, B. J., Jarrard, L. E., & Robbins, T. W. (1991). Complementary roles for the amygdala and hippocampus in aversive conditioning to explicit and contextual cues. *Neuroscience, 42*(2), 335-350.

Shaban, H., Humeau, Y., Herry, C., Cassasus, G., Shigemoto, R., Ciocchi, S., . . . Luthi, A. (2006). Generalization of amygdala LTP and conditioned fear in the absence of presynaptic inhibition. *Nat Neurosci, 9*(8), 1028-1035. doi:10.1038/nn1732

Sheremet, A., Burke, S. N., & Maurer, A. P. (2016). Movement Enhances the Nonlinearity of Hippocampal Theta. *J Neurosci, 36*(15), 4218-4230. doi:10.1523/JNEUROSCI.3564-15.2016

Sheremet, A., Kennedy, J. P., Qin, Y., Zhou, Y., Lovett, S. D., Burke, S. N., & Maurer, A. P. (2019). Theta-gamma cascades and running speed. *J Neurophysiol, 121*(2), 444-458. doi:10.1152/jn.00636.2018

Silva, B. A., Gross, C. T., & Graff, J. (2016). The neural circuits of innate fear: detection, integration, action, and memorization. *Learn Mem, 23*(10), 544-555. doi:10.1101/lm.042812.116

Slawinska, U., & Kasicki, S. (1998). The frequency of rat's hippocampal theta rhythm is related to the speed of locomotion. *Brain Res, 796*(1-2), 327-331.

Smith, D. M., & Mizumori, S. J. (2006). Learning-related development of context-specific neuronal responses to places and events: the hippocampal role in context processing. *J Neurosci, 26*(12), 3154-3163. doi:10.1523/JNEUROSCI.3234-05.2006

Smith, Y., & Pare, D. (1994). Intra-amygdaloid projections of the lateral nucleus in the cat: PHA-L anterograde labeling combined with postembedding GABA and glutamate immunocytochemistry. *J Comp Neurol, 342*(2), 232-248. doi:10.1002/cne.903420207

Stuber, G. D., Sparta, D. R., Stamatakis, A. M., van Leeuwen, W. A., Hardjoprajitno, J. E., Cho, S., . . . Bonci, A. (2011). Excitatory transmission from the amygdala to nucleus accumbens facilitates reward seeking. *Nature, 475*(7356), 377-380. doi:10.1038/nature10194

Stujenske, J. M., Likhtik, E., Topiwala, M. A., & Gordon, J. A. (2014). Fear and safety engage competing patterns of theta-gamma coupling in the basolateral amygdala. *Neuron, 83*(4), 919-933. doi:10.1016/j.neuron.2014.07.026

Sun, H., & Frost, B. J. (1998). Computation of different optical variables of looming objects in pigeon nucleus rotundus neurons. *Nat Neurosci, 1*(4), 296-303. doi:10.1038/1110

Takahashi, L. K. (2014). Olfactory systems and neural circuits that modulate predator odor fear. *Front Behav Neurosci, 8*, 72. doi:10.3389/fnbeh.2014.00072

Tannenholz, L., Jimenez, J. C., & Kheirbek, M. A. (2014). Local and regional heterogeneity underlying hippocampal modulation of cognition and mood. *Front Behav Neurosci, 8*, 147. doi:10.3389/fnbeh.2014.00147

Telensky, P., Svoboda, J., Blahna, K., Bures, J., Kubik, S., & Stuchlik, A. (2011). Functional inactivation of the rat hippocampus disrupts avoidance of a moving object. *Proc Natl Acad Sci U S A, 108*(13), 5414-5418. doi:10.1073/pnas.1102525108

Telensky, P., Svoboda, J., Pastalkova, E., Blahna, K., Bures, J., & Stuchlik, A. (2009). Enemy avoidance task: a novel behavioral paradigm for assessing spatial avoidance of a moving subject. *J Neurosci Methods, 180*(1), 29-33. doi:10.1016/j.jneumeth.2009.02.010

Terada, S., Takahashi, S., & Sakurai, Y. (2013). Oscillatory interaction between amygdala and hippocampus coordinates behavioral modulation based on reward expectation. *Front Behav Neurosci, 7*, 177. doi:10.3389/fnbeh.2013.00177

Van den Oever, M. C., Rotaru, D. C., Heinsbroek, J. A., Gouwenberg, Y., Deisseroth, K., Stuber, G. D., . . . Smit, A. B. (2013). Ventromedial prefrontal cortex pyramidal cells have a

temporal dynamic role in recall and extinction of cocaine-associated memory. *J Neurosci, 33*(46), 18225-18233. doi:10.1523/JNEUROSCI.2412-13.2013

Wei, P., Liu, N., Zhang, Z., Liu, X., Tang, Y., He, X., . . . Wang, L. (2015). Processing of visually evoked innate fear by a non-canonical thalamic pathway. *Nat Commun, 6*, 6756. doi:10.1038/ncomms7756

Weinberger, N. M. (2011). The medial geniculate, not the amygdala, as the root of auditory fear conditioning. *Hear Res, 274*(1-2), 61-74. doi:10.1016/j.heares.2010.03.093

Weingarten, H. W., N. (1978). Exploration evoked by electrical stimulation of the amygdala of rats. *Physiological Psychology, 6*(2), 229-235. doi:https://doi.org/10.3758/BF03326718

Wilensky, A. E., Schafe, G. E., Kristensen, M. P., & LeDoux, J. E. (2006). Rethinking the fear circuit: the central nucleus of the amygdala is required for the acquisition, consolidation, and expression of Pavlovian fear conditioning. *J Neurosci, 26*(48), 12387-12396. doi:10.1523/JNEUROSCI.4316-06.2006

Wilensky, A. E., Schafe, G. E., & LeDoux, J. E. (1999). Functional inactivation of the amygdala before but not after auditory fear conditioning prevents memory formation. *J Neurosci, 19*(24), RC48.

Wilson, J. C., Kesler, M., Pelegrin, S. L., Kalvi, L., Gruber, A., & Steenland, H. W. (2015). Watching from a distance: A robotically controlled laser and real-time subject tracking software for the study of conditioned predator/prey-like interactions. *J Neurosci Methods, 253*, 78-89. doi:10.1016/j.jneumeth.2015.06.015

Wolff, S. B., Grundemann, J., Tovote, P., Krabbe, S., Jacobson, G. A., Muller, C., . . . Luthi, A. (2014). Amygdala interneuron subtypes control fear learning through disinhibition. *Nature, 509*(7501), 453-458. doi:10.1038/nature13258

Wu, C. T., Haggerty, D., Kemere, C., & Ji, D. (2017). Hippocampal awake replay in fear memory retrieval. *Nat Neurosci, 20*(4), 571-580. doi:10.1038/nn.4507

Yilmaz, M., & Meister, M. (2013). Rapid innate defensive responses of mice to looming visual stimuli. *Curr Biol, 23*(20), 2011-2015. doi:10.1016/j.cub.2013.08.015

Young, B. J., Fox, G. D., & Eichenbaum, H. (1994). Correlates of hippocampal complex-spike cell activity in rats performing a nonspatial radial maze task. *J Neurosci, 14*(11 Pt 1), 6553-6563.

Young, S. L., Bohenek, D. L., & Fanselow, M. S. (1994). NMDA processes mediate anterograde amnesia of contextual fear conditioning induced by hippocampal damage: immunization against amnesia by context preexposure. *Behav Neurosci, 108*(1), 19-29.

# VITA

Mi-Seon Kong was born in Chuncheon, South Korea. She currently lives in Lynnwood, Washington, with her husband Sung and two sons; Enoch and Ezra. She received her Bachelor of Arts degree in Psychology at Korea University in Seoul, Korea, 2010, and her Master of Science degree in Biological Psychology at Korea University in Seoul, Korea, 2012. In 2019, she earned a Doctor of Philosophy in Psychology at the University of Washington in Seattle, Washington.